Electronic Supplementary Information

Facile Interconversion of Mesitylcopper into A CuMes-Cu_2bis(amidinate) Triangle and A Tetracuprous Möbius Strip

Keri Dowling,[†[a]] Tomasz Kruczyński,[†[a]] Sanjay Dutta,[a] Ngan Le,[b] Samer Gozem,[b] Colin D. McMillen,[c] Nattamai Bhuvanesh,[d] and Michael Stollenz*[a]

[a] Department of Chemistry and Biochemistry, Kennesaw State University, 370 Paulding Avenue NW, MD#1203, Kennesaw, Georgia 30144. [b] Department of Chemistry, Georgia State University, 145 Piedmont Ave SE, Atlanta, Georgia 30303, P. O. Box 3945, Atlanta, Georgia 30302-3945. [c] Department of Chemistry, Clemson University, 379 Hunter Laboratories, Clemson, SC 29634-0973. [d] Department of Chemistry, Texas A&M University, P.O. Box 30012, College Station, Texas 77842-3012.

[†]These authors contributed equally to this work.

This work is dedicated to Professor Dr. Dirk Walther on the occasion of his 85th birthday.

*E-mail: Michael.Stollenz@kennesaw.edu

Table of Contents

Experimental and Computational Section

General Procedures. All synthetic procedures involving air- and moisture-sensitive compounds were carried out by using Schlenk or glovebox techniques under an atmosphere of dry argon. Glassware and NMR tubes were heat-sealed with a heat gun under vacuum. ***Caution!*** *Extreme care should be taken both in the handling of the cryogen liquid nitrogen and its use in the Schlenk line trap to avoid the condensation of oxygen from air.*

Solvents: Prior to use, dichloromethane (CH_2Cl_2, VWR, ≥ 99.5%) was freshly distilled from CaH_2. Diethyl ether (Thermo Fisher, ≥ 99.0%), hexanes (mixture of isomers, VWR, ≥ 98.5%), *n*-hexane (VWR, 97%), tetrahydrofuran (THF, Thermo Fisher, 99.9%), and toluene (VWR, ≥ 99.5%) were freshly distilled from sodium/benzophenone. *Deuterated solvents*: Chloroform-*d* (Cambridge Isotope Laboratories, Inc., D, 99.8% + 0.03% v/v tetramethylsilane, TMS) was distilled from CaH_2. Benzene-d_6 (C_6D_6, Cambridge Isotope Laboratories, Inc., D, 99.5%) and toluene-d_8 (Cambridge Isotope Laboratories, Inc., D, 99.5%) were distilled from sodium.

Reactants: Triethylamine (Alfa Aesar, 99%) was distilled from sodium. 1,3-Diaminopropane (Acros, 99+%) was dried over molecular sieves (3 Å), 2-amino-6-methylpyridine (Thermo Fisher, 98%) was recrystallized from a mixture of dichloromethane and hexanes (1:4 v/v) and dried in oil pump vacuum for ≈ 20 min. Pivaloyl chloride (Thermo Fisher, 99%) and Phosphorus pentachloride (PCl_5, Thermo Fisher, 99.5%) were used as received. Mesitylcopper were prepared according to the literature procedure.[S2]

Elemental analyses were performed by Atlantic Microlab, Inc., Norcross, Georgia, and Robertson Microlit Laboratories, Ledgewood, New Jersey.

Melting points were determined with an SRS (Stanford Research Systems) Digi Melt instrument, using capillaries sealed with Teflon grease; values are uncorrected (the heating rate was 2 K/min).

NMR measurements were recorded on a Bruker Avance III 400 and a Bruker Avance III 600 spectrometers, equipped with a PRODIGY cryoprobe, at ambient probe temperatures regulated by a BCU unit unless noted at 400.1 MHz or 600.2 MHz (^{1}H) and 100.6 MHz or 150.9 MHz (^{13}C), respectively. ^{13}C NMR resonances were obtained with proton broadband decoupling and referenced to the solvent signals of $CDCl_3$ at 77.16 ppm and C_6D_6 at 128.06 ppm (^{1}H NMR: 7.26 ppm ($CDCl_3$) and 7.16 (benzene), respectively).[S3] ^{13}C NMR assignments are based on COSY, NOESY, HSQC, and HMBC 2D experiments. ^{15}N chemical shifts were measured using a ^{15}N HMBC at 600.2 MHz (^{1}H)/60.8 MHz (^{15}N) (^{15}N, optimized for $^nJ_{HN}$ couplings of 5 Hz) and calibrated indirectly to Ξ ($MeNO_2$) = 0.10136767.[S4,S5]

Mass spectrometric analyses of $\mathbf{L^2}H_2$, **1**, and **2** (electrospray ionization, ESI, in acetonitrile, **1** and **2** prepared under argon atmosphere) were performed on a Thermo Scientific LTQ XL Linear Ion Quadrupole Mass Spectrometer ($\mathbf{L^2}H_2$, low resolution) and on an Orbitrap Exploris 240 Mass Spectrometer (**1** and **2**, high resolution).

IR spectra were measured on a PerkinElmer Spectrum One FTIR Spectrometer equipped with a Universal ATR Sampling Accessory.

Photoluminescence measurements were performed on a Horiba Scientific Fluorolog-QM (model: FL-QM-75-11C) spectrofluorometer. In solution, emission spectra of **1** and **2** were recorded in THF as solvent with a concentration of 1 mM. For solids, a quartz cuvette with path length of 0.5 mm was used to record the spectra. Fluorescence quantum yields for both in solution and solid were performed at room temperature using an integrating sphere installed in the sample chamber of the spectrofluorometer. Variable-temperature experiments were performed in a quartz capillary (diameter of 2 mm) under *vacuum* (0.2 mbar) using a Janis VPF-100 liquid nitrogen cryostat system equipped with a sample holder window. The operating temperature ranges were 150–300 K for solutions and 77–300 K for solids.

Absorbance spectra for all samples were recorded on a Cary 5000 UV-Vis-NIR spectrophotometer, in THF as solvent with a concentration of 20 µM.

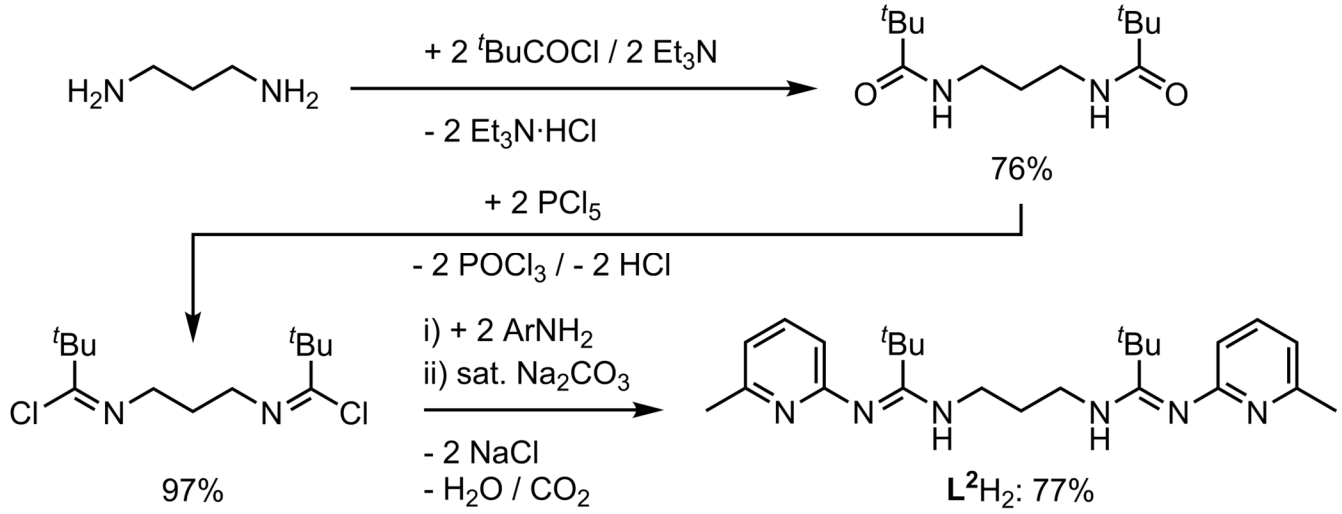

Scheme S1: Synthesis of $\mathbf{L^2}H_2$.

Synthesis of *N*,*N*′-1,3-propanediylbis(2,2-dimethylpropanamide). This synthetic protocol was adapted from a procedure from *Burton*[S6] and modified as follows: Pivaloyl chloride (6.507 g, 53.97 mmol) was added dropwise via a syringe to a stirring solution of 1,3-diaminopropane (2.30 mL, 2.02 g, 27.3 mmol) and Et_3N (7.50 mL, 5.45 g, 53.9 mmol) in CH_2Cl_2 (90 mL) at 0 °C to form a colorless precipitate. The suspension was warmed to room temperature. After ~ 18 h, the reaction mixture was washed with deionized water (4 × 40 mL), dried over anhydrous Na_2SO_4, and filtered. Volatiles were removed from the filtrate using a rotary evaporator and the residue was finally dried in oil pump vacuum for 18 h to give a colorless powder. Yield: 4.979 g (20.54 mmol, 76%).

^{1}H NMR ($CDCl_3$, 400.1 MHz): δ 1.21 (s, 18 H; CH_3), 1.56–1.62 (m, 2 H; $NCH_2C\underline{H_2}$, β), 3.25 (dt, , $^3J_{H,H}$ = 6.3 Hz, 6.0 Hz, 4 H; $NC\underline{H_2}$, α), 6.39 (s, 2 H; NH). ^{13}C NMR ($CDCl_3$, 100.6 MHz): δ 27.8 (CH_3), 30.0 ($NCH_2\underline{C}H_2$, β), 35.4 ($N\underline{C}H_2CH_2$, α), 38.9 (C, ^{t}Bu), 179.5 ($\underline{C}$=O).

Synthesis of *N*,*N*′-1,3-propanediylbis(2,2-dimethylpropanimidoyl chloride). A synthetic protocol was earlier reported by *Kretschmer et al.* and modified by us based on ref.[S7]: *N*,*N*'-1,3-propanediylbis(2,2-dimethylpropanamide) (10.640 g, 43.90 mmol) and PCl_5 (18.054 g, (86.70 mol) were suspended in CH_2Cl_2 (80 mL) with stirring to give a pale yellow solution. After 19 h, volatiles were removed by oil pump vacuum to give a yellow to beige viscous solid. Hexanes (100 mL) and then triethylamine (11.9 mL. 8.64 g, 85.4 mmol) were added. The resulting pale yellow suspension was filtered to give an off-white filter cake and a yellow filtrate. The filter cake was washed with hexanes (1 × 10 mL). The volatiles of the filtrate were removed by oil pump vacuum to leave a pale yellow oil.

Yield: 11.906 g (42.64 mmol, 97%).

^{1}H NMR ($CDCl_3$, 400.1 MHz): δ 1.19 (s, 18 H; CH_3), 1.84 (quint, $^3J_{H,H}$ = 6.8 Hz, 2 H; $NCH_2C\underline{H_2}$, β), 3.47 (t, $^3J_{H,H}$ = 6.8 Hz, 4 H; $NC\underline{H_2}$, α). ^{13}C{^{1}H} NMR ($CDCl_3$, 100.6 MHz): δ 28.4 (CH_3), 29.6 ($NCH_2\underline{C}H_2$, β), 43.6 (C, ^{t}Bu), 50.8 ($N\underline{C}H_2$, α), 152.6 ($\underline{C}$=N).

Synthesis of L^2H_2. A solution of 2-amino-6-methylpyridine (6.500 g, 60.11 mmol) in toluene (50 mL) was added by a cannula to a cooled (0 °C) solution of *N*,*N*′-1,3-propanediylbis(2,2-dimethylpropanimidoyl chloride) (8.388 g, 30.04 mmol) in toluene (80 mL) with stirring, resulting in the formation of an orange, waxy solid at the bottom of the flask. The reaction mixture was warmed to room temperature, then heated to 87 °C for 40 h, and subsequently cooled to 0 °C. The clear solution was removed from the solid residue by decantation. A solution of saturated aqueous Na_2CO_3 (75 mL) was added to the reaction flask and resulted in the formation of an off-white precipitate. The suspension was stirred at room temperature for 20 min. The solid was isolated by filtration, then washed with water (3 × 70 mL), followed by hexanes (1 × 10 mL), and then dried in in air at ≈ 40 °C for 19 h. The crude product was subsequently dried in oil pump vacuum for 18 h to give a pale yellow powder, then washed with cold acetonitrile (1 × 30 mL, ≈ -20 °C) until all orange/red impurities were removed and finally dried for 18 h in oil pump vacuum. $\mathbf{L^2}H_2$ was obtained as a white powder.

Yield: 9.773 g (23.13 mmol, 77%). Mp: 144.5 °C.

^{1}H NMR ($CDCl_3$, 600.2 MHz,) δ 1.14 (s, 18 H, CH_3, ^{t}Bu), 1.56 (quint, $^3J_{H,H}$ = 6.4 Hz, 2 H, $NCH_2C\underline{H_2}$, β), 2.41 (s, 6 H, CH_3, 6-py), 3.01 (q, $^3J_{H,H}$ = 6.0 Hz, 4 H, $NC\underline{H_2}CH_2$, α), 5.47 (broad s, 2 H, NH), 6.44 (d, $^3J_{H,H}$ = 8.0 Hz, 2 H, CH, py H^3), 6.60 (d, $^3J_{H,H}$ = 7.3 Hz, 2 H, CH, py H^5), 7.32 (t, $^3J_{H,H}$ = 7.6 Hz, 2 H, CH, py H^4). ^{1}H NMR (C_6D_6, 600.2 MHz): δ 1.19 (s, 18 H; CH_3, ^{t}Bu), 1.47 (quint, $^3J_{H,H}$ = 6.0 Hz, 2 H; $NCH_2C\underline{H_2}$, β), 2.38 (s, 6 H; CH_3, 6-py), 3.17 (q, $^3J_{H,H}$ = 6.0 Hz, 4 H, $NC\underline{H_2}CH_2$, α), 6.42 (d, $^3J_{H,H}$ = 7.9 Hz, 2 H; CH, py H^5), 6.74 (d, $^3J_{H,H}$ = 7.9 Hz, 2 H; CH, py H^3), 7.12 (t, $^3J_{H,H}$ = 7.6 Hz, 2 H; CH, *4*-py py H^4), NH signal was not observed. ^{13}C{^{1}H} NMR ($CDCl_3$, 150.9 MHz,) δ 24.6 (CH_3, 6-py), 29.4 (CH_3, ^{t}Bu), 30.1 ($NCH_2\underline{C}H_2$, β), 39.2 (C, ^{t}Bu), 40.1 ($N\underline{C}H_2$, α), 113.6 (CH, py C^3), 115.4 (CH, py C^5), 137.0 (CH, py C^4), 156.6 (C, py C^6), 162.2 (C, ^{t}Bu$\underline{C}N_2$), 163.0 (C, py C^2). ^{13}C{^{1}H} NMR (C_6D_6, 150.9 MHz):

δ 24.6 (CH_3, 6-py), 29.4 (CH_3, ^{t}Bu), 30.7 ($NCH_2\underline{C}H_2$, β), 39.2 (C, ^{t}Bu), 40.1 ($N\underline{C}H_2$, α), 115.2 (CH, py C^5), 115.3 (CH, py C^3), 137.0 (C, py C^4), 155.9 (C, py C^6), 163.1 (C, ^{t}Bu$\underline{C}N_2$), 163.6 (C, py C^2). ^{15}N NMR (C_6D_6, 60.8 MHz):[S8] δ -91.6 (*N*-py), -284.1 ((*N*H)CH_2).

MS (ESI in MeCN): *m/z* (relative intensity) 423.4 (100), 424.4 (29), 425.4 (4) $[M + H]^+$.

IR (neat, cm^{-1}): $\tilde{\nu}$ = 3353, 3311, 3297, 3290, 3283 (w, ν(N–H)), 3063, 3007 (w, ν-(C–H)), 2958, 2951 (m, ν-(C–H)), 2906, 2868, 2836 (w, ν-(C–H)), 1644, 1604, 1585 (s), 1560, 1528, 1515 (vs), 1486 (m), 1436 (vs), 1397, 1372 (m), 1362 (s), 1347, 1282 (m), 1272 (s), 1233 (m), 1222 (s), 1206 (m), 1185, 1154, 1150 (s), 1087, 1077, 1033 (m), 1019 (w), 1000, 991 (m), 963, 934 (w), 890, 868, 838 (m), 822 (w), 811 (m), 800, 782, 760 (s), 740, 729, 720 (m).

Elemental analysis: Anal. Calcd for $C_{25}H_{38}N_6$: C, 71.05; H, 9.06; N, 19.89. Found: C, 71.23; H 9.21; N 19.64.

Synthesis of 1. A solution of $\mathbf{L^2}H_2$ (0.452 g, 1.07 mmol) in toluene (25 mL) was added to a cooled (–78 °C) solution of CuMes (0.597 g, 3.27 mmol) in toluene (25 mL) with stirring. Formation of pale yellow precipitate was observed. The resulting suspension was allowed to warm to room temperature in the cold bath as the dry ice evaporated overnight (18 h). The solvent was removed by decantation from the solid, which was washed with *n*-hexane (2 × 2 mL) and dried in oil pump vacuum for 18 h. Yield: (0.545 g, 0.746 mmol, 70%). Mp: ≈ 227 °C (onset of decomposition into a brown solid).

^{1}H NMR (C_6D_6, 600.2 MHz) δ 1.51 (s, 18 H, CH_3, ^{t}Bu), 1.83 (s, 6 H, CH_3, 6-py), 2.14 (s, 6 H, CH_3, *p*-Mes), 2.47–2.50 (m, 2 H, 2 H, $NCH_2C\underline{H_2}$, β), 2.84 (s, 6 H CH_3, *o*-Mes), 3.44 (dt, $^3J_{H,H}$ = 8.7 Hz, $|^2J_{H,H}| \approx$ 13 Hz, 2 H, $NC\underline{H_2}$, α_a), 4.14–4.18 (m, 2 H, 2 H, $NC\underline{H_2}$, α_b), 5.62 (d, $^3J_{H,H}$ = 6.8 Hz, 2 H, CH, py H^5), 5.95 (d, $^3J_{H,H}$ = 8.6 Hz, 2 H, CH, py H^3), 6.67 (dd, $^3J_{H,H}$ = 8.6 Hz, 6.9 Hz, 2 H, CH, py H^4), 6.85 (s, 2 H, CH, Mes). ^{13}C{^{1}H} NMR (C_6D_6, 150.9 MHz): δ 21.5 (*p*-CH_3, Mes), 24.3 (CH_3, 6-*py*), 29.6 (CH_3, *o*-Mes), 30.3 (CH_3, ^{t}Bu), 32.1 ($NCH_2\underline{C}H_2$, β), 42.0 (C, ^{t}Bu), 45.6 ($N\underline{C}H_2$, α), 107.8 (CH, py C^5), 109.0 (CH, py C^3), 126.8 (CH, Mes), 137.6 (C, *i*-, *p*-Mes), 138.6 (CH, py C^4), 141.9 (C, *i*-, *p*-Mes), 154.7 (C, py C^6), 155.6 (C, *o*-Mes), 165.5 (C, py C^2), 169.6 (C, ^{t}Bu$\underline{C}N_2$).[S9]

MS (ESI in MeCN): *m/z* (relative intensity) 485.2463 (100), 486.2489 (28), 487.2450 (48), 488.2475 (12), 489.2518 (1) $[(L^2H_2)Cu]^+$; 574.1800 (4), 575.1833 (1), 576.1778 (4), 577.1822 (1), 578.1751(1), 579.1789 (0.2), 580.1828 (0.03) $[(L^2H_2)Cu_2CN]^+$.

IR (neat, cm^{-1}): $\tilde{\nu}$ = 2965, 2945, 2915 (m, ν-(C–H)), 2882, 2865, 2844, 2835 (w, ν-(C–H)), 1621 (m), 1602 (s), 1546 (m), 1464, 1455 (vs), 1385, 1382, 1368 (s), 1268, 1223 (m), 1203, 1163 (w), 1138 (vs), 1056 (s), 1033, 1008 (vs), 943 (m), 921 (w), 879, 858, 849 (m), 782 (vs), 729, 709, 631 (w).

Anal. Calcd for $C_{34}H_{47}Cu_3N_6$: C, 55.91; H, 6.49; N, 11.51. Found: C, 56.08; H 6.44; N 11.26.

Synthesis of 2. *Method A*: A solution of CuMes (1.286 g, 7.04 mmol) in toluene (100 mL) was added dropwise over 1.5 h to a suspension of $\mathbf{L^2}H_2$ (1.488 g, 3.52 mmol) in toluene (90 mL) with stirring at

room temperature. The resulting lime green solution was stirred for 48 h. After cooling to room temperature, the volatiles were removed using oil pump vacuum. A lime green solid was obtained and washed with *n*-hexane (2 × 1 mL). The supernatant was removed by decantation and the solid was dried using oil pump vacuum. The crude product was recrystallized from a 2:1 mixture of THF and *n*-hexane (20 mL) at –35 °C, washed with *n*-hexane (2 × 1 mL), and dried in oil pump vacuum for 19 h. Complex **2** was isolated as a yellow microcrystalline solid. Yield: 0.750 g (0.68 mmol, 39 %).

Method B: A solution of **1** (25.2 mg, 0.035 mmol) and $\mathbf{L^2}H_2$ (8.1 mg, 0.019 mmol) in toluene (60 mL) was heated with stirring to 75 °C for 18 h. After cooling to room temperature, all volatiles were removed using oil pump vacuum and the resulting olive yellow solid was dried for additional 2 h in vacuo. The ^{1}H NMR spectrum indicated a conversion of **1** and $\mathbf{L^2}H_2$ into **2**, **3**, and **4** as major products in an approximate ratio of 3:1:1.

Characterization details of isolated **2**: Mp: ≈ 178 °C (onset of decomposition into a brownish-yellow melt). ^{1}H NMR (C_6D_6, 600.2 MHz): δ 1.33 (s, 18 H; ^{t}Bu'), 1.50 (s, 18 H; ^{t}Bu), 1.90 (s, 6 H; CH_3, 6-py), 2.36 (s, 6 H; CH_3, 6'-py), 2.42–2.47 (m, 2 H; $NCH_2C\underline{H_2}$, β), 2.73 (qt, $J_{H,H}$ = 12.8 Hz, 3.1 Hz, 2 H; $NCH_2C\underline{H_2}$, β'), 3.09 (ddd, $^3J_{H,H}$ = 12.4 Hz, 6.2 Hz, $|^2J_{H,H}|$ = 16.0 Hz, 2 H; $NC\underline{H_2}$, α_a), 3.29 (dt, $^3J_{H,H}$ = 3.5 Hz, $|^2J_{H,H}|$ =16.5 Hz, 2 H; $NC\underline{H_2}$, α_a'), 3.59 (ddd, $^3J_{H,H}$ 12.9 Hz, 1.5 Hz, $|^2J_{H,H}|$ = 14.9 Hz, 2 H, $NC\underline{H_2}$, α_b'), 4.19 (ddd, $^3J_{H,H}$ = 13.0 Hz, 2.9 Hz, $|^2J_{H,H}|$ = 15.9 Hz, 2 H, $NC\underline{H_2}$, α_b), 5.70 (d, $^3J_{H,H}$ = 6.8 Hz, 2 H; CH, py H^5), 5.80 (d, $^3J_{H,H}$ = 6.8 Hz, 2 H; CH, py $H^{5'}$), 5.97 (d, $^3J_{H,H}$ = 8.8 Hz, 2 H, py $H^3/H^{3'}$), 5.99 (d, $^3J_{H,H}$ = 8.7 Hz, 2 H, py $H^3/H^{3'}$) 6.64 (dd, $^3J_{H,H}$ = 8.3 Hz, 7.3 Hz, 4 H; CH, py $H^4/H^{4'}$). ^{13}C{^{1}H} NMR (C_6D_6, 150.9 MHz): δ 26.2 (CH_3, 6-py), 26.8 (CH_3, 6'-py), δ 30.3 (CH_3, ^{t}Bu), 30.5 (CH_3, ^{t}Bu'), 34.5 ($NCH_2\underline{C}H_2$, β), 40.3 (C, ^{t}Bu'), 40.7 (C, ^{t}Bu), 46.3 ($N\underline{C}H_2$, α'), 48.9 ($N\underline{C}H_2$, α), 107.7 (CH, py C^5), 108.2 (CH, py $C^{5'}$), 108.3 (CH, py $C^{3'}$), 108.9 (CH, py C^3), 138.1 (CH, py $C^{4'}$), 138.6 (CH, py C^4), 154.6 (C, py C^6), 154.8 (C, py $C^{6'}$), 164.9 (2 × C, py C^2, py $C^{2'}$), 169.7 (C, ^{t}Bu$\underline{C}N_2$'), 169.8 (C, ^{t}Bu$\underline{C}N_2$). ^{15}N NMR (C_6D_6, 60.8 MHz, 288.0 K):[S8] δ -83.3 ($N$$CH_2$'), -85.4 ($N$$CH_2$), -174.3 ($N$-py), -175.3 ($N$-py').

MS (ESI in MeCN): *m/z* (relative intensity) 423.3225 (38), 424.3283 (11), 425.3275 (2) $[L^2H_2 + H]^+$; 485.2488 (100), 486.2515 (30), 487.2444 (49), 488.2532 (13), 489.2527 (2) $[(L^2H_2)Cu]^+$; 574.1815 (11), 575.1744 (3), 576.1858 (10), 577.1834 (3), 578.1837(3), 579.1873 (1), 580.1805 (0.1) $[(L^2H_2)Cu_2CN]^+$.

IR (neat cm^{-1}): $\tilde{\nu}$ = 2946 (m, ν-(C–H)), 2868 (w, ν-(C–H)), 1606 (s), 1550 (m), 1466 (vs), 1382, 1368 (s), 1300 (w), 1264 (m), 1226 (w), 1140 (s), 1094 (w), 1056, 1012 (m), 944, 902, 840 (w), 770 (s), 730 (w).

Anal. Calcd for $C_{50}H_{72}Cu_4N_{12}$: C, 54.82; H, 6.63; N, 15.34. Found: C, 54.93; H 6.62; N 14.74.

Characterization details of **3**: ^{1}H NMR (C_6D_6, 600.2 MHz) δ 1.45 (s, 18 H, CH_3, ^{t}Bu), 1.96 (s, 6 H, CH_3, 6-py), 5.55 (d, $^3J_{H,H}$ = 6.8 Hz, 2 H, CH, py H^5), 5.89 (d, $^3J_{H,H}$ = 8.7 Hz, 2 H, CH, py H^3), 6.54 (dd, $^3J_{H,H}$ = 8.7 Hz, 6.9 Hz, 2 H, CH, py H^4). ^{13}C{^{1}H} NMR (C_6D_6, 150.9 MHz): 26.2 (CH_3, 6-py), δ 29.5 (CH_3, ^{t}Bu), 40.1 (C, ^{t}Bu), ≈ 107.7 (CH, overlaid by **2**, py C^5), 108.9 (CH, py C^3), 137.9 (CH, py C^4), 154.1 (C, py

C^6), 164.9 (C, py C^2), ~ 168−169 (C, ^{t}Bu$\underline{C}$N$_2$). Due to overlapping signals from **2** and **4**, the CH$_2$ groups of **3** could not be unambiguously assigned.

Characterization details of **4**: ^{1}H NMR (600. MHz, C$_6$D$_6$) δ 1.50 (s, 18 H, CH$_3$, ^{t}Bu), 2.01 (s, 6 H, CH$_3$, 6-py), 2.23–2.26 (m, 2 H, NCH$_2\underline{C}$H$_2$, β), ≈ 3.53–3.60 (m, overlaid by **2**, 2 H, N$\underline{C}$H$_2$CH$_2$, α$_a$), 3.85 (dt, $^3J_{H,H}$ = 7.2 Hz, $|^2J_{H,H}|$ = 14.3 Hz, 2 H; NC$\underline{H_2}$, α$_b$), 5.73 (d, $^3J_{H,H}$ = 6.9 Hz, 2 H, CH, py H^5), 6.05 (d, $^3J_{H,H}$ = 8.7 Hz, 2 H, CH, py H^3), 6.67 (dd, $^3J_{H,H}$= 8.7, 6.9 Hz, 2H, CH, py H^4). ^{13}C{^{1}H} NMR (C$_6$D$_6$, 150.9 MHz, 298.1 K): δ 26.2 (CH$_3$, 6-py), 30.0 (CH$_3$, ^{t}Bu), 33.3 (NCH$_2\underline{C}$H$_2$, β), 47.9 (N$\underline{C}$H$_2$CH$_2$, α), ≈ 107.7 (CH, overlaid by **2**, py C^5), 110.0 (CH, py C^3), ≈ 138.1 (CH, overlaid by **2**, py C^4), 154.1 (C, py C^6), 165.9 (C, py C^2), ~ 168−169 (C, ^{t}Bu$\underline{C}$N$_2$). Due to overlapping signals from **2** and **4**, the quaternary C atom resonance of the ^{t}Bu groups of **3** could not be unambiguously assigned.

X-ray Crystallography. Colorless, block-shaped single crystals of **L^2**H$_2$ were obtained from a saturated solution in Et$_2$O in an NMR tube using a recrystallization method described by *Watkin*.[S10] Yellow column-shaped single crystals of complex **1** suitable for X-ray diffraction analysis were obtained by layering a solution in toluene with *n*-hexane at room temperature and formed over the course of 5 d. Single crystals of complex **2** were grown as greenish yellow blocks from a saturated solution in toluene at –35 °C for 3 d. X-ray data for **L^2**H$_2$ and **2**·2C$_7$H$_8$ were collected on a Bruker Venture X-ray diffractometer (CuKα radiation, λ = 1.54178 Å) and for **1** on a Bruker Bruker Quest (PHOTON III) diffractometer (MoKα radiation, λ = 0.71073 Å) by using ω and φ scans at 100 K (**L^2**H$_2$ and **2**·2C$_7$H$_8$) or 110 K (**1**, Table S1). The integrated intensities for each reflection were obtained by reduction of the data frames with the program APEX4.[S11] Cell parameters were obtained and refined with 15607 (5099 unique, **L^2**H$_2$), 19251 (19251 unique, **1**), and 74123 (11687 unique, **2**·2C$_7$H$_8$) reflections, respectively. The integrated intensity information for each reflection was obtained by reduction of the data frames by using APEX4. The integrated were corrected for absorption by using SADABS.[S12] For **1**, twinned crystals were found and data was integrated that included both of the components of the twinned crystal. TWINABS[S13] was used for integrated data correction as well as to generate the hklf4 file with non-overlapping peaks and the hklf5 file with all the reflections including both twin components. While the hklf4 file was used for structure solution, hklf5 data served for the final least squares refinement. The structures were solved by intrinsic phasing and refined (weighted least squares refinement on F^2) by using SHELXT-2016/6 and SHELXL.[S14] The hydrogen atoms were placed in idealized positions, and refined by using a riding model. Non-hydrogen atoms were refined with anisotropic thermal parameters. For all structures, absence of additional symmetry and void was confirmed using PLATON (ADDSYM).[S15] The absolute structure of **L^2**H$_2$, refined in the noncentrosymmetric space group $P\,2_1\,2_1\,2_1$ is supported by the Flack parameter of 0.08(15). CCDC 2373847 (**L^2**H$_2$), 2362330 (**1**), and 2373848 (**2**·2C$_7$H$_8$) contain the supplementary

crystallographic data (CIF) for this paper. These data can be obtained free of charge from The Cambridge Crystallographic Data Centre *via* www.ccdc.cam.ac.uk/data_request/cif.

Computational details. All complexes were optimized using PBE0 (also known as PBE1PBE),[S16] a hybrid density functional that uses 25% exact Hartree-Fock exchange and 75% DFT exchange from the PBE functional. Hybrid functionals such as PBE0 have been widely used to optimize geometries of transition metal complexes[S17] as well as to evaluate thermodynamic quantities.[S18] The 6-311+G* basis set was employed for the Cu atoms while 6-31G* was used for C, H, and N atoms. A similar basis set has been used in earlier calculations on copper Cu(I) systems.[S19,20,21,22] All ground state structures were validated to be at energy minima with frequency calculations, which also provided the Gibbs free energy of each system through enthalpy, entropy, and thermal corrections at 298.15 K temperature and 1 atm pressure. The calculations were performed using Gaussian16.[S23] The relative free energies for different *E* and *Z* isomers (**IIa**–**d**, **IIIa**, and **IIIb**) were calculated with respect to two units of the proposed intermediate **I** as reference in the gas phase, as shown in equation **Eq. 1**. The relative free energy of complex **1** was obtained by subtracting the free energy of the reference state and a quarter of the free energy of $[Cu_4Mes_4]$, as shown in equation **Eq. 2**. The relative free energy of reaction for the intermediate **I** ($\Delta_rG = \Delta G_I$) was calculated from the free energies of $\mathbf{L^2}H_2$, ½ of $[Cu_4Mes_4]$, and mesitylene (MesH, **Eq. 3**).

$$\Delta G_{dimerization} = G_{dimer} - 2 \times G_I \qquad \textbf{(Eq. 1)}$$

$$\Delta G_1 = G_1 - G_I - \tfrac{1}{4}\, G_{[Cu_4Mes_4]} \qquad \textbf{(Eq. 2)}$$

$$\Delta G_I = (G_I + 2 \times G_{MesH}) - (\tfrac{1}{2}\, G_{[Cu_4Mes_4]} + G_{L^2H_2}) \qquad \textbf{(Eq. 3)}$$

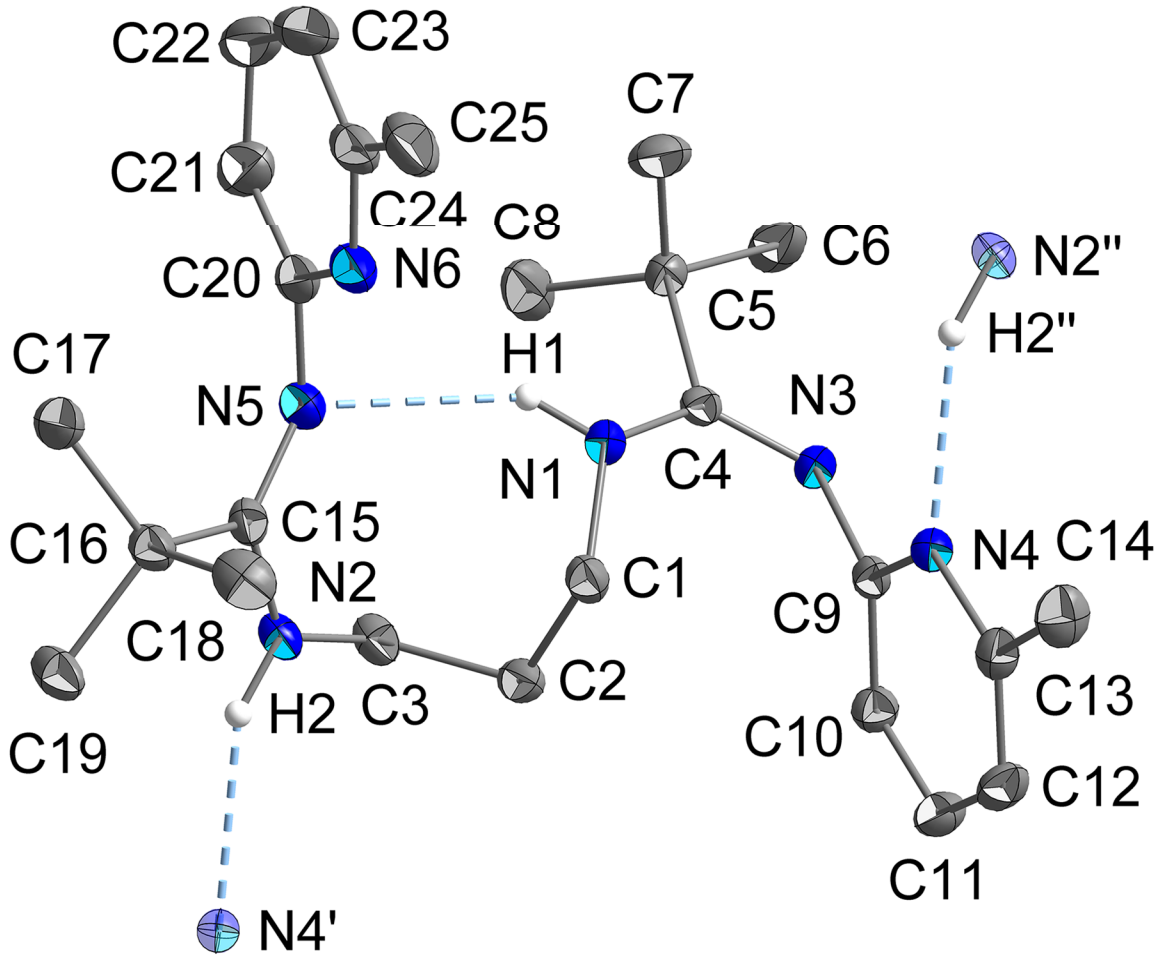

Figure S1: Molecular structure of $\mathbf{L^2}H_2$ showing ellipsoids with anisotropic displacement factors of 50% probability. Hydrogen atoms except for NH functionalities have been omitted for clarity. Selected interatomic distances (Å), bond angles (deg), and torsion angles (deg): C2–C1 1.531(3), C1–N1 1.458(3), N1–C4 1.361(3), C4–N3 1.287(3), N3–C9 1.393(3), C9–N4 1.344(3), N4–C13 1.351(3), C2–C3 1.523(3), C3–N2 1.461(2), N2–C15 1.348(3), C15–N5 1.294(3), N5–C20 1.401(3), C20–N6 1.343(3), N6–C24 1.350(3), C3–C2–C1 113.36(18), C2–C1–N1 111.98(17), C1–N1–C4 126.34(18), N1–C4–N3 127.69(19), C4–N3–C9 126.01(17), N3–C9–N4 117.79(18), C9–N4–C13 118.58(18), C2–C3–N2 112.86(17), C3–N2–C15 124.31(18), N2–C15–N5 118.02(19), C15–N5–C20 127.41(19), N5–C20–N6 119.5(2), C20–N6–C24 118.6(2), C3–C2–C1–N1 –63.2(2), C2–C1–N1–C4 –74.1(3), C1–N1–C4–N3 –21.8(3), N1–C4–N3–C9 –6.3(3), C4–N3–C9–N4 –76.9(3), N3–C9–N4–C13 –174.18(18), C2–C3–N2–C15 95.4(2), C3–N2–C15–N5 2.2(3), N2–C15–N5–C20 –171.0(2), C15–N5–C20–N6 61.5(3), N5–C20–N6–C24 176.2(2). Hydrogen bonds (Å) and associated angles (deg): N1···N5 3.042(3), N2···N4' 2.942(3), H1···N5 2.30(3), H2···N4' 2.18(3), N1–H1···N5 143.(3), N2–H2···N4' 148.(2). Symmetry operation used to generate equivalent atoms: (') 1 + *x*, *y*, *z*; (") –1 + *x*, *y*, *z*.

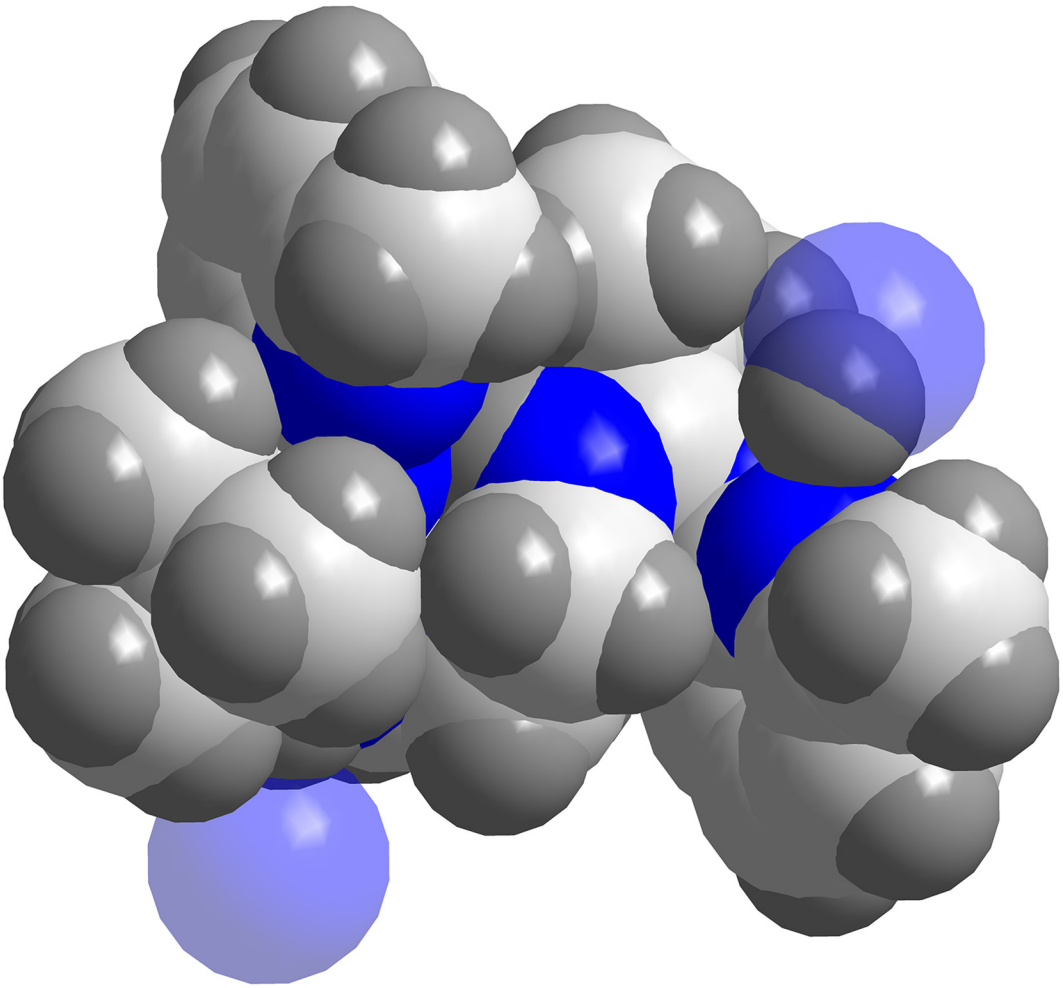

Figure S2: Space filling representation of the molecular structure of $\mathbf{L^2}H_2$.

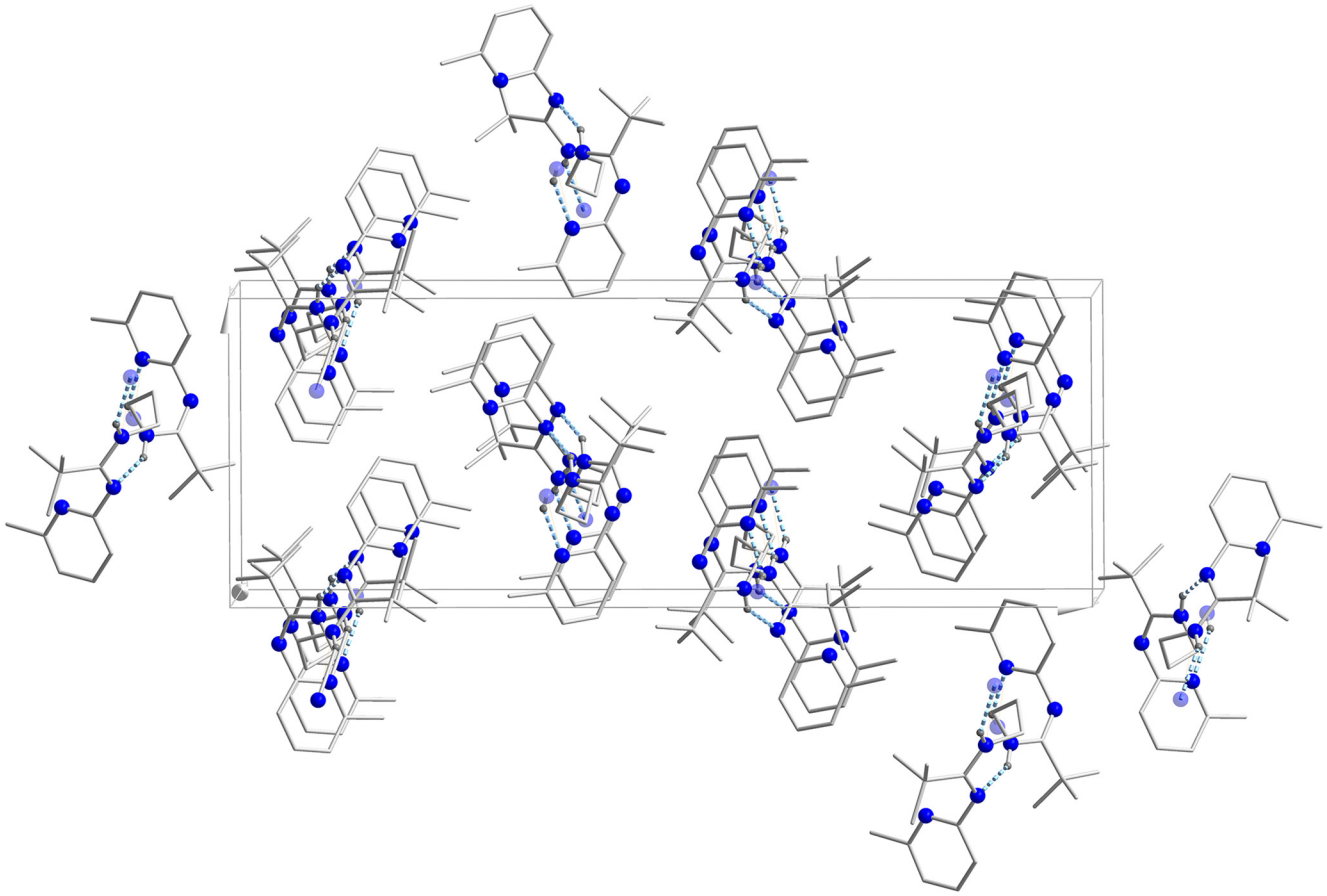

Figure S3: Crystal packing diagram and unit cell of $\mathbf{L^2}H_2$. Hydrogen atoms except for NH functionalities have been omitted for clarity.

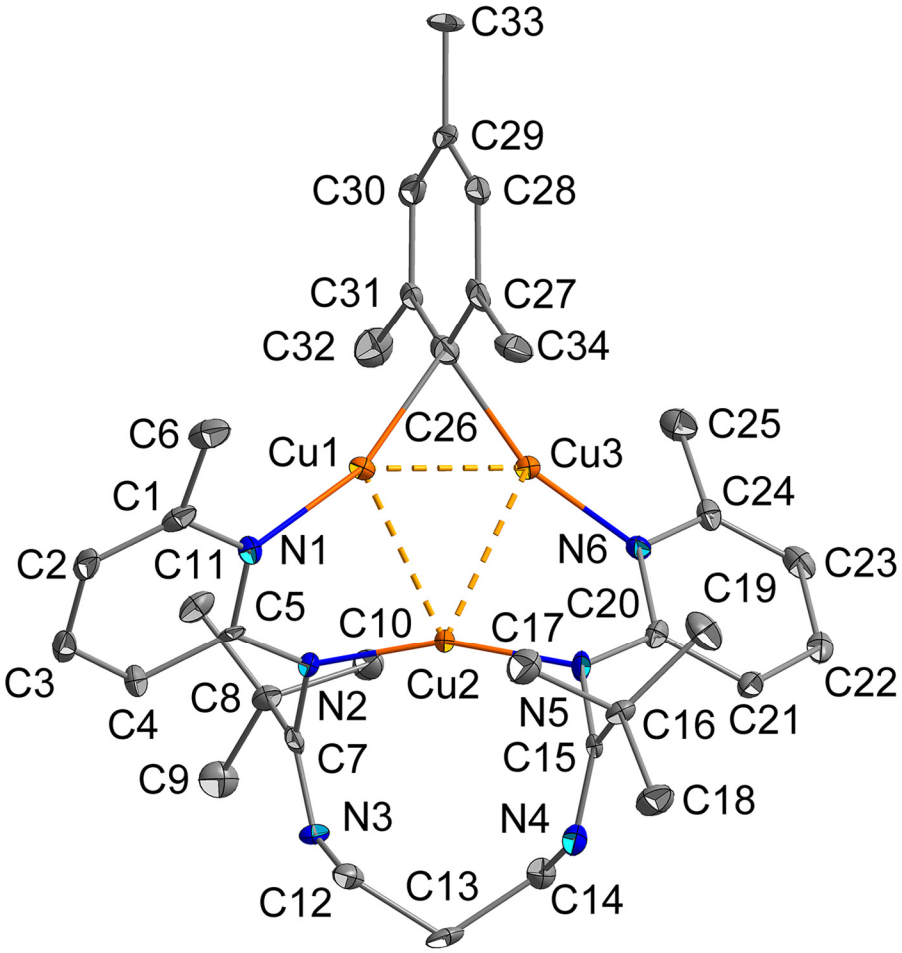

Figure S4: Molecular structure of **1** showing ellipsoids with anisotropic displacement factors of 50% probability. Hydrogen atoms have been omitted for clarity. Selected interatomic distances (Å), bond angles (deg), and torsion angles (deg): Cu1···Cu3 2.4554(11), Cu1···Cu2 2.6002(14), Cu3···Cu2 2.6006(14), Cu1–C26 1.990(8), Cu3–C26 1.981(9), Cu1–N1 1.930(7), Cu3–N6 1.919(7), Cu2–N2 1.860(7), Cu2–N5 1.869(8), C13–C12 1.524(13), C12–N3 1.470(10), N3–C7 1.275(12), C7–N2 1.419(11), N2–C5 1.342(10), C5–N1 1.365(12), N1–C1 1.364(10), C13–C14 1.534(14), C14–N4 1.460(11), N4–C15 1.279(12), C15–N5 1.415(11), N5–C20 1.346(10), C20–N6 1.373(11), N6–C24 1.374(10), Cu1–Cu3–Cu2 61.82(5), Cu1–Cu2–Cu3 56.34(3), Cu1–C26–Cu3 76.4(3), Cu1–C26–C27 110.9(5), Cu1–C26–C31 116.8(7), N1–Cu1–C26 161.8(4), N6–Cu3–C26 161.6(3), N2–Cu2–N5 159.7(3), C13–C12–N3 110.1(6), C12–N3–C7 121.1(7), N3–C7–N2 125.6(7), C7–N2–C5 121.2(7), N2–C5–N1 116.2(8), C5–N1–C1 119.8(8), C13–C14–N4 110.4(6), C14–N4–C15 119.9(7), N4–C15–N5 126.0(7), C15–N5–C20 122.1(7), N5–C20–N6 116.2(8), C20–N6–C24 119.3(7), N1–Cu1–C26–C27 79.1(12),[S24] N1–Cu1–C26–C31 –60.5(14),[S24] N6–Cu3–C26–C27 –64.2(13),[S24] N6–Cu3–C26–C31 75.1(12),[S24] N1–Cu1–Cu2–N2 34.5(3),[S24] N6–Cu3–Cu2–N5 34.7(3),[S24] C13–C12–N3–C7 –128.3(8), C12–N3–C7–N2 5.1(13), N3–C7–N2–C5 –98.5(10), C7–N2–C5–N1 –169.2(7), N2–C5–N1–C1 –174.1(7), C13–C14–N4–C15 –129.3(9), C14–N4–C15–N5 4.1(13), N4–C15–N5–C20 –94.4(11), C15–N5–C20–N6 –170.9(7), N5–C20–N6–C24 –174.8(7).

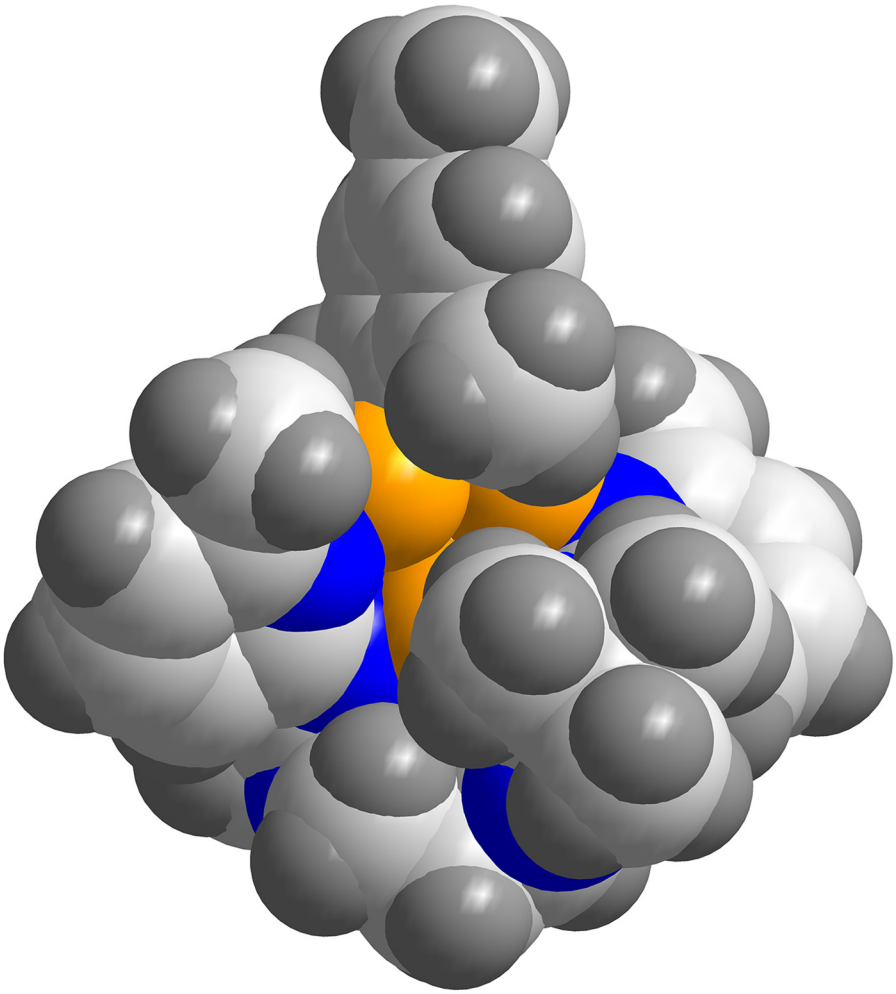

Figure S5: Space filling representation of the molecular structure of **1**.

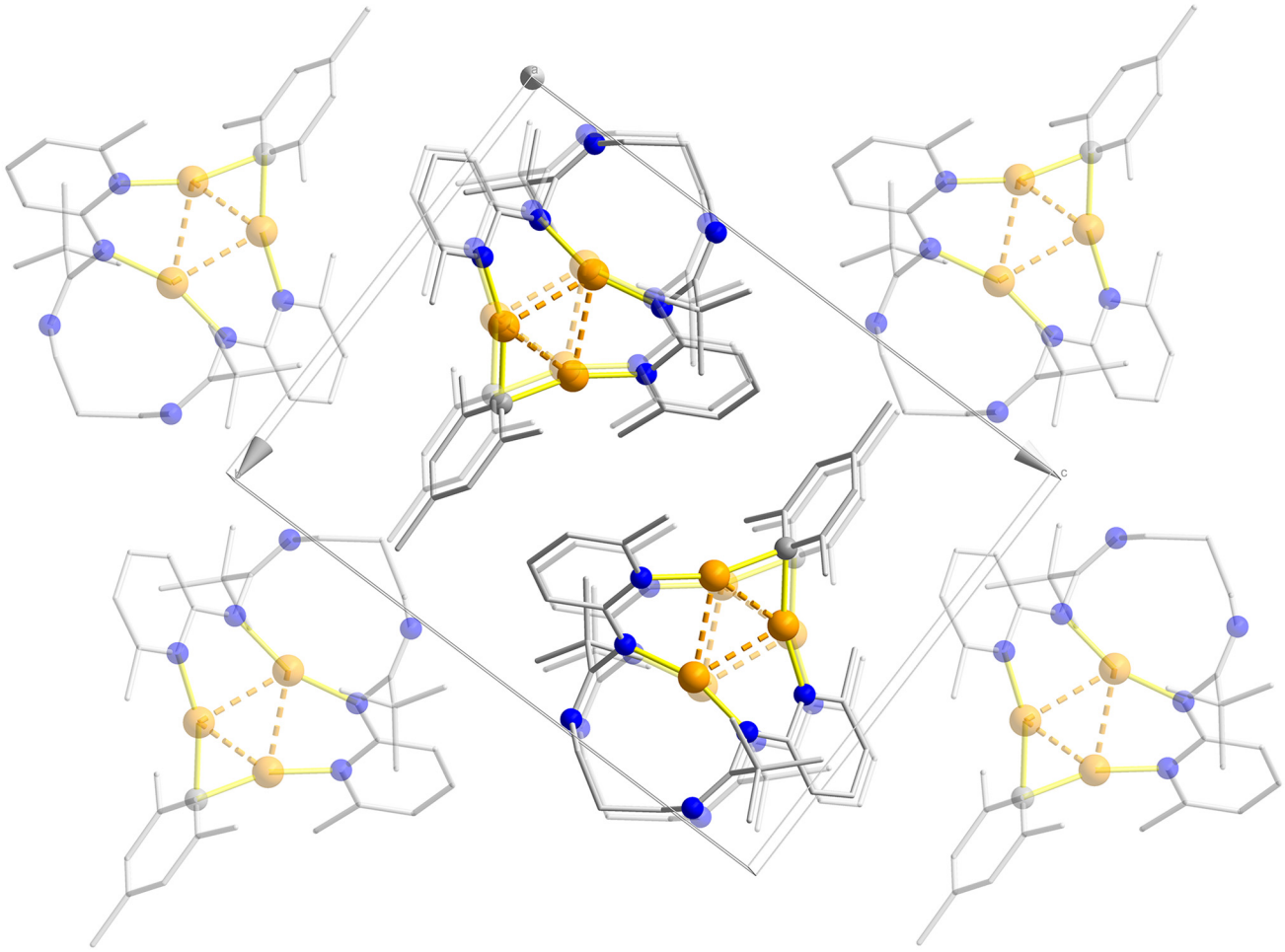

Figure S6: Crystal packing diagram and unit cell of **1**. Hydrogen atoms have been omitted for clarity.

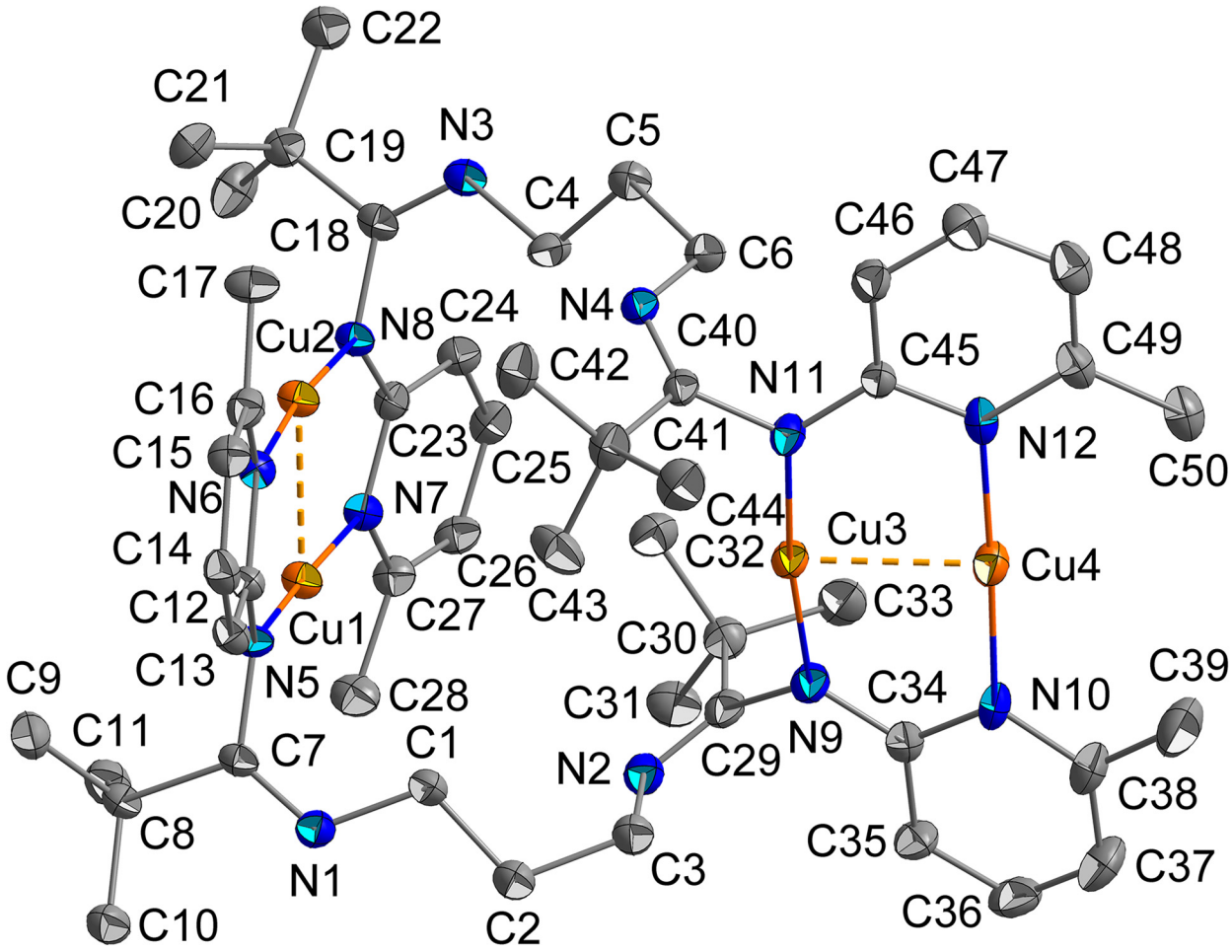

Figure S7: Molecular structure of **2** showing ellipsoids with anisotropic displacement factors of 50% probability. Hydrogen atoms have been omitted for clarity. Selected interatomic distances (Å), bond angles (deg), and torsion angles (deg): Cu2···Cu1 2.4477(8), Cu4···Cu3 2.4493(9), Cu2···Cu3 6.3833(8),[S24] Cu1···Cu3 6.4174(8),[S24] Cu2–N8 1.861(3), Cu2–N6 1.891(3), Cu1–N7 1.884(3), Cu1–N5 1.869(3), C2–C1 1.519(6), C1–N1 1.463(6), N1–C7 1.263(5), C7–N5 1.438(5), N5–C12 1.355(5), C12–N6 1.370(5), N6–C16 1.356(5), C2–C3 1.532(6), C3–N2 1.464(6), N2–C29 1.262(6), C29–N9 1.430(6), N9–C34 1.340(6), C34–N10 1.376(6), N10–C38 1.358(6), N8–Cu2–Cu1 87.07(11), N6–Cu2–Cu1 89.53(11), N8–Cu2–N6 173.18(15), Cu2–N8–C23 124.0(3), Cu2–N6–C12 120.2(3), Cu2–N8–C18 116.9(3), Cu2–N6–C16 119.5(3), N7–Cu1–Cu2 89.50(11), N5–Cu1–Cu2 87.10(10), N7–Cu1–N5 173.78(15), Cu1–N7–C23 120.0(3), Cu1–N5–C12 123.9(3), Cu1–N7–C27 119.9(3), Cu1–N5–C7 117.0(2), C2–C1–N1 111.6(3), C1–N1–C7 118.9(4), N1–C7–N5 124.0(4), C7–N5–C12 118.5(3), N5–C12–N6 118.3(4), C12–N6–C16 120.0(4), C2–C3–N2 108.1(4), C3–N2–C29 119.8(4), N2–C29–N9 126.5(4), C29–N9–C34 117.5(4), N9–C34–N10 118.4(4), C34–N10–C38 120.2(4), Cu4–N10 1.905(4), Cu4–N12 1.911(4), Cu3–N9 1.864(4), Cu3–N11 1.861(4), C5–C6 1.525(6), C6–N4 1.460(5), N4–C40 1.263(6), C40–N11 1.429(5), N11–C45 1.348(5), C45–N12 1.363(5), N12–C49 1.364(6), C5–C4 1.512(6), C4–N3 1.467(5), N3–C18 1.272(6), C18–N8 1.431(5), N8–C23 1.351(5), C23–N7 1.377(5),

N7–C27 1.371(5), N10–Cu4–Cu3 88.24(11), N12–Cu4–Cu3 89.61(11), N10–Cu4–N12 177.85(15), Cu4–N10–C34 119.7(3), Cu4–N12–C45 118.5(3), Cu4–N10–C38 119.9(3), Cu4–N12–C49 120.3(3), N9–Cu3–Cu4 87.29(12), N11–Cu3–Cu4 86.10(11), N9–Cu3–N11 173.30(16), Cu3–N9–C34 124.0(3), Cu3–N11–C45 125.2(3), Cu3–N9–C29 118.1(3), Cu3–N11–C40 116.6(3), C5–C6–N4 110.1(4), C6–N4–C40 119.1(4), N4–C40–N11 124.2(4), C40–N11–C45 117.8(3), N11–C45–N12 118.8(4), C45–N12–C49 121.1(4), C5–C4–N3 110.1(3), C4–N3–C18 118.6(4), N3–C18–N8 124.7(4), C18–N8–C23 118.1(3), N8–C23–N7 117.8(4), C23–N7–C27 119.4(3), N8–Cu2–Cu1–N7 1.7(1),[S24] N8–Cu2–Cu1–N5 176.5(1),[S24] N7–Cu1–Cu2–N6 – 172.4(1),[S24] N10–Cu4–Cu3–N9 –11.3(2),[S24] N10–Cu4–Cu3–N11 169.8(2),[S24] N9–Cu3–Cu4–N12 168.8(2)[S24].

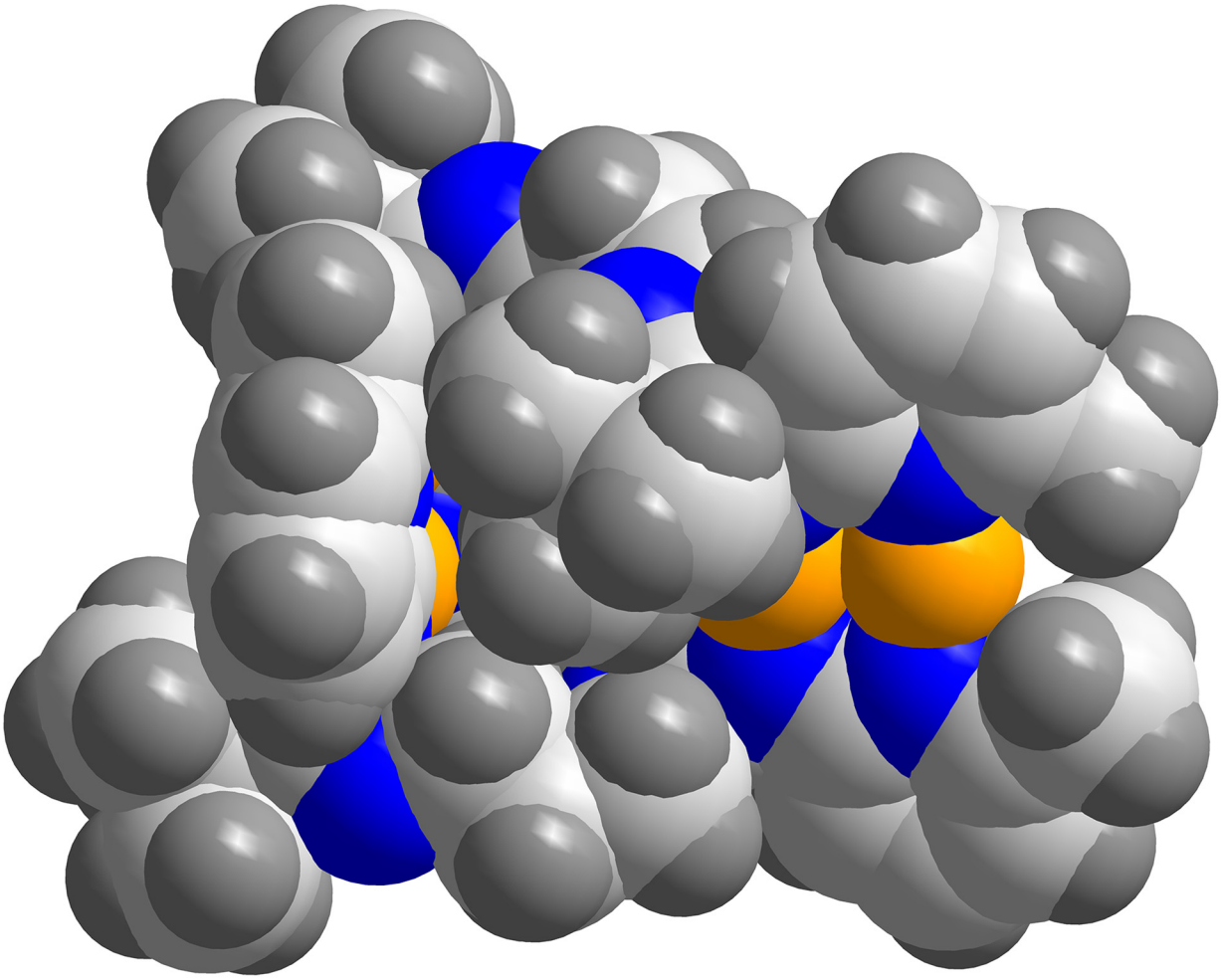

Figure S8: Space filling representation of the molecular structure of **2**.

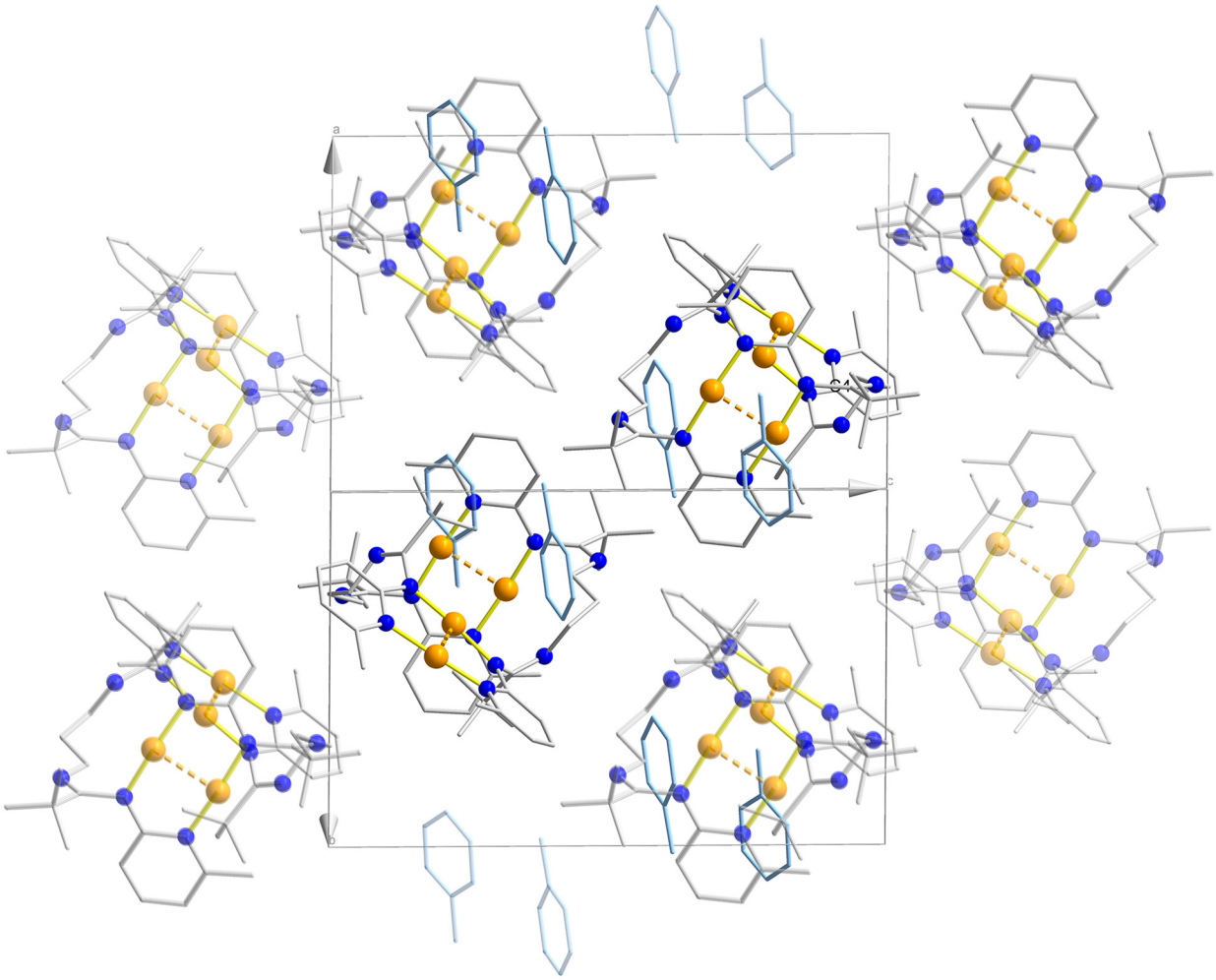

Figure S9: Crystal packing diagram and unit cell of **2**·C_7H_8. Hydrogen atoms have been omitted for clarity.

Table S1. Crystal data and refinement details for $\mathbf{L^2}H_2$, **1**, and **2**·2C_7H_8.

	$\mathbf{L^2}H_2$	**1**	**2**·2C_7H_8
Empirical formula	$C_{25}H_{38}N_6$	$C_{34}H_{47}N_6Cu_3$	$C_{50}H_{72}N_{12}Cu_4$·2C_7H_8
M_r	422.61	730.39	1279.62
Crystal size [mm]	0.052 × 0.061 × 0.401	0.28 × 0.10 × 0.03	0.061 × 0.082 × 0.112
Crystal system	orthorhombic	triclinic	triclinic
Space group	$P\,2_1\,2_1\,2_1$	$P\,\bar{1}$	$P\,\bar{1}$
a [Å], α [°]	7.9087(2), 90	8.6701(10), 88.712(4)	12.4666(3), 91.7413(14)
b [Å], β [°]	10.6914(3), 90	12.8540(15), 86.426(4)	15.4770(4), 90.1643(14)
c [Å], γ [°]	29.7770(8), 90	15.977(2), 71.457(4)	17.6182(4), 110.6086(13)
V [Å^3]	2517.80(12)	1684.8(3)	3180.01(14)
Z	4	2	2
$\rho_{calcd.}$ [g cm^{-3}]	1.115	1.440	1.336
F(000)	920	760	1344
μ [mm^{-1}]	0.526	1.909	1.872
T_{max}/T_{min}	0.9730 / 0.8170	0.429 / 0.371	0.8940 / 0.8180
hkl range	–9 +8, –13 +12, –21 +37	±10, ±15, ±19	±15, ±18, ±21
θ range [°]	2.97 – 74.61	2.482 – 25.853	3.05 – 68.50
Measured refl.	15607	19251	74123
Unique refl. [R_{int}]	5099 [0.0342]	19251 [0.0786]	11687 [0.0707]
Data / restr. / param.	5099 / 0 / 296	19251 / 0 / 400	11687 / 0 / 739
Goodness-of-fit	1.154	1.040	1.172
$R1$ (I>2σ(I))	0.0379	0.0682	0.0669
$wR2$ (all data)	0.1132	0.2074	0.1464
Resid. electron dens. [e Å^{-3}]	0.305 / –0.358	1.040 / –1.063	1.162 / –0.555

Table S2: Key crystallographic interatomic distances of $\mathbf{L^2}H_2$, **1**, and **2**·2C_7H_8.

	$\mathbf{L^2}H_2$	**1**	**2**·2C_7H_8	
	bond/angle [Å]/[°]			
Cu···Cu	-	2.4554(11)	2.4477(8)	
		2.6002(14)	2.4493(9)	
		2.6006(14)		
Cu–C	-	1.990(8)	-	
		1.981(9)		
Cu–N	-	1.930(7)	1.861(3)	1.905(4)
		1.919(7)	1.891(3)	1.911(4)
		1.860(7)	1.884(3)	1.864(4)
		1.869(8)	1.869(3)	1.861(4)
CH_2–CH_2	1.531(3)	1.524(13)	1.519(6)	1.525(6)
	1.523(3)	1.534(14)	1.532(6)	1.512(6)
CH_2–N	1.458(3)	1.470(10)	1.463(6)	1.460(5)
	1.461(2)	1.460(11)	1.464(6)	1.467(5)
$C_{amidine}$–N(CH_2)	1.361(3)	1.275(12)	1.263(5)	1.263(6)
	1.348(3)	1.279(12)	1.262(6)	1.272(6)
$C_{amidine}$–N($C_{Py\text{-}2}$)	1.287(3)	1.419(11)	1.438(5)	1.429(5)
	1.294(3)	1.415(11)	1.430(6)	1.431(5)
$N_{amidine}$–$C_{Py\text{-}2}$	1.393(3)	1.342(10)	1.355(5)	1.348(5)
	1.401(3)	1.346(10)	1.340(6)	1.351(5)
$C_{Py\text{-}2}$–N_{Ar}	1.344(3)	1.365(12)	1.370(5)	1.363(5)
	1.343(3)	1.373(11)	1.376(6)	1.377(5)

Table S3: Key crystallographic angles of $\mathbf{L^2}H_2$, **1**, and **2**·2C_7H_8.

	$\mathbf{L^2}H_2$	**1**	**2**·2C_7H_8	
		bond/angle [Å]/[°]		
N–Cu–C	-	161.8(4) 161.6(3)	-	
N–Cu–N	-	159.7(3)	173.18(15) 173.78(15)	177.85(15) 173.30(16)
CH_2–N–$C_{amidine}$	126.34(18) 124.31(18)	121.1(7) 119.9(7)	118.9(4) 119.8(4)	119.1(4) 118.6(4)
N–$C_{amidine}$–N	127.69(19) 118.02(19)	125.6(7) 126.0(7)	124.0(4) 126.5(4)	124.2(4) 124.7(4)
$C_{amidine}$–N–$C_{Py\text{-}2}$	126.01(17) 127.41(19)	121.2(7) 122.1(7)	118.5(3) 117.5(4)	117.8(3) 118.1(3)
$N_{amidine}$–$C_{Py\text{-}2}$–N_{Ar}	117.79(18) 119.5(2)	116.2(8) 116.2(8),	118.3(4) 118.4(4)	118.8(4) 117.8(4)

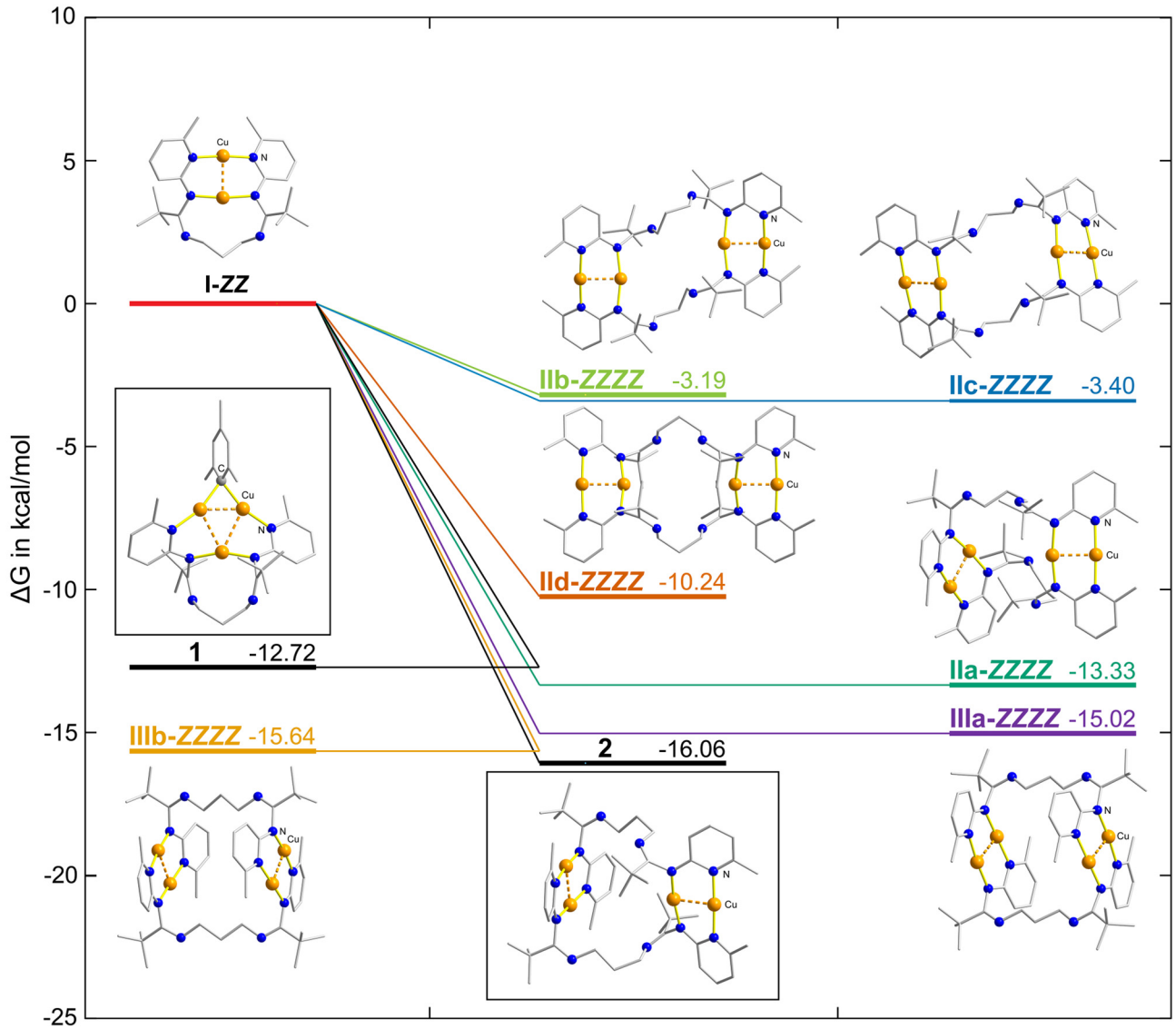

Figure S10: Free energy diagram of the computational structures **I-*ZZ***, **IIa–d-*ZZZZ***, **IIIa-*ZZZZ***, **IIIb-*ZZZZ***, and computationally geometry-optimized structures of **1** and **2** (PBE1PBE). The free energy values are relative to **I-*ZZ***. Hydrogen atoms have been omitted for clarity.

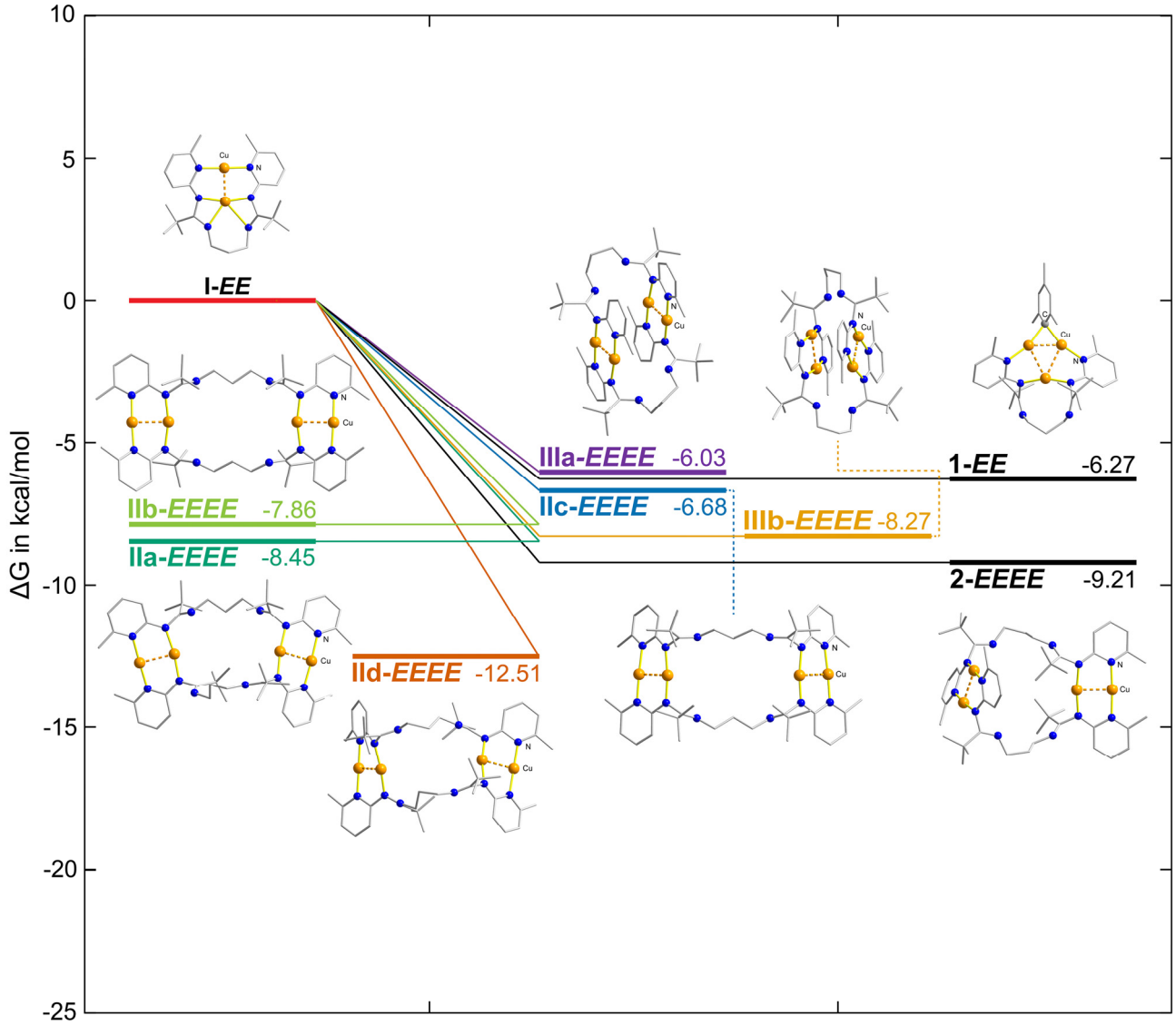

Figure S11: Free energy diagram of the computational structures **I-*EE***, **IIa**–**d-*EEEE***, **IIIa-*EEEE***, **IIIb-*EEEE***, **1-*EE***, and **2-*EEEE*** (PBE1PBE). The free energy values are relative to **I-*EE***. Hydrogen atoms have been omitted for clarity.

Table S4: Calculated free energies of computational structures.

	[kcal·mol^{-1}]		
1-*ZZ*	-4123082.92	**1-*EE***	-4123060.81
2-*ZZZZ*	-5749618.51	**2-*EEEE***	-5749580.36
I-*ZZ*	-2874801.22	**I-*EE***	-2874785.57
IIa-*ZZZZ*	-5749615.78	**IIa-*EEEE***	-5749579.60
IIb-*ZZZZ*	-5749605.64	**IIb-*EEEE***	-5749579.00
IIc-*ZZZZ*	-5749605.85	**IIc-*EEEE***	-5749577.82
IId-*ZZZZ*	-5749612.68	**IId-*EEEE***	-5749583.65
IIIa-*ZZZZ*	-5749617.47	**IIIa-*EEEE***	-5749577.17
IIIb-*ZZZZ*	-5749618.09	**IIIb-*EEEE***	-5749579.41
$\mathbf{L^2}H_2$	-817002.16	MesH	-219384.09

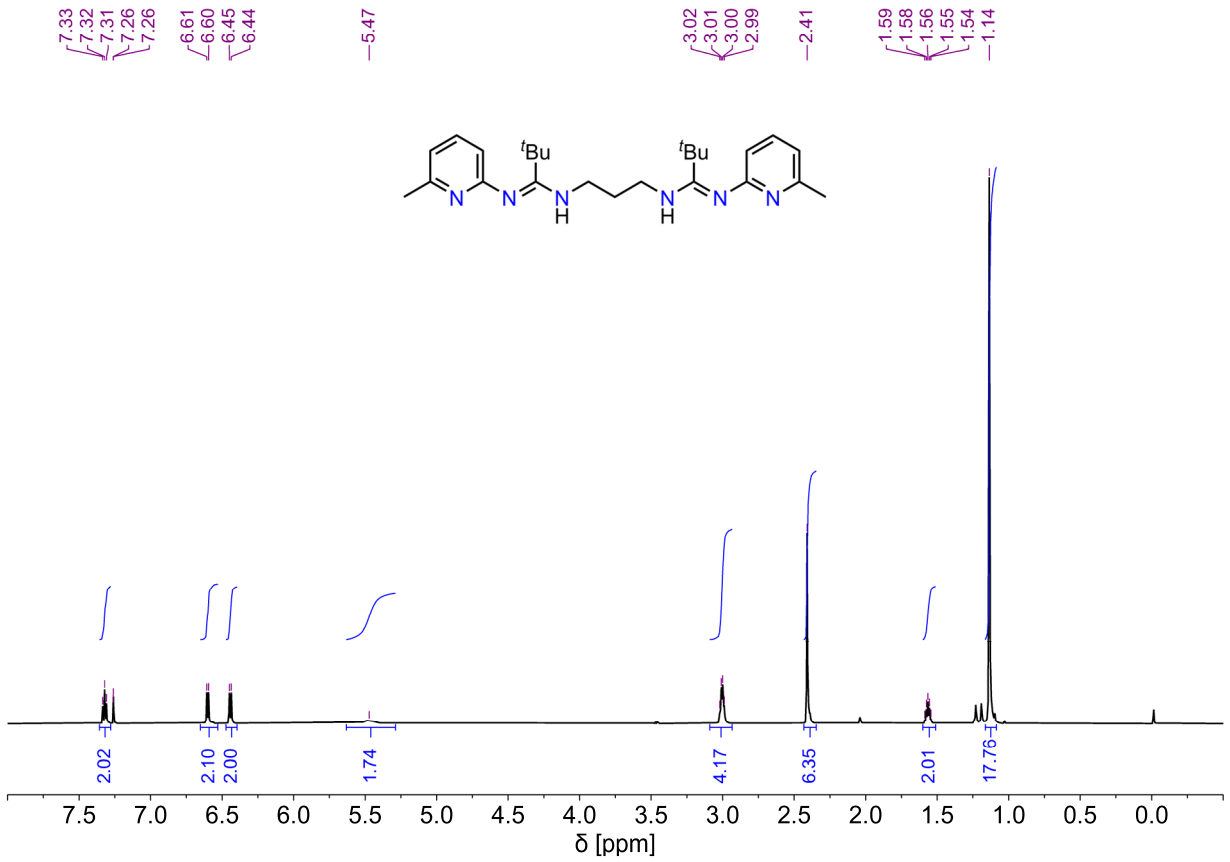

Figure S12: ^{1}H NMR spectrum of $\mathbf{L^2}H_2$ ($CDCl_3$, 600.2 MHz).

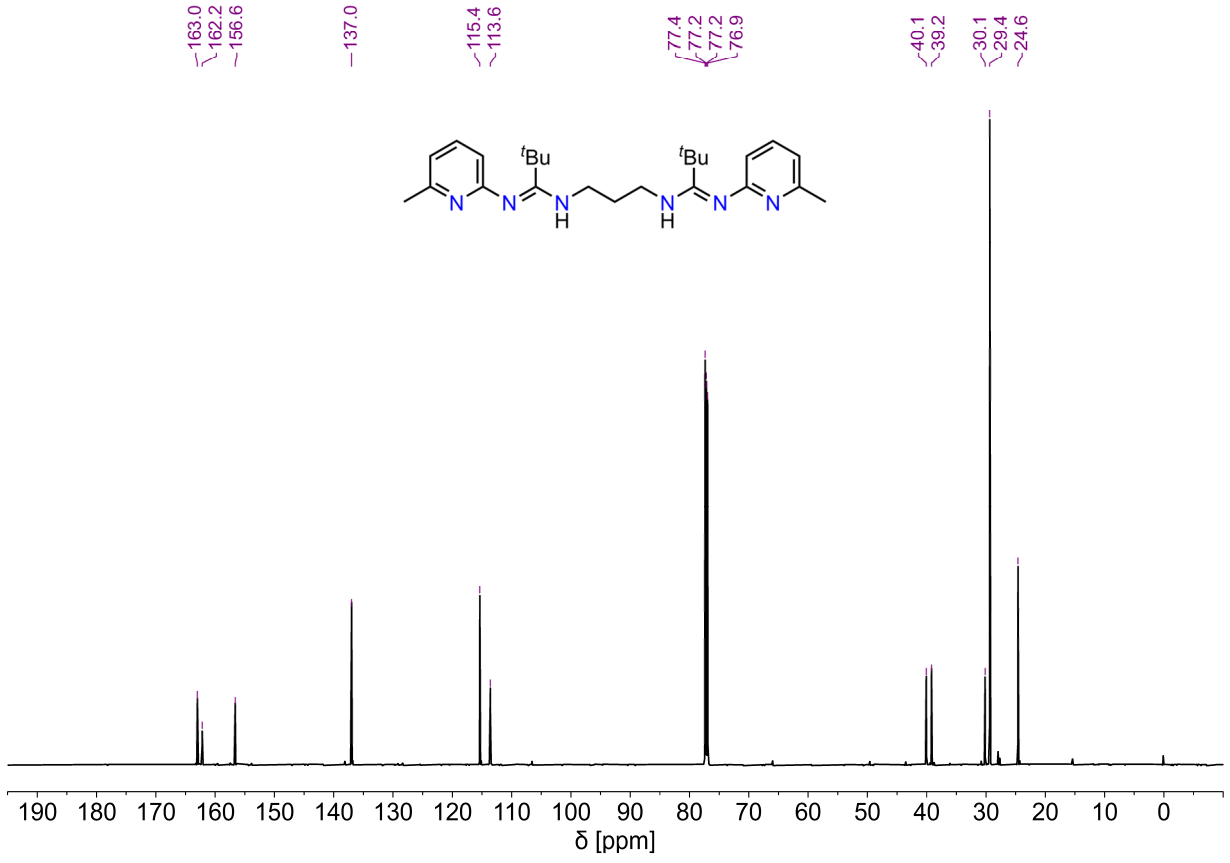

Figure S13: $^{13}C\{^{1}H\}$ NMR spectrum of $\mathbf{L^2}H_2$ ($CDCl_3$, 150.9 MHz).

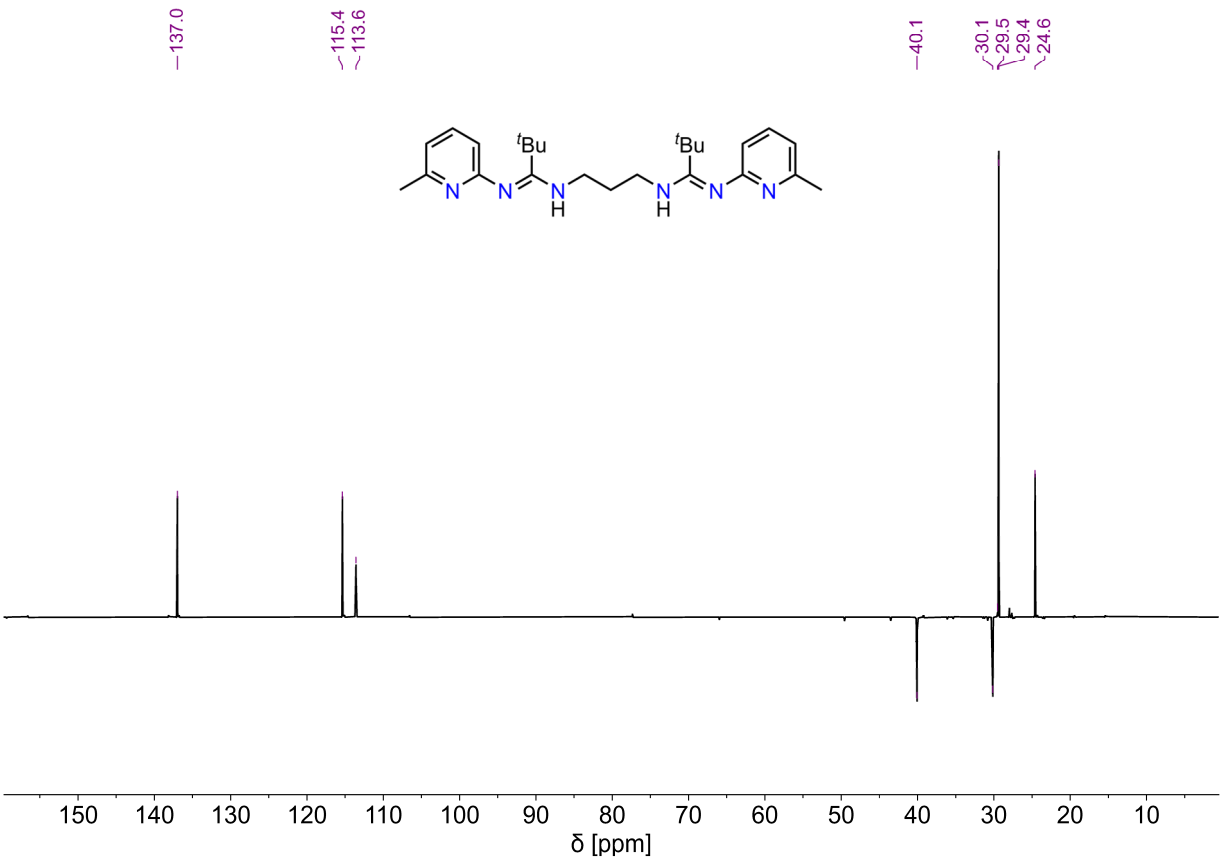

Figure S14: DEPT 135 NMR spectrum of $\mathbf{L^2}H_2$ ($CDCl_3$, 150.9 MHz).

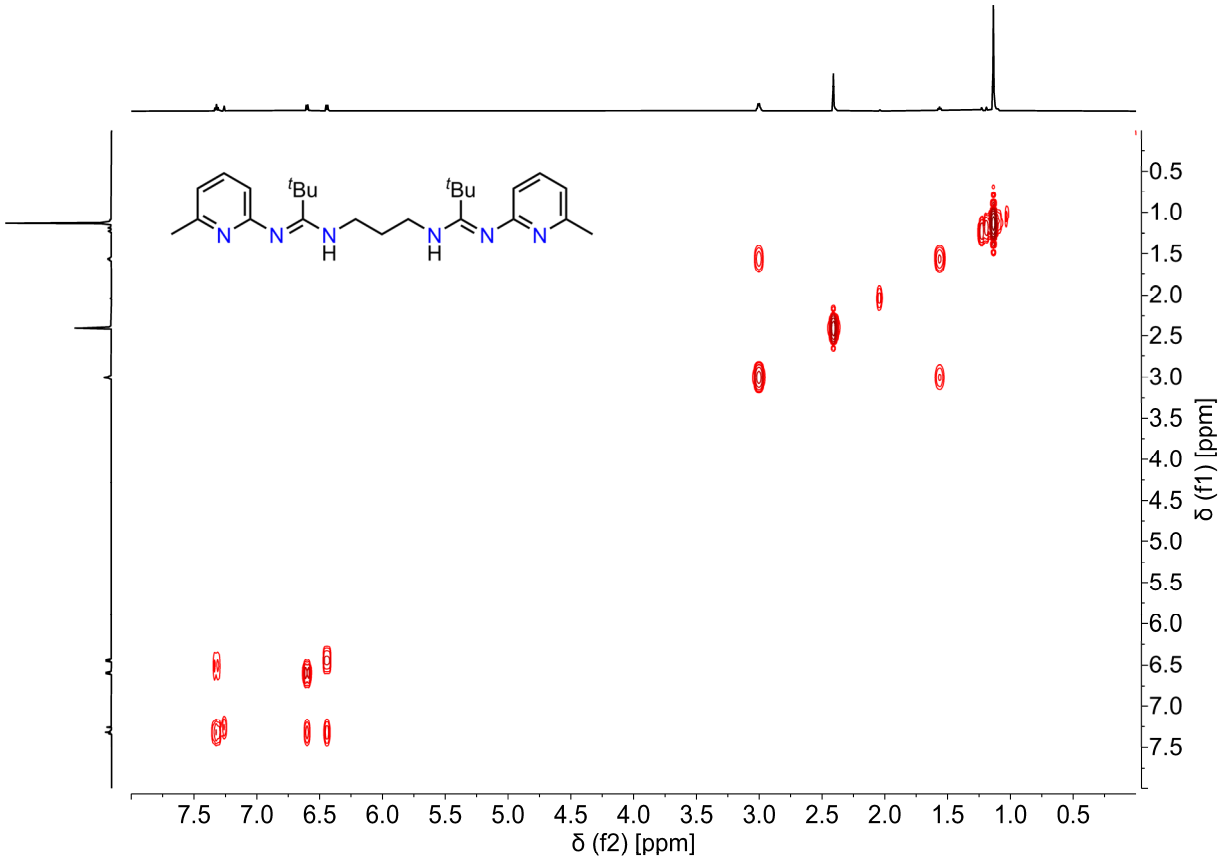

Figure S15: (^{1}H, ^{1}H)-COSY NMR spectrum of $\mathbf{L^2}H_2$ ($CDCl_3$, 600.2 MHz).

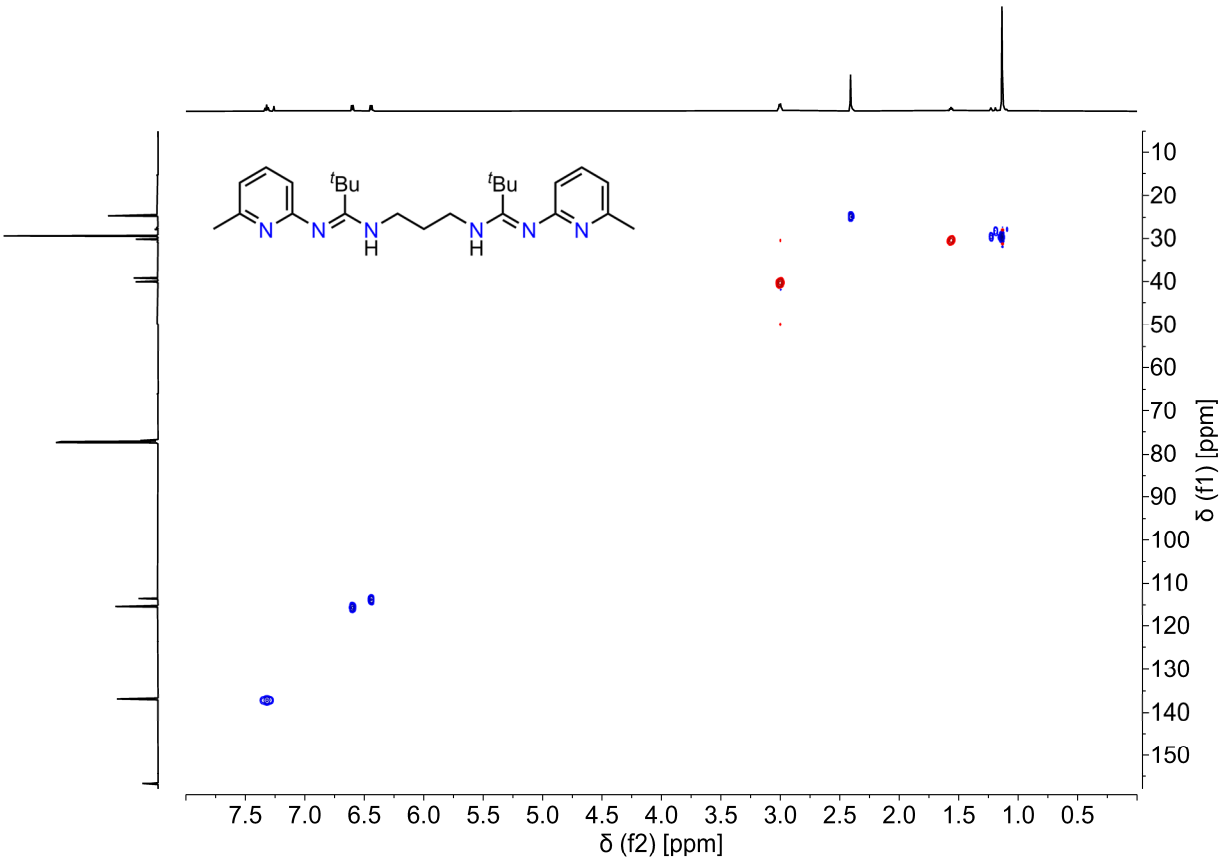

Figure S16: (^{1}H, ^{13}C)-HSQC NMR spectrum of **L²**H$_2$ (CDCl$_3$, 150.9 MHz).

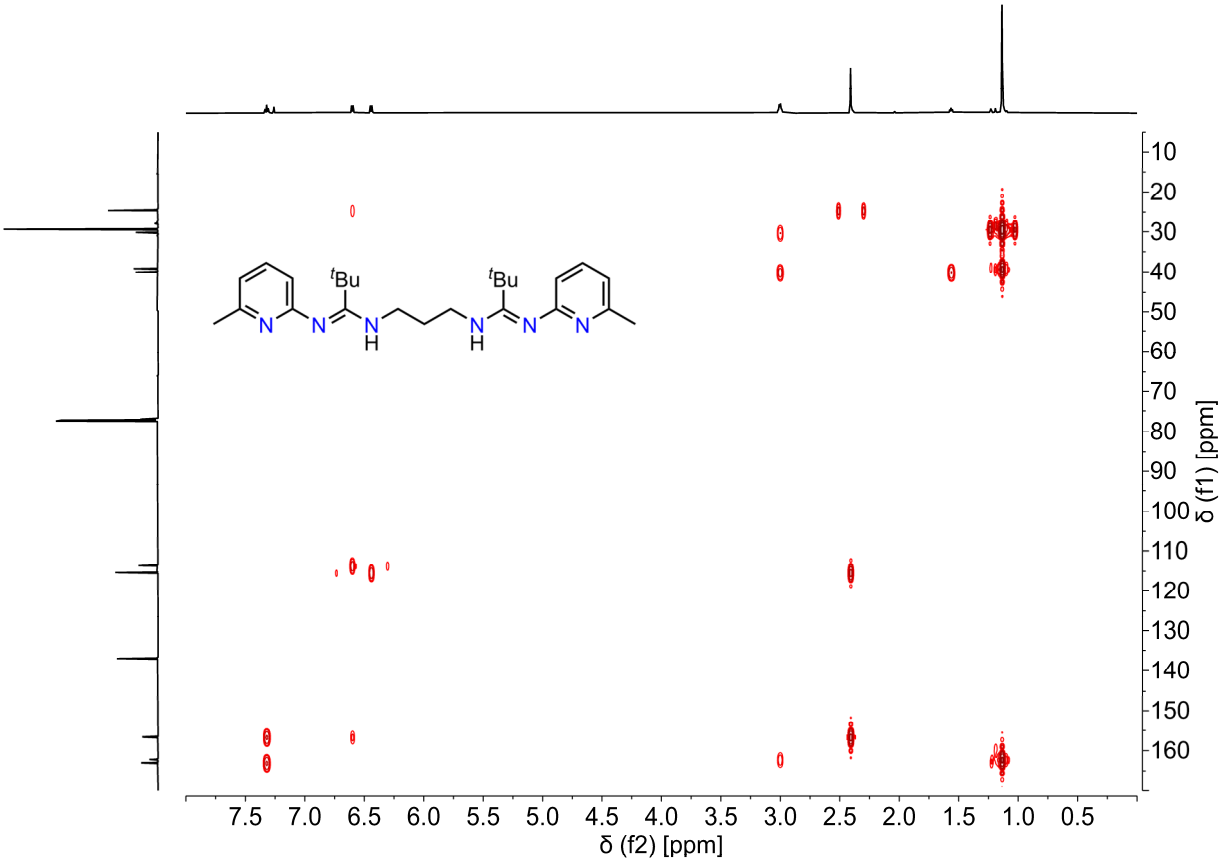

Figure S17: (^{1}H, ^{13}C)-HMBC NMR spectrum of **L²**H$_2$ (CDCl$_3$, 150.9 MHz).

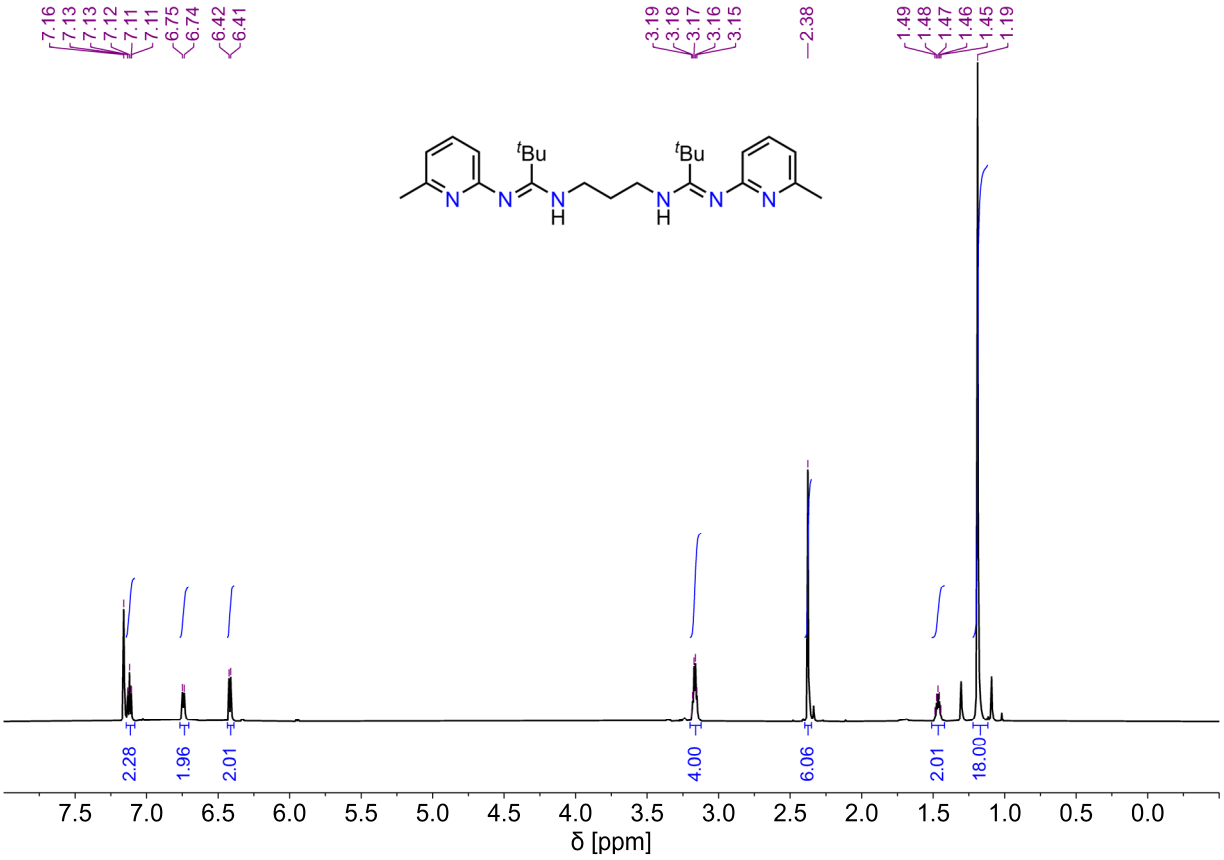

Figure S18: ^{1}H NMR spectrum of $\mathbf{L^2}H_2$ (C_6D_6, 600.2 MHz).

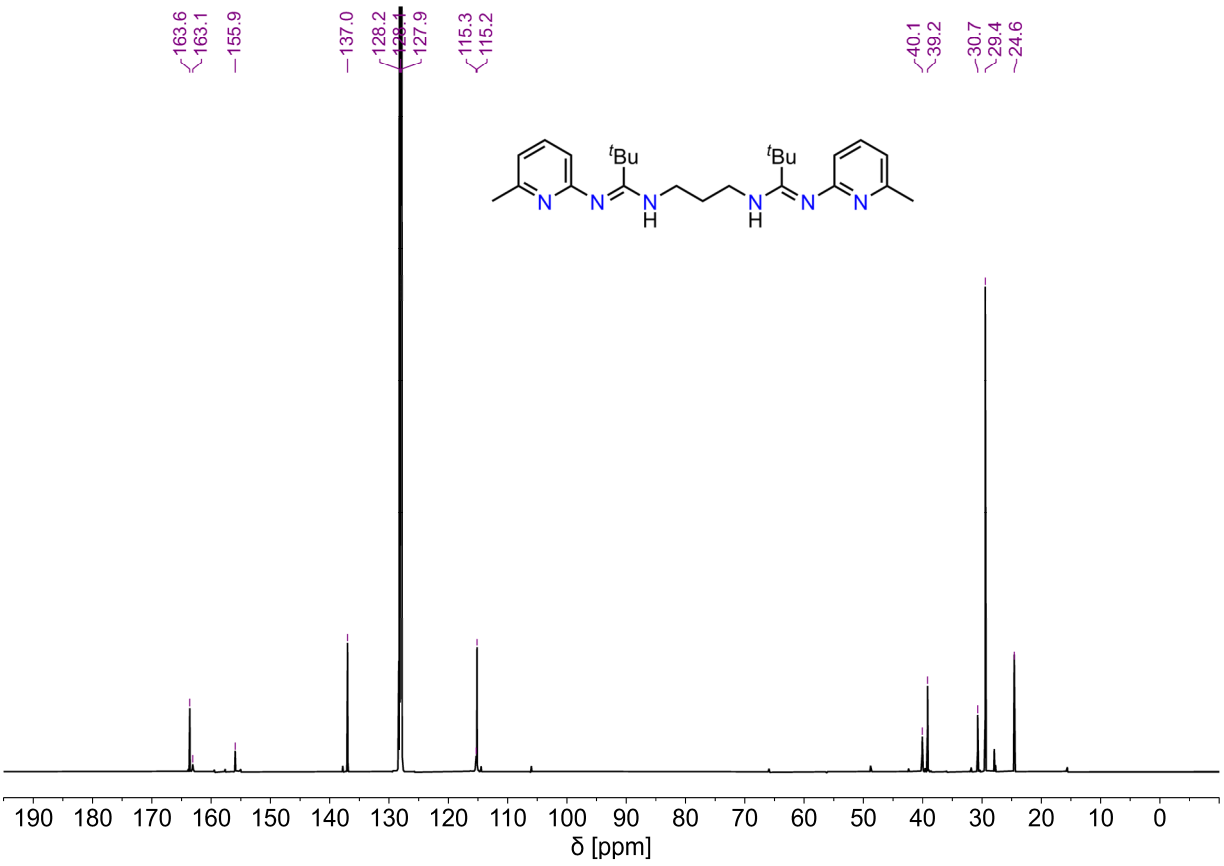

Figure S19: $^{13}C\{^{1}H\}$ NMR spectrum of $\mathbf{L^2}H_2$ (C_6D_6, 150.9 MHz).

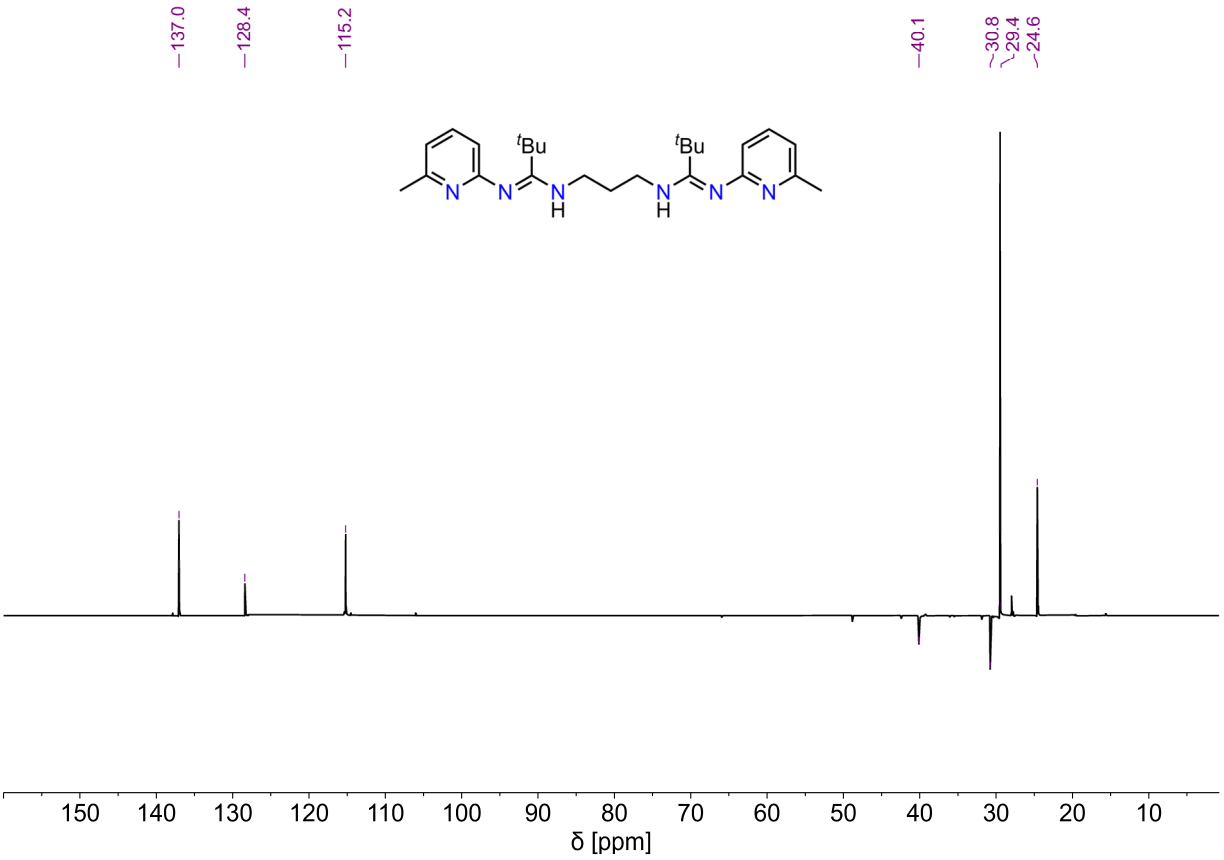

Figure S20: DEPT 135 NMR spectrum of $\mathbf{L^2}H_2$ (C_6D_6, 150.9 MHz).

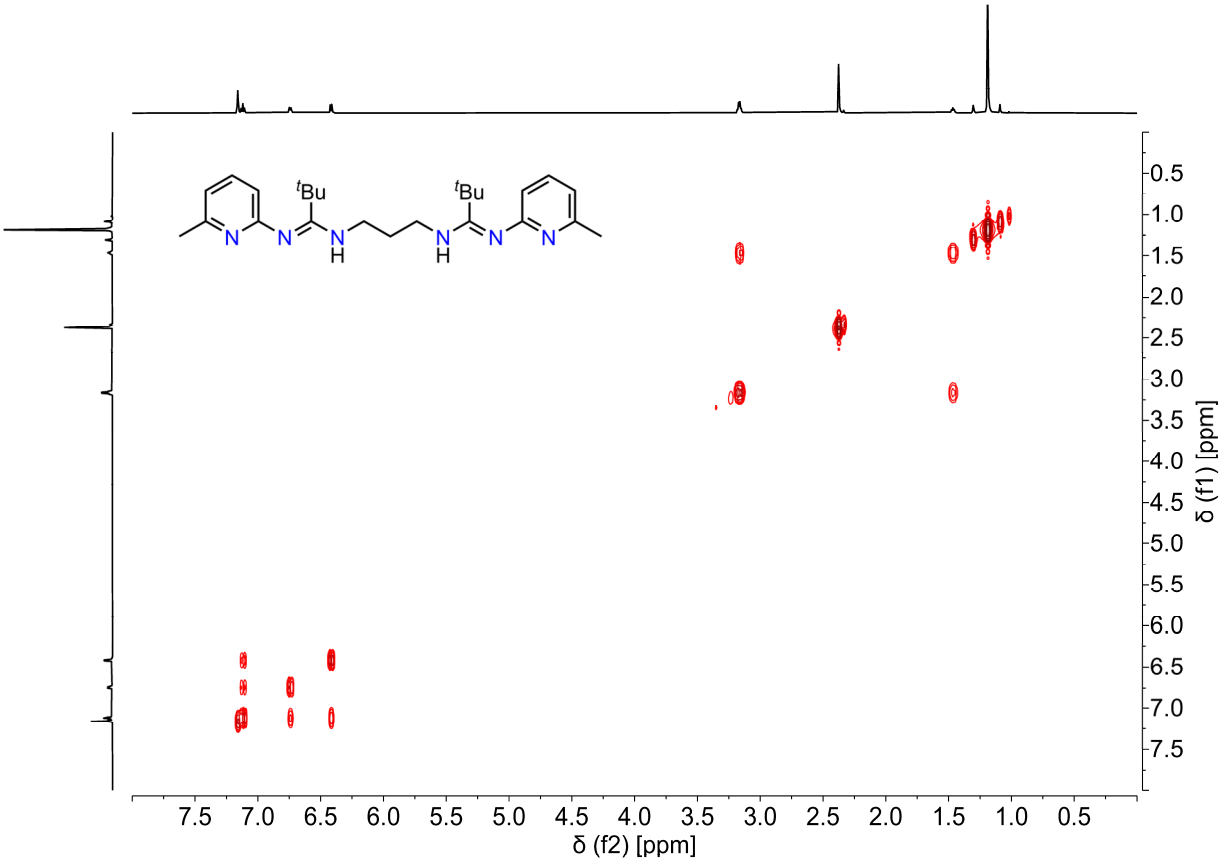

Figure S21: (^{1}H, ^{1}H)-COSY NMR spectrum of $\mathbf{L^2}H_2$ (C_6D_6, 600.2 MHz).

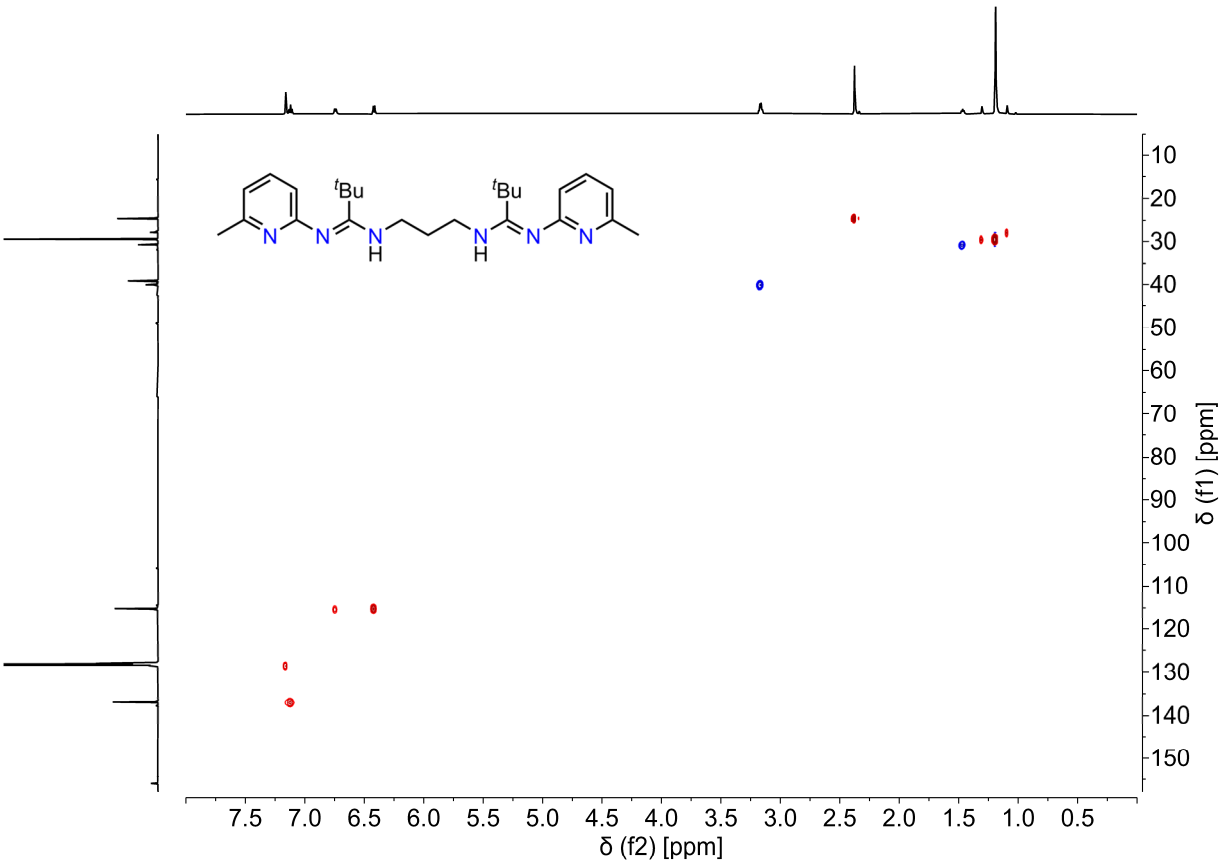

Figure S22: (^{1}H, ^{13}C)-HSQC NMR spectrum of **L²**H$_2$ (C$_6$D$_6$, 150.9 MHz).

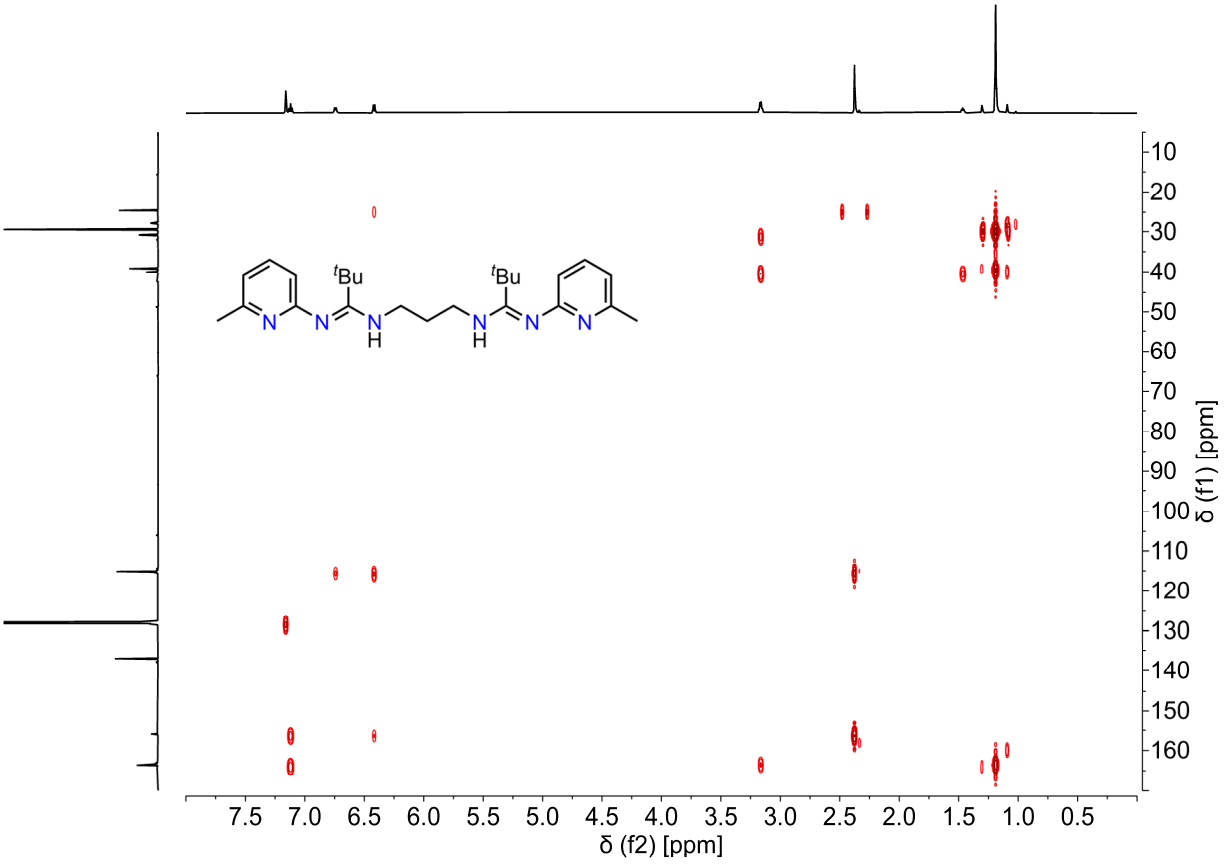

Figure S23: (^{1}H, ^{13}C)-HMBC NMR spectrum of **L²**H$_2$ (C$_6$D$_6$, 150.9 MHz).

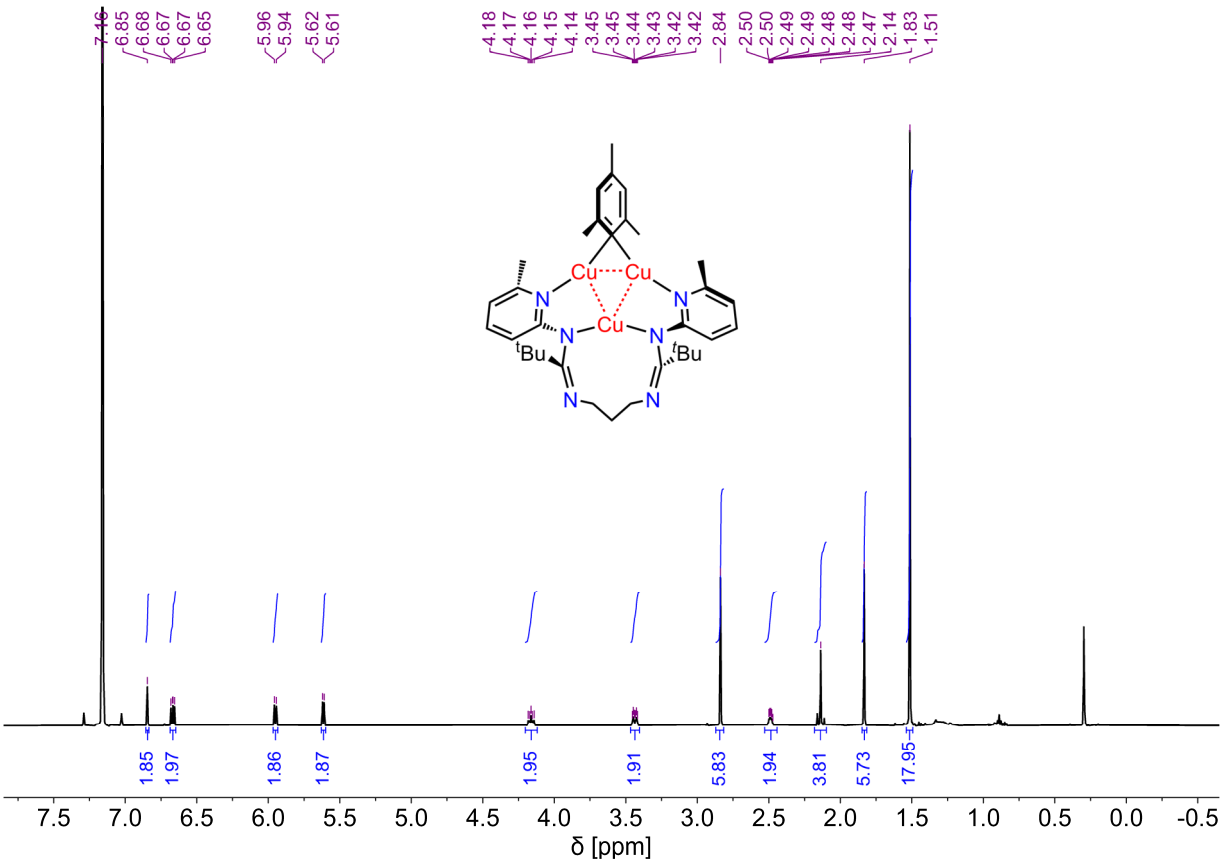

Figure S24: ^{1}H NMR spectrum of **1** (C_6D_6, 600.2 MHz).

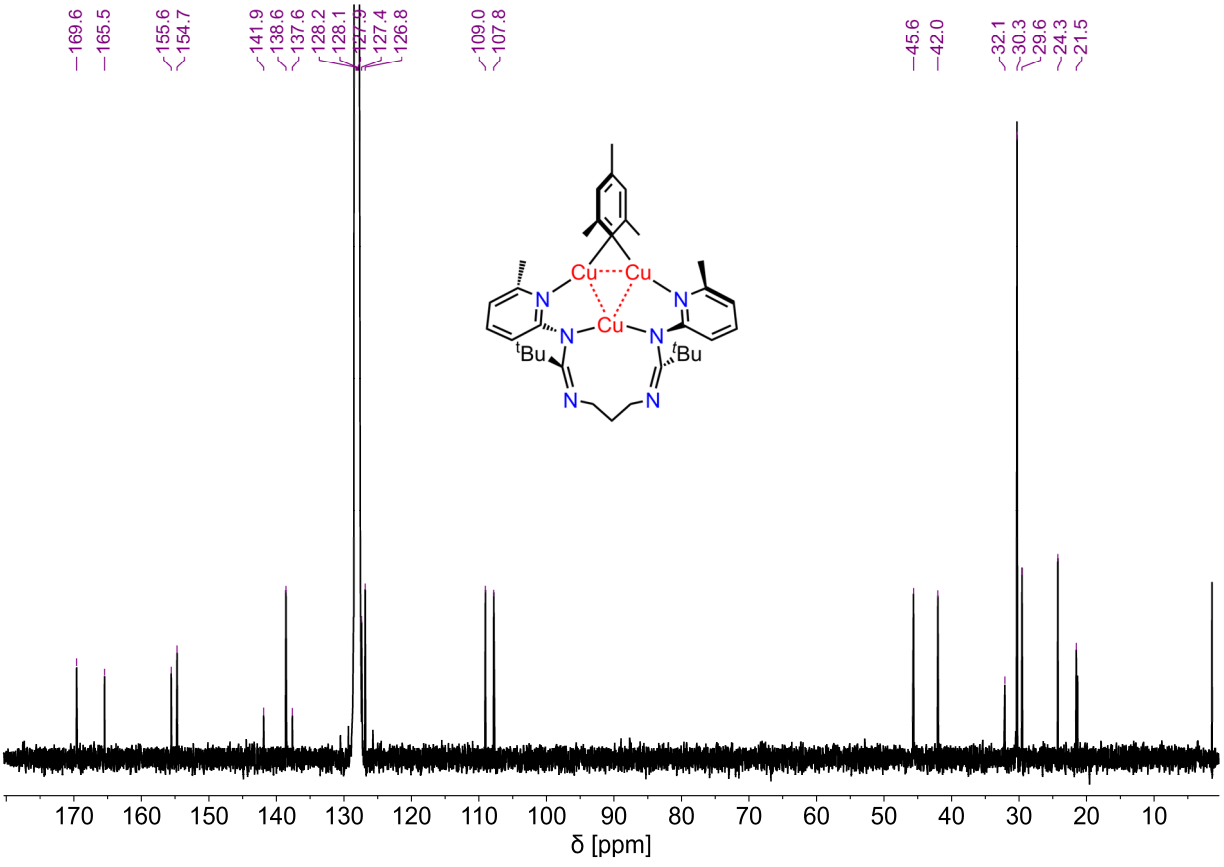

Figure S25: ^{13}C{^{1}H} NMR spectrum of **1** (C_6D_6, 150.9 MHz).

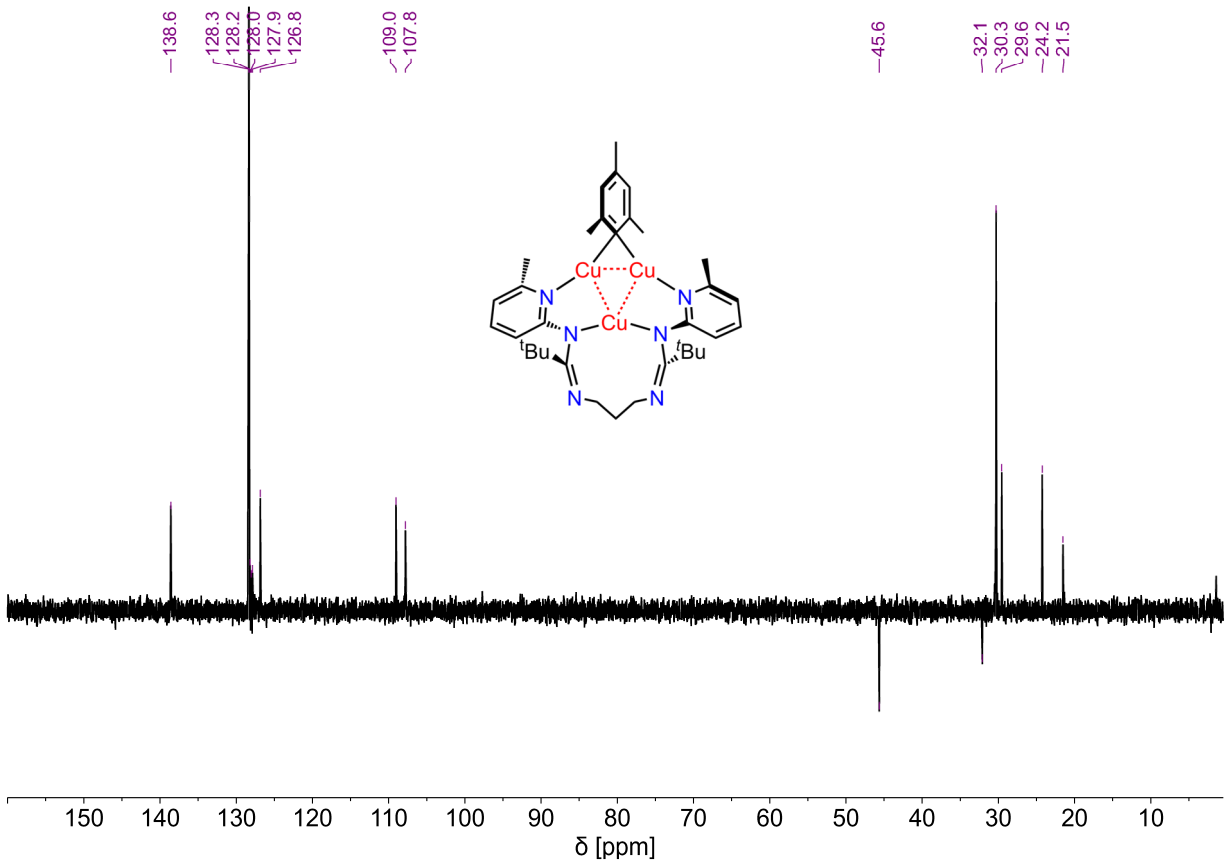

Figure S26: DEPT 135 NMR spectrum of **1** (C_6D_6, 150.9 MHz).

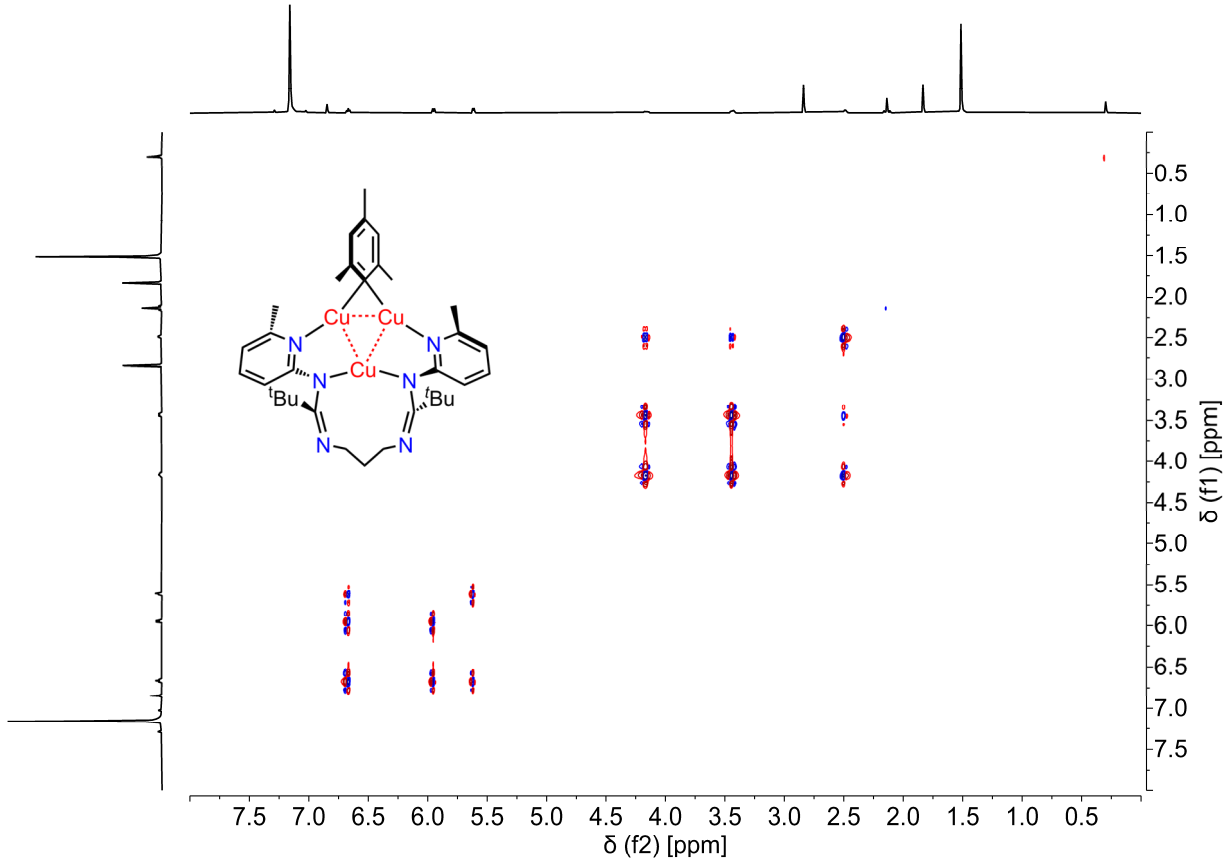

Figure S27: (^{1}H, ^{1}H)-COSY NMR spectrum of **1** (C_6D_6, 600.2 MHz).

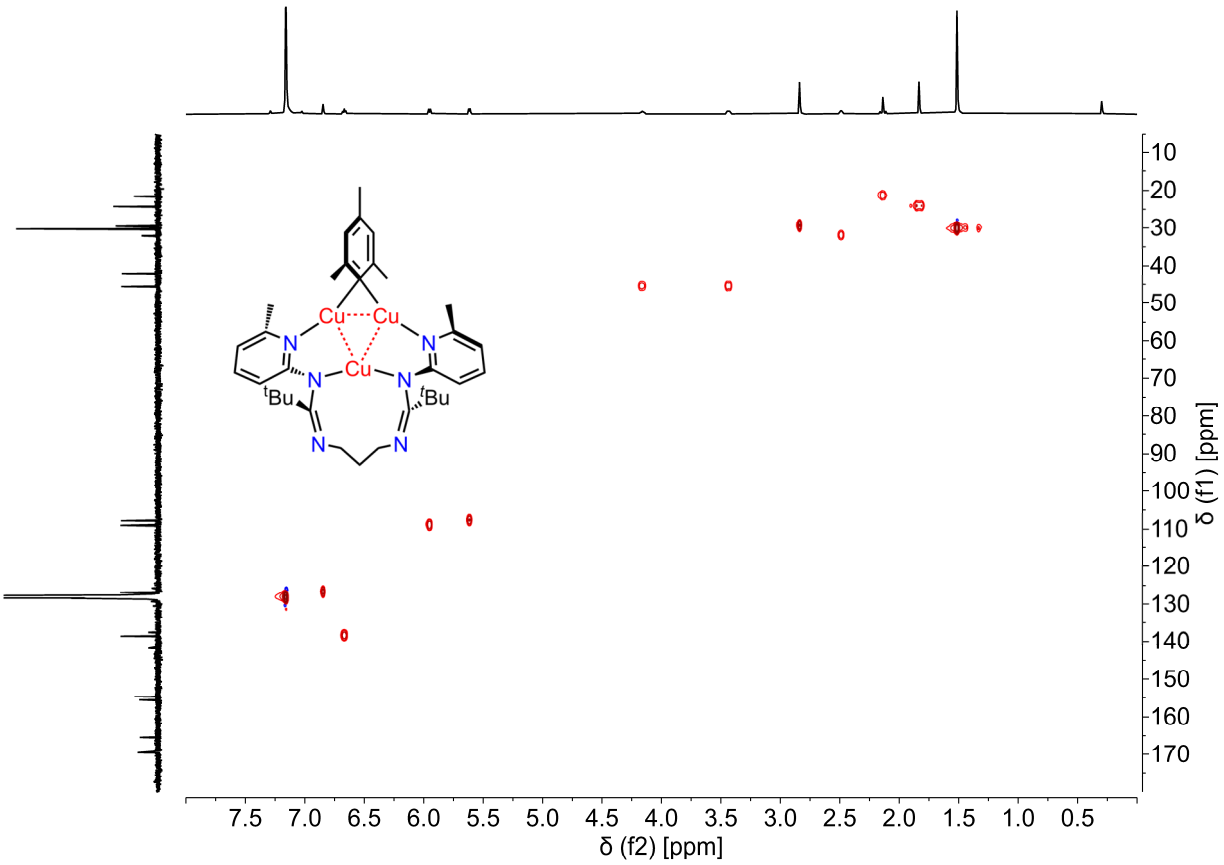

Figure S28: (^{1}H, ^{13}C)-HSQC NMR spectrum of **1** (C_6D_6, 600.2, 150.9 MHz).

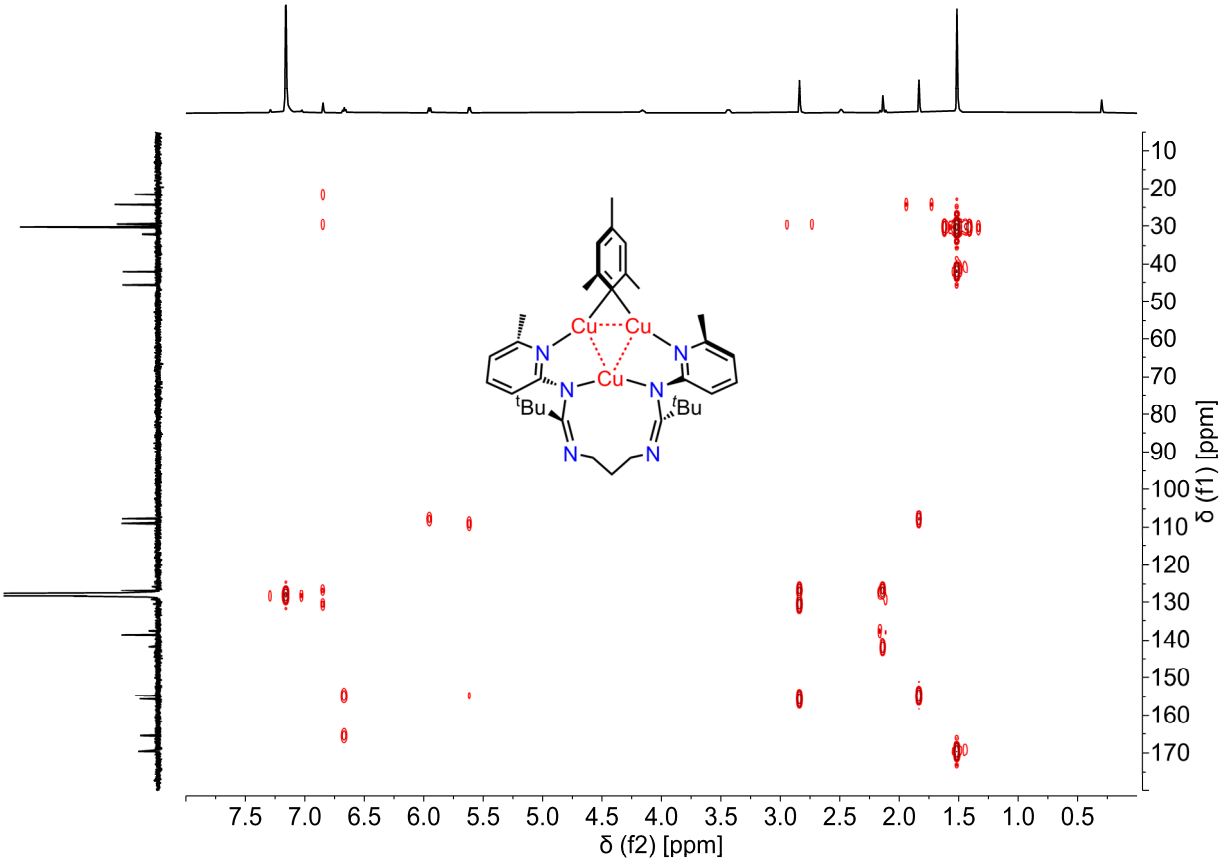

Figure S29: (^{1}H, ^{13}C)-HMBC NMR spectrum of **1** (C_6D_6, 600.2, 150.9 MHz).

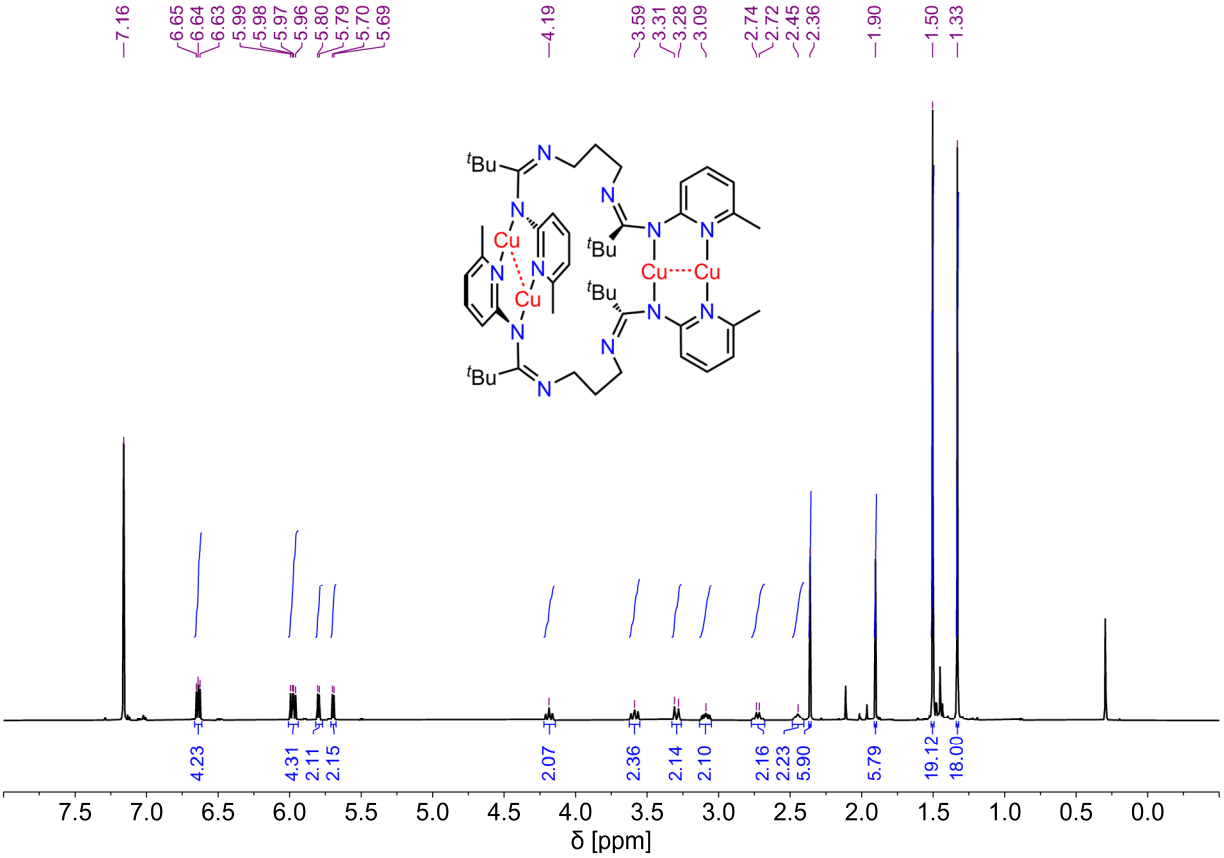

Figure S30: ^{1}H NMR spectrum of **2** (C_6D_6, 600.2 MHz).

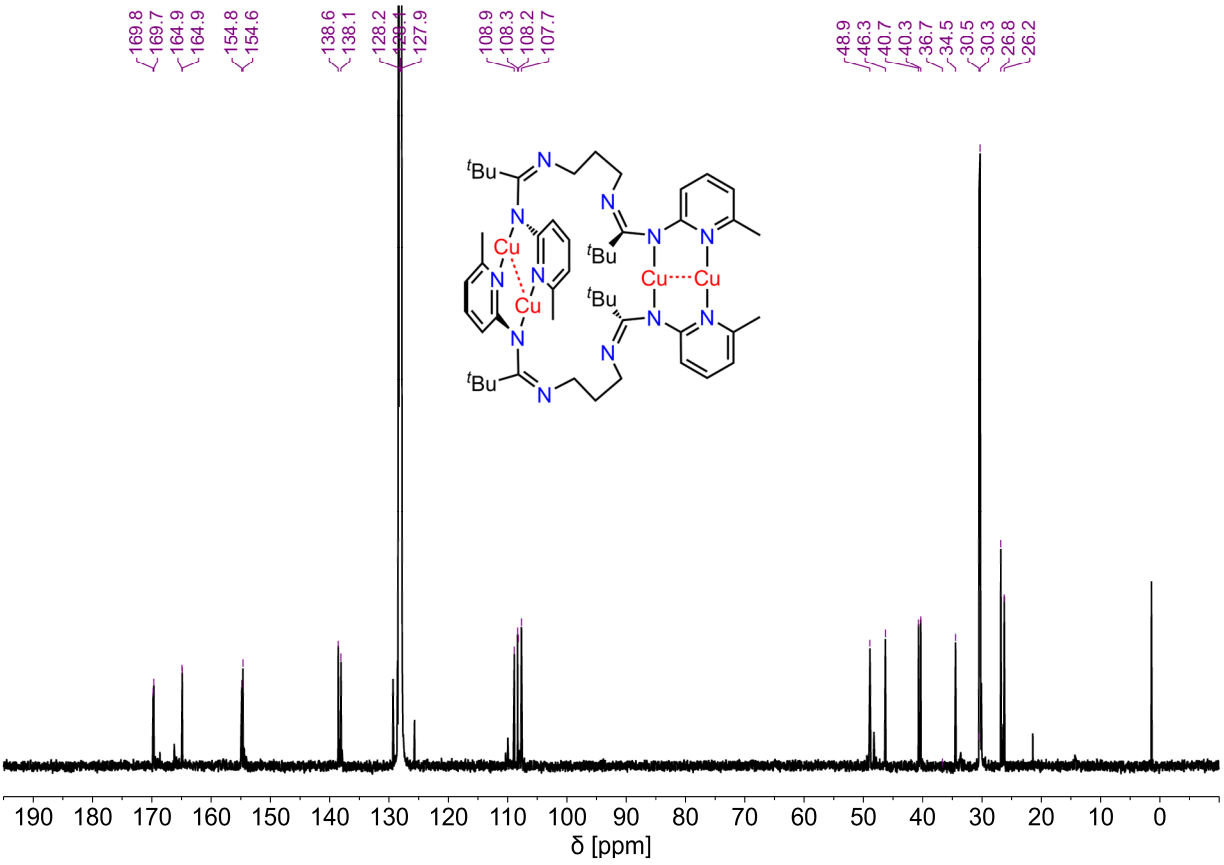

Figure S31: ^{13}C{^{1}H} NMR spectrum of **2** (C_6D_6, 150.9 MHz).

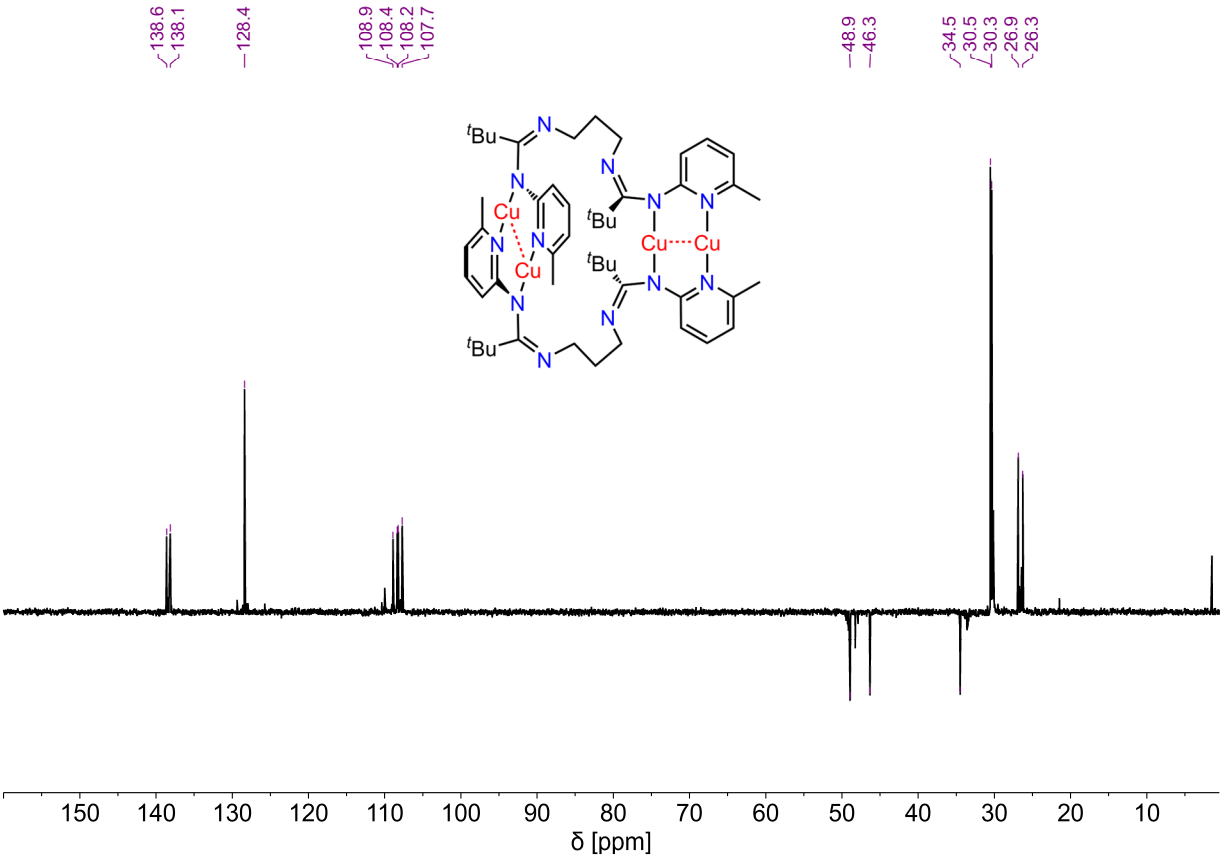

Figure S32: DEPT 135 NMR spectrum of **2** (C_6D_6, 150.9 MHz).

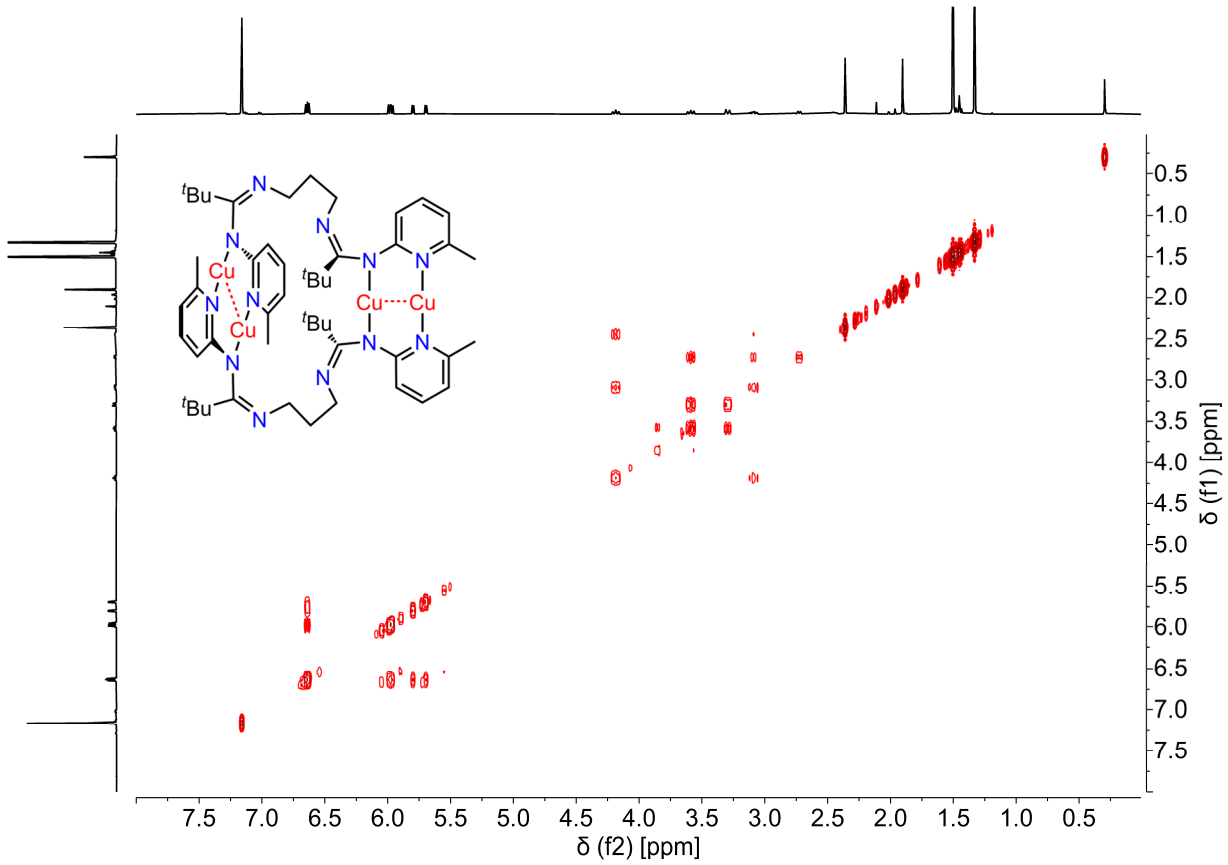

Figure S33: (^{1}H, ^{1}H)-COSY NMR spectrum of **2** (C_6D_6, 600.2 MHz).

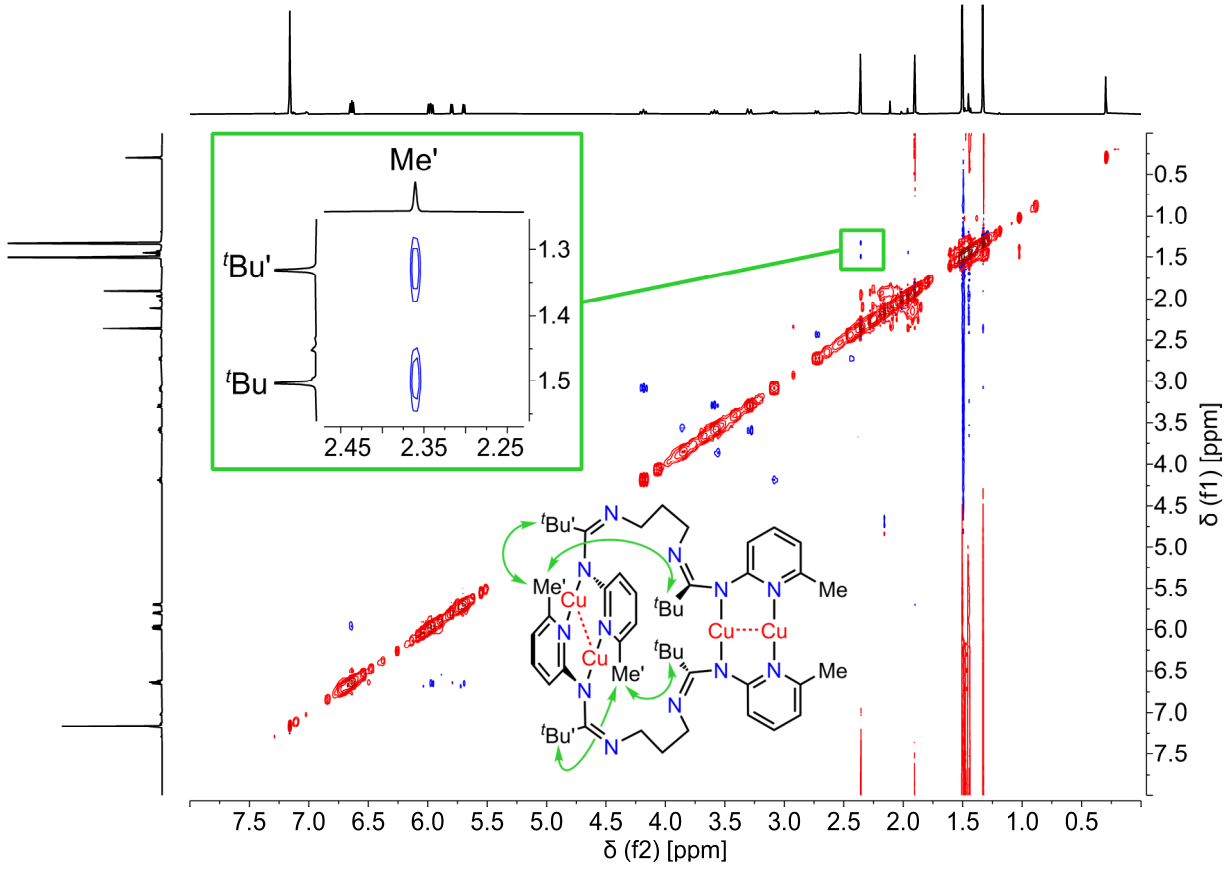

Figure S34: (^{1}H, ^{1}H)-ROESY NMR spectrum of **2** (C_6D_6, 600.2 MHz).

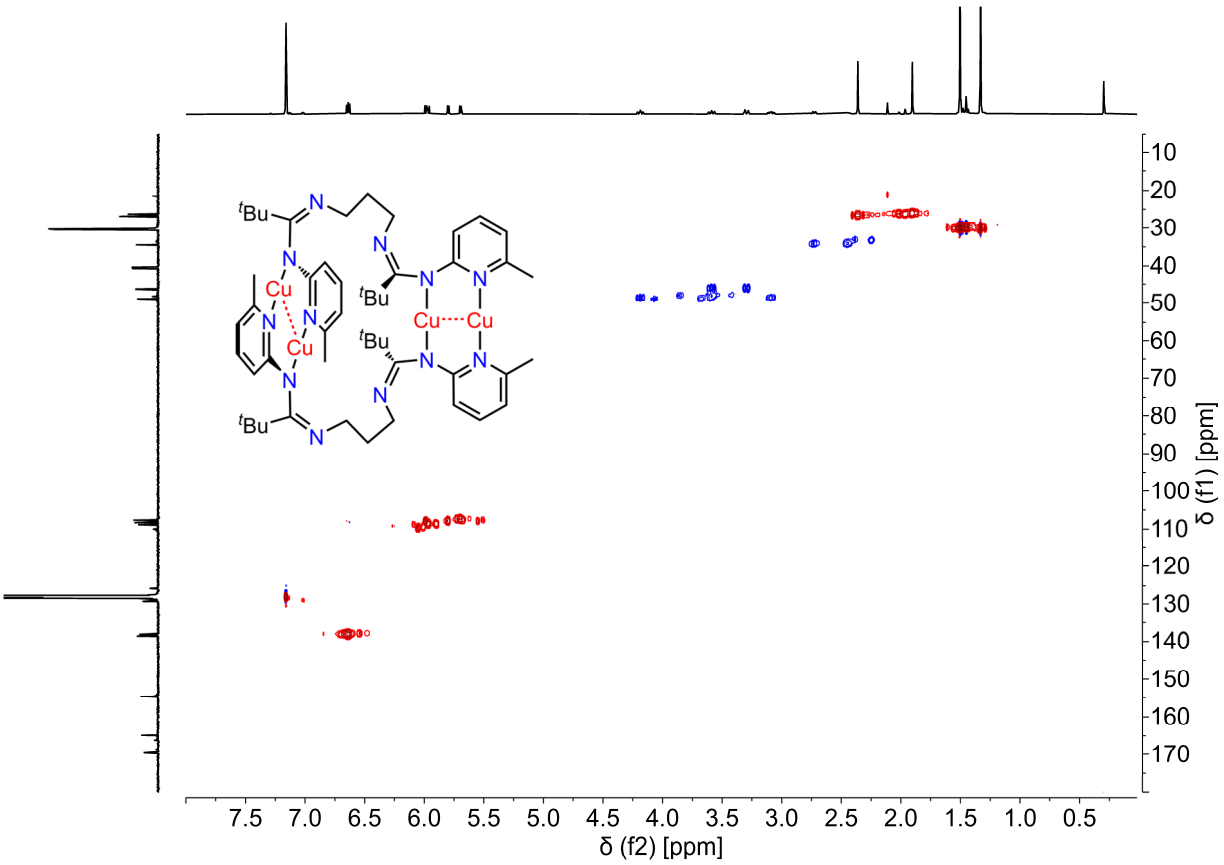

Figure S35: (^{1}H, ^{13}C)-HSQC NMR spectrum of **2** (C_6D_6, 600.2, 150.9 MHz).

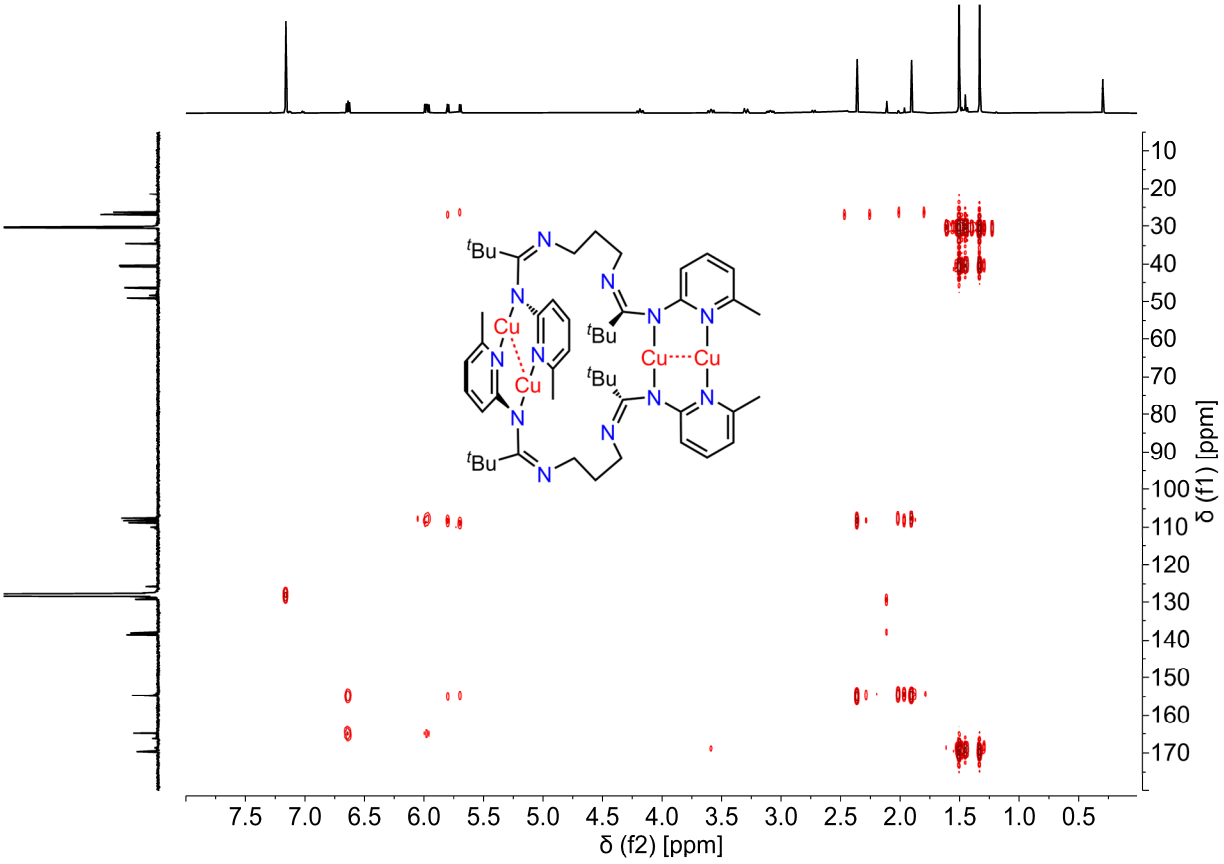

Figure S36: (^{1}H, ^{13}C)-HMBC NMR spectrum of **2** (C_6D_6, 600.2, 150.9 MHz).

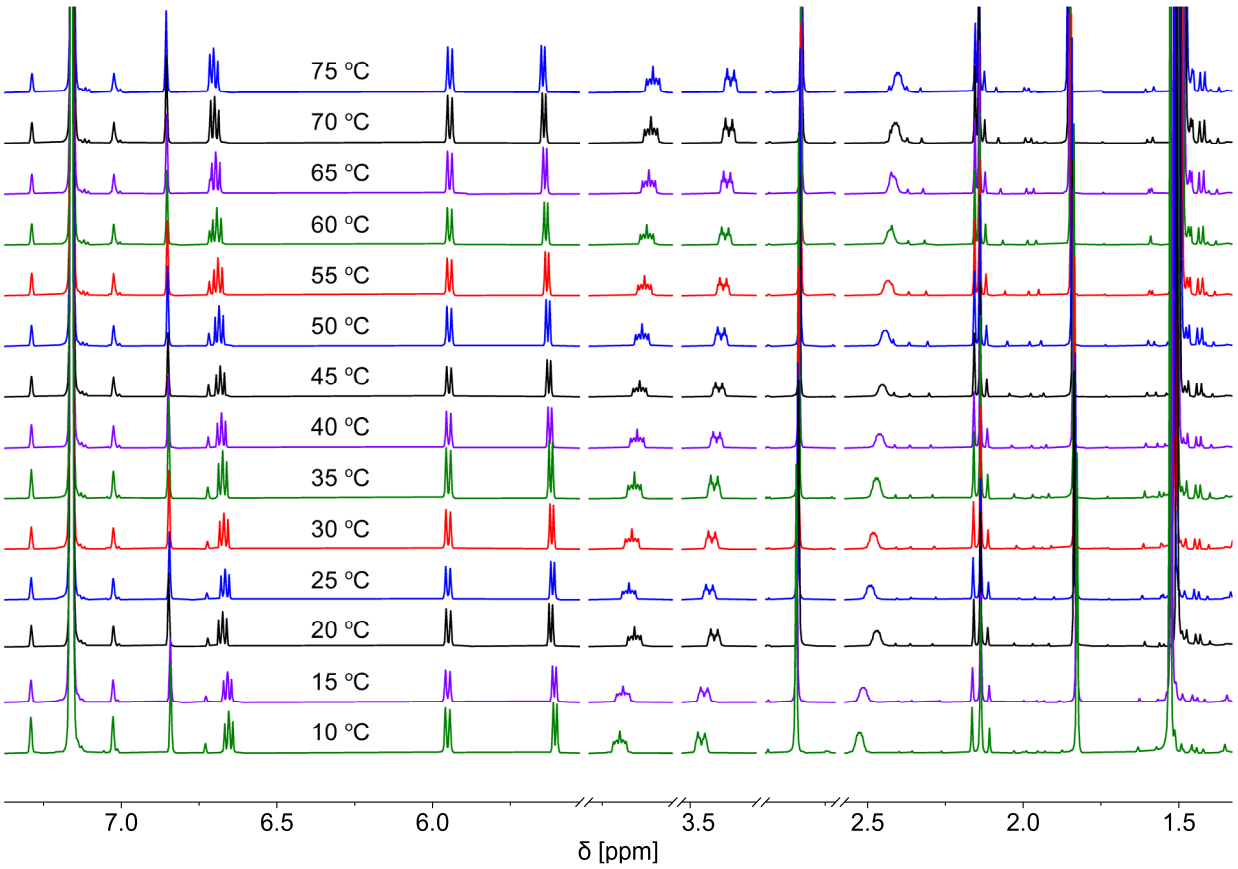

Figure S37: VT ^{1}H NMR spectra of **1** (C_6D_6, 600.2 MHz, +27…75 °C).

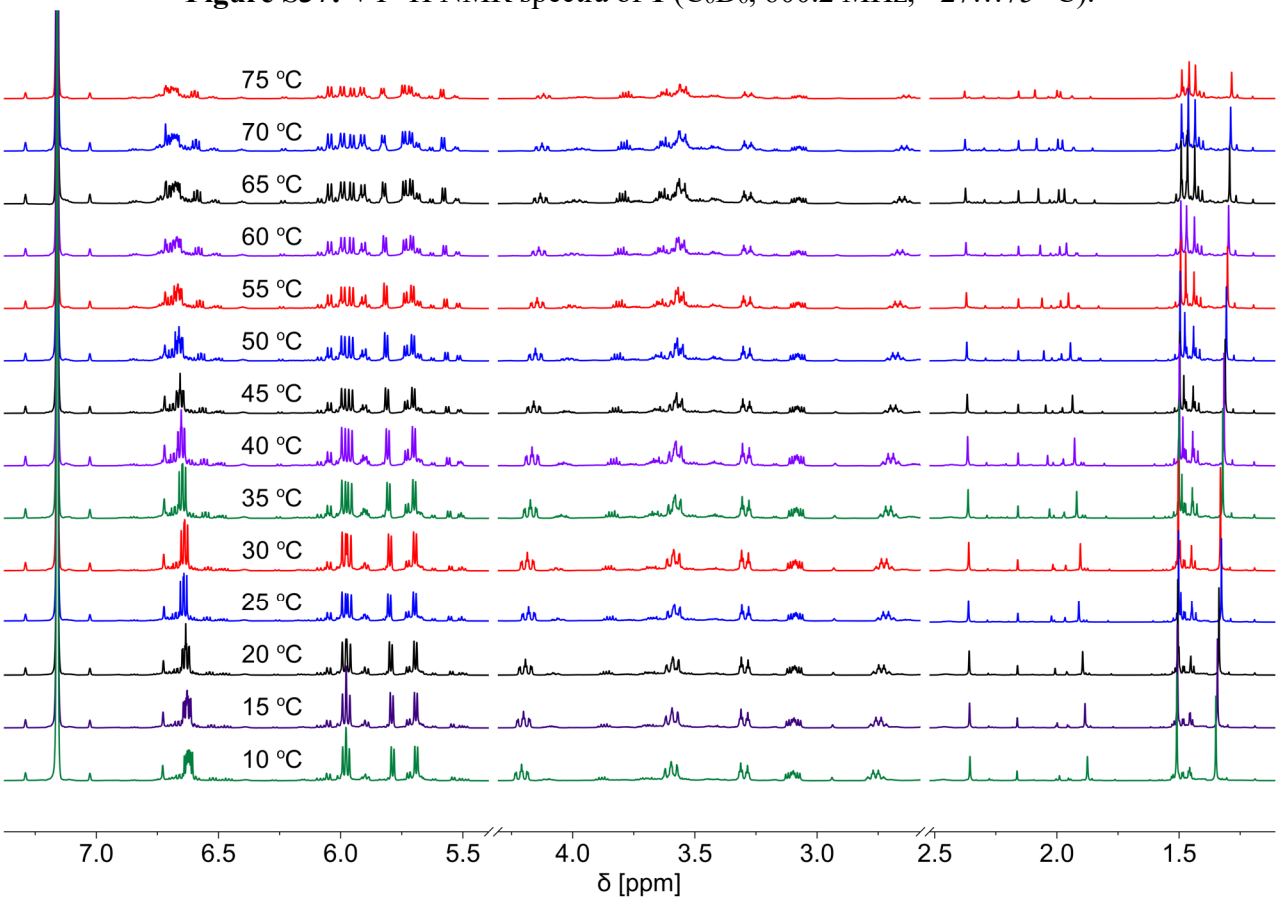

Figure S38: VT ^{1}H NMR spectra of **2** (C_7D_8, 600.2 MHz, +25…75 °C).

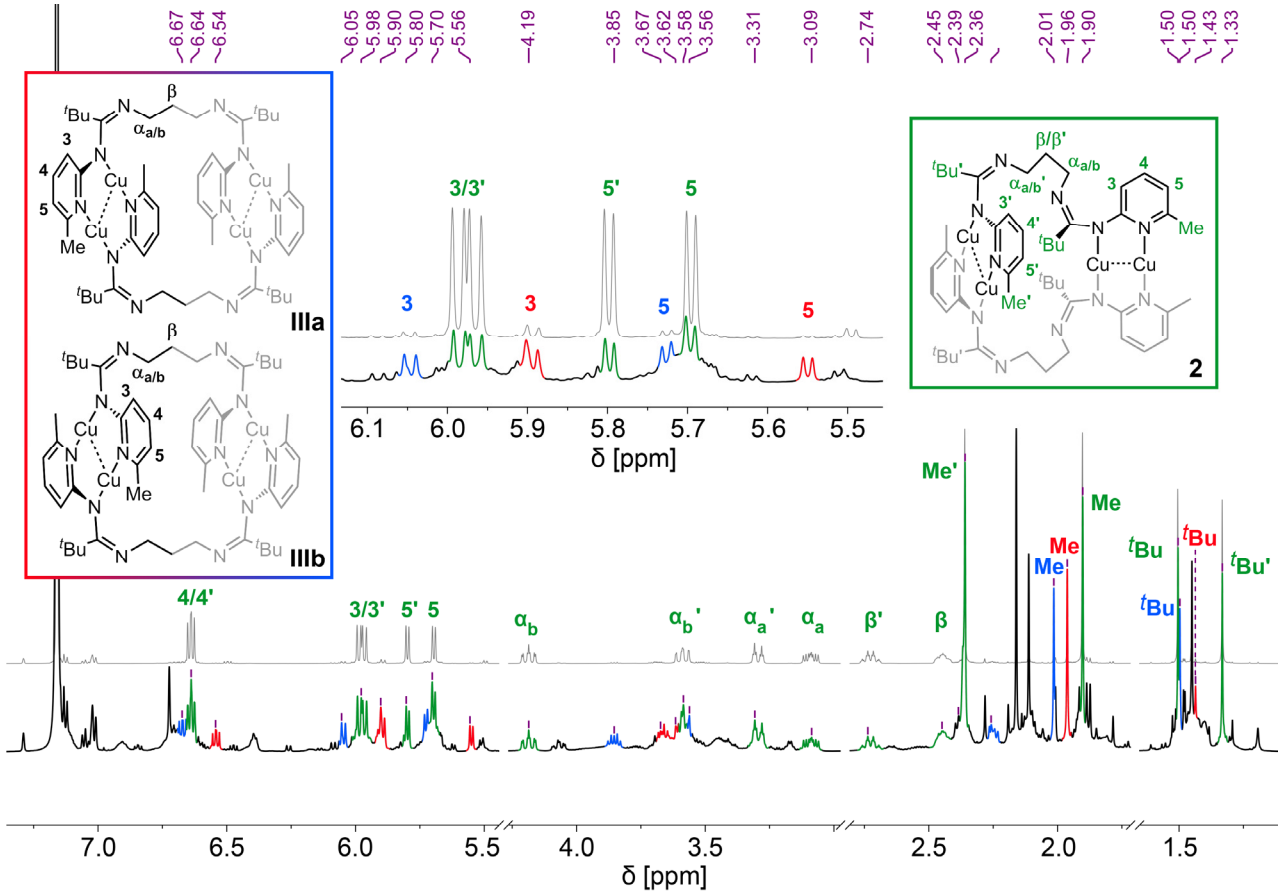

Figure S39: ^{1}H NMR spectra of **2** (method A) and of **2**, **3**, and **4**, (method B, C_6D_6, 600.2 MHz).

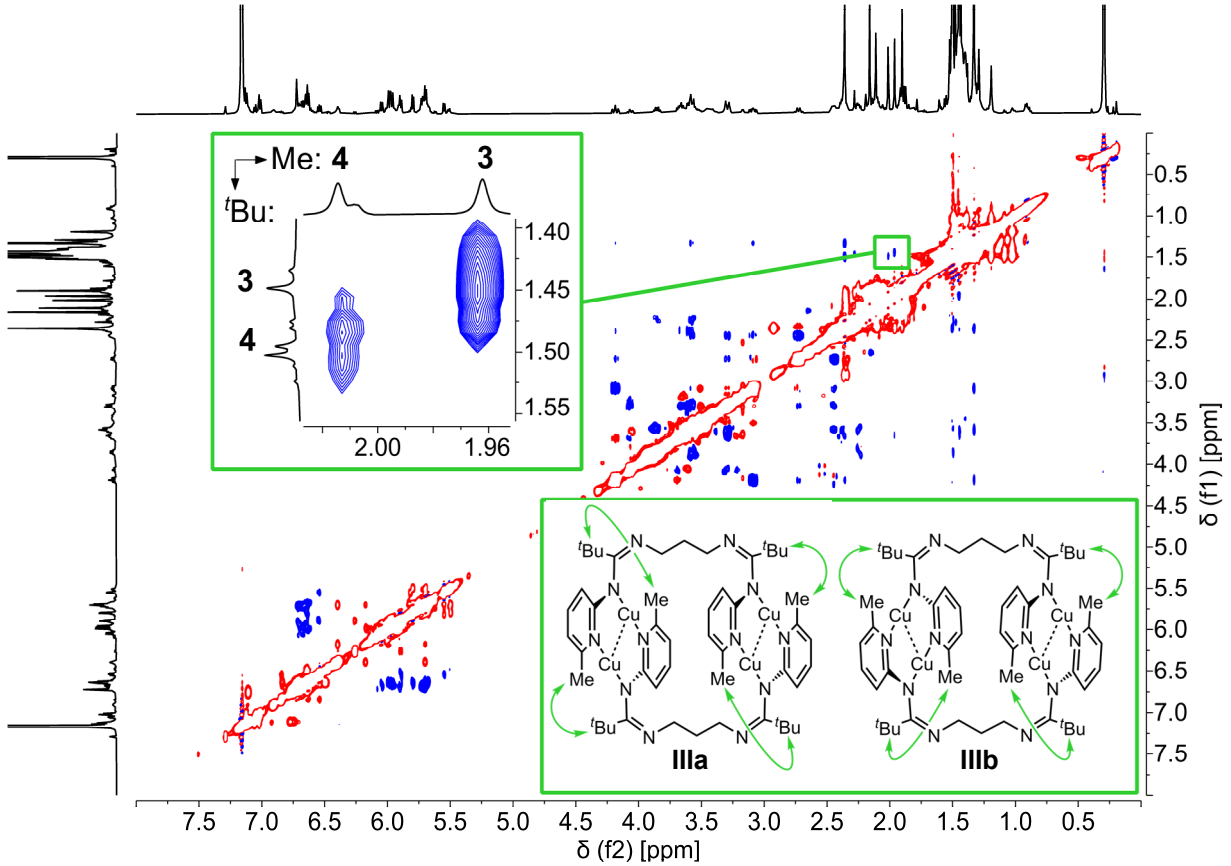

Figure S40: (^{1}H, ^{1}H)-ROESY NMR spectrum of **2**–**4** after heating of **2** to 75 °C (C_6D_6, 600.2 MHz).

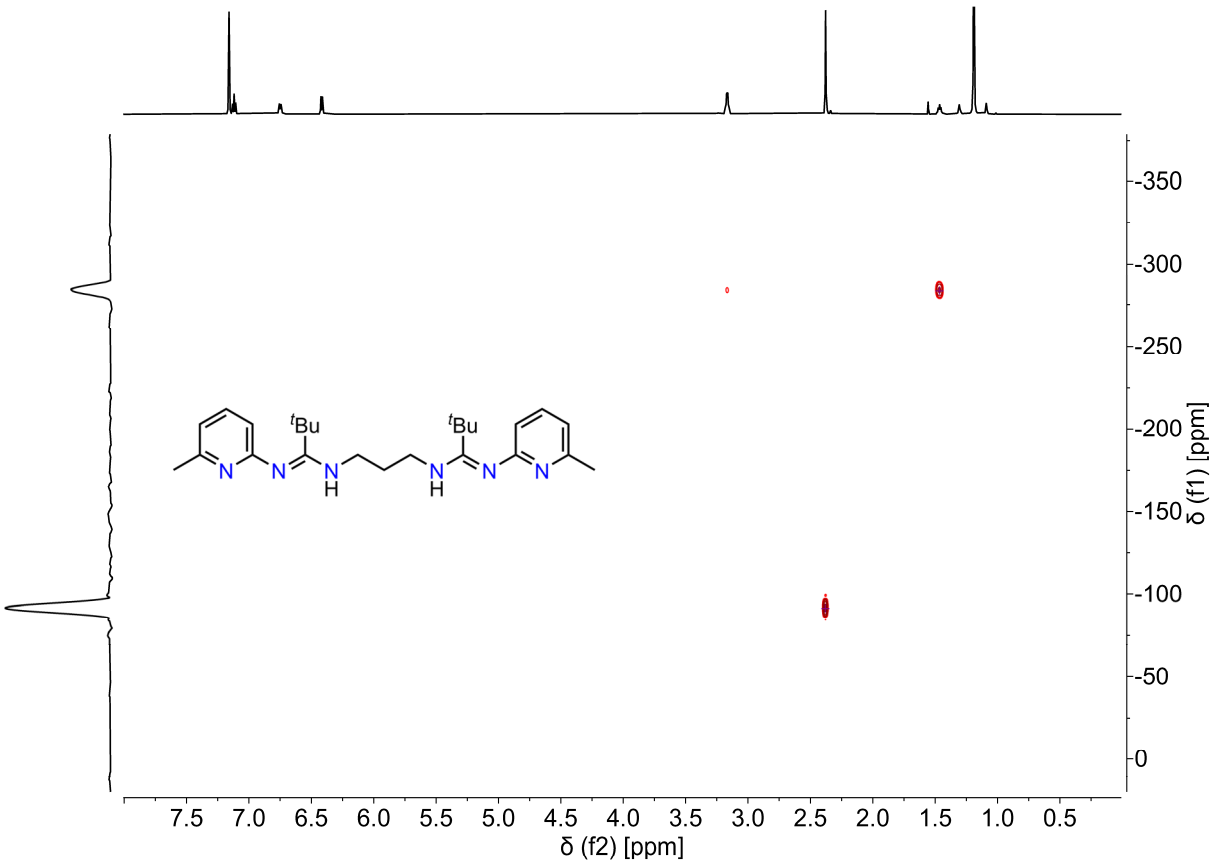

Figure S41: (^{1}H, ^{15}N)-HMBC NMR spectrum of $\mathbf{L^2H_2}$ (C_6D_6, 600.2, 60.8 MHz).

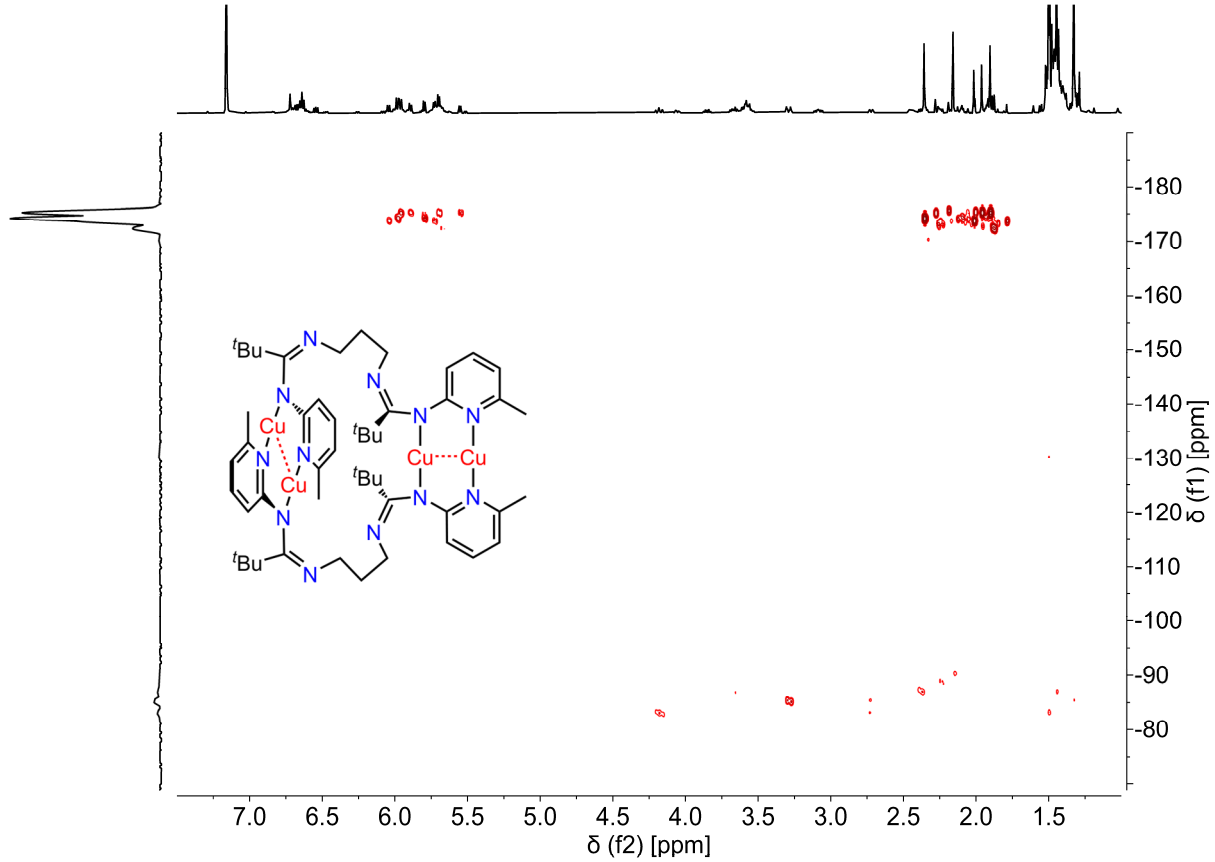

Figure S42: (^{1}H, ^{15}N)-HMBC NMR spectrum of **2** (C_6D_6, 600.2, 60.8 MHz, 288.0 K).

Table S5: Selected ^{1}H NMR shifts of $\mathbf{L^2}H_2$, **1**, and **2**.

	$\mathbf{L^2}H_2$	**1**	**2**
		δ (C_6D_6) [ppm]	
CH_3 (^{t}Bu)	1.19 (s)	1.51 (s)	1.33 (s), 1.50 (s)
CH_3 (6-py)	2.38 (s)	1.83 (s)	1.90 (s), 2.36 (s)
$NCH_2C\underline{H_2}$	1.47 (quint, $^3J_{HH}$ = 6.0 Hz)	2.47–2.50 (m)	2.42–2.47 (m) 2.73 (qt, J_{HH} = 12.8 Hz, 3.1 Hz)
$NC\underline{H_2}$	3.17 (q, $^3J_{HH}$ = 6.0 Hz)	3.44 (dt, $^3J_{H,H}$ = 8.7 Hz, $\lvert^2J_{H,H}\rvert \approx$ 13 Hz) 4.15–4.18 (m)	3.09 (ddd, $^3J_{H,H}$ = 12.4 Hz, 6.2 Hz, $\lvert^2J_{H,H}\rvert$ = 16.0 Hz) 3.29 (dt, $^3J_{H,H}$ = 3.5 Hz, $\lvert^2J_{H,H}\rvert$ =16.5 Hz) 3.59 (ddd, $^3J_{H,H}$ 12.9 Hz, 1.5 Hz, $\lvert^2J_{H,H}\rvert$ = 14.9 Hz) 4.19 (ddd, $^3J_{H,H}$ = 13.0 Hz, 2.9 Hz, $\lvert^2J_{H,H}\rvert$ = 15.9 Hz)
py H^3	6.74 (d, $^3J_{HH}$ = 7.9 Hz)	5.95 (d, $^3J_{HH}$ = 8.6 Hz)	5.97 (d, $^3J_{HH}$ = 8.8 Hz) 5.99 (d, $^3J_{HH}$ = 8.7 Hz)
py H^4	7.12 (t, $^3J_{HH}$ = 7.6 Hz)	6.67 (dd, $^3J_{HH}$ = 8.6 Hz, 6.9 Hz)	6.64 (dd, $^3J_{HH}$ = 8.3 Hz, 7.3 Hz)
py H^5	6.42 ($^3J_{HH}$ = 7.9 Hz)	5.62 (d, $^3J_{HH}$ = 6.8 Hz)	5.70 (d, $^3J_{HH}$ = 6.8 Hz) 5.80 (d, $^3J_{HH}$ = 6.8 Hz)

Table S6: Selected $^{13}C\{^{1}H\}$ NMR shifts of $\mathbf{L^2}H_2$, **1**, and **2**.

	$\mathbf{L^2}H_2$	**1**	**2**
	δ (C_6D_6) [ppm]		
CH_3, ^{t}Bu	29.4	30.3	30.3 30.5
C, ^{t}Bu	39.2	42.0	40.3 40.7
CH_3 (6-py)	24.6	24.3	26.2 26.8
$NCH_2\underline{C}H_2$	30.7	32.1	34.5
$N\underline{C}H_2$	40.1	45.6	46.3 48.9
C (py C^2)	163.6	165.5	164.9 (2 ×)
CH (py C^3)	115.3	109.0	108.3 108.9
CH (py C^4)	137.0	138.6	138.1 138.6
CH (py C^5)	115.2	107.8	107.7 108.2
C (py C^6)	155.9	154.7	154.6 154.8
^{t}Bu$\underline{C}N_2$	163.1	169.6	169.7 169.8

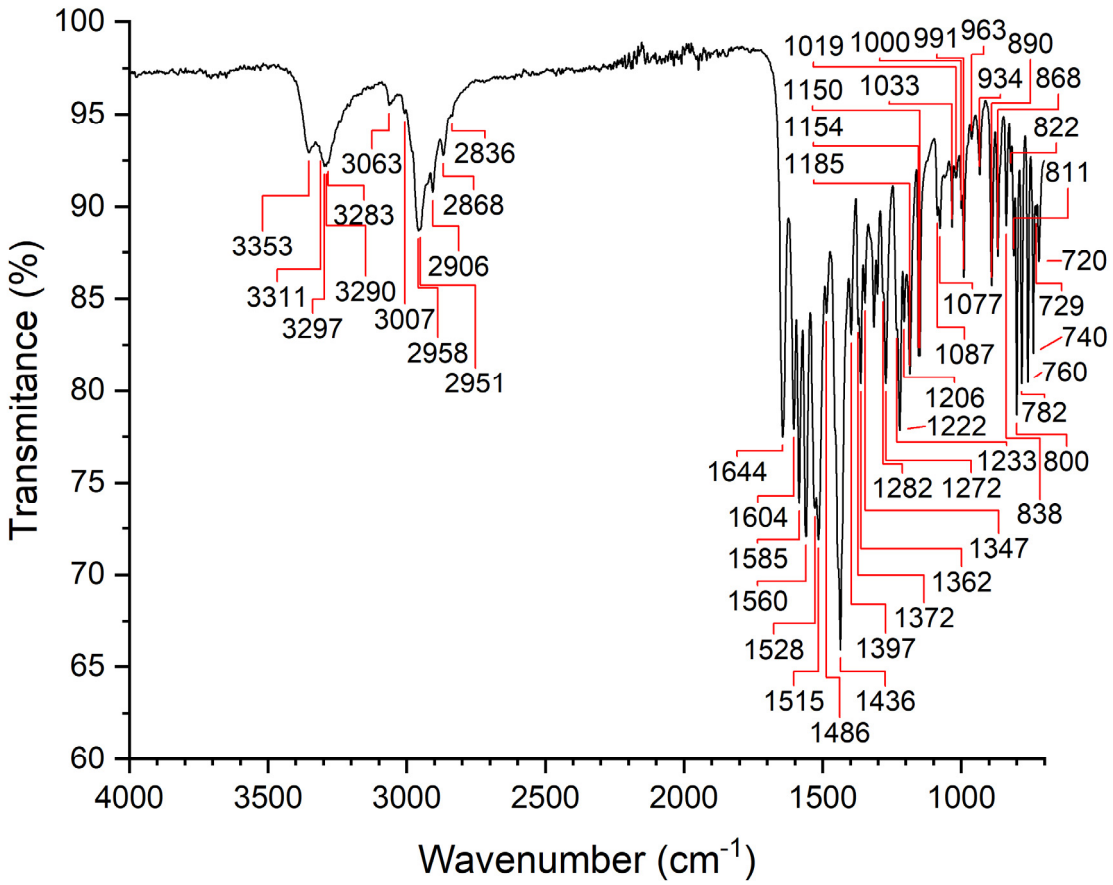

Figure S43: IR spectrum of $\mathbf{L^2}H_2$ (ATR).

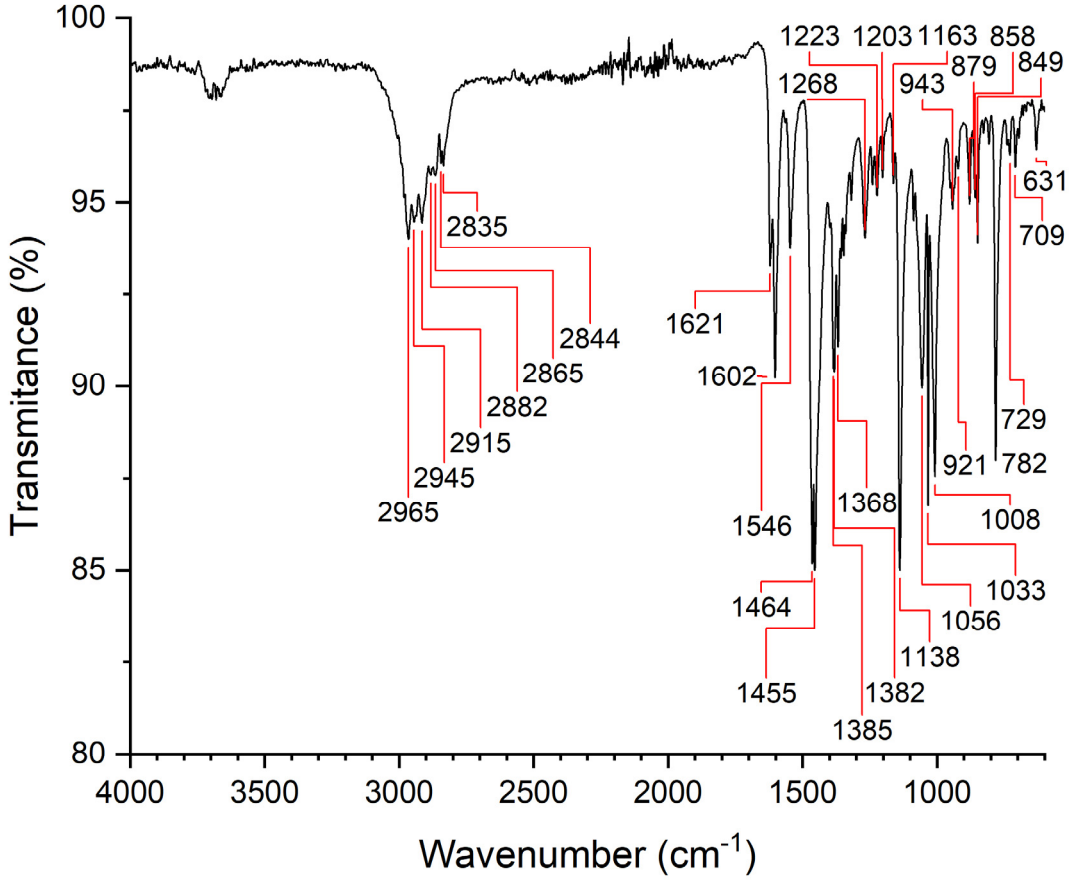

Figure S44: IR spectrum of **1** (ATR).

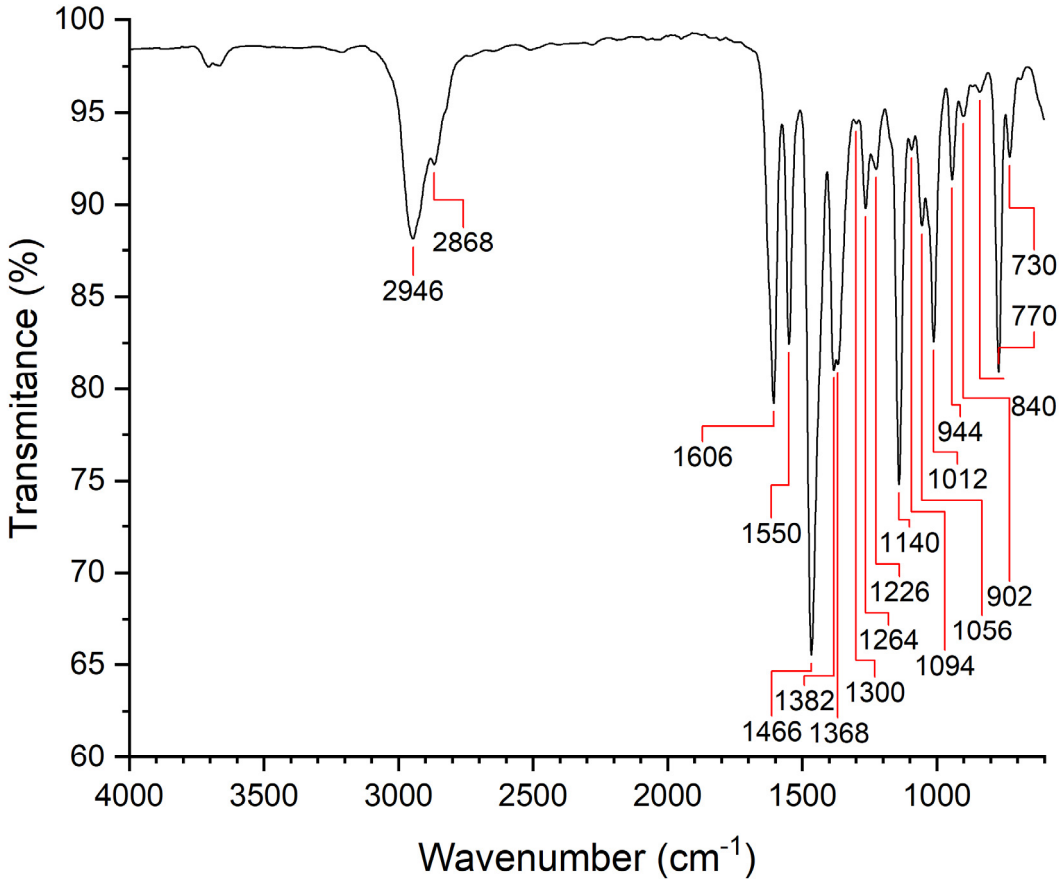

Figure S45: IR spectrum of **2** (ATR).

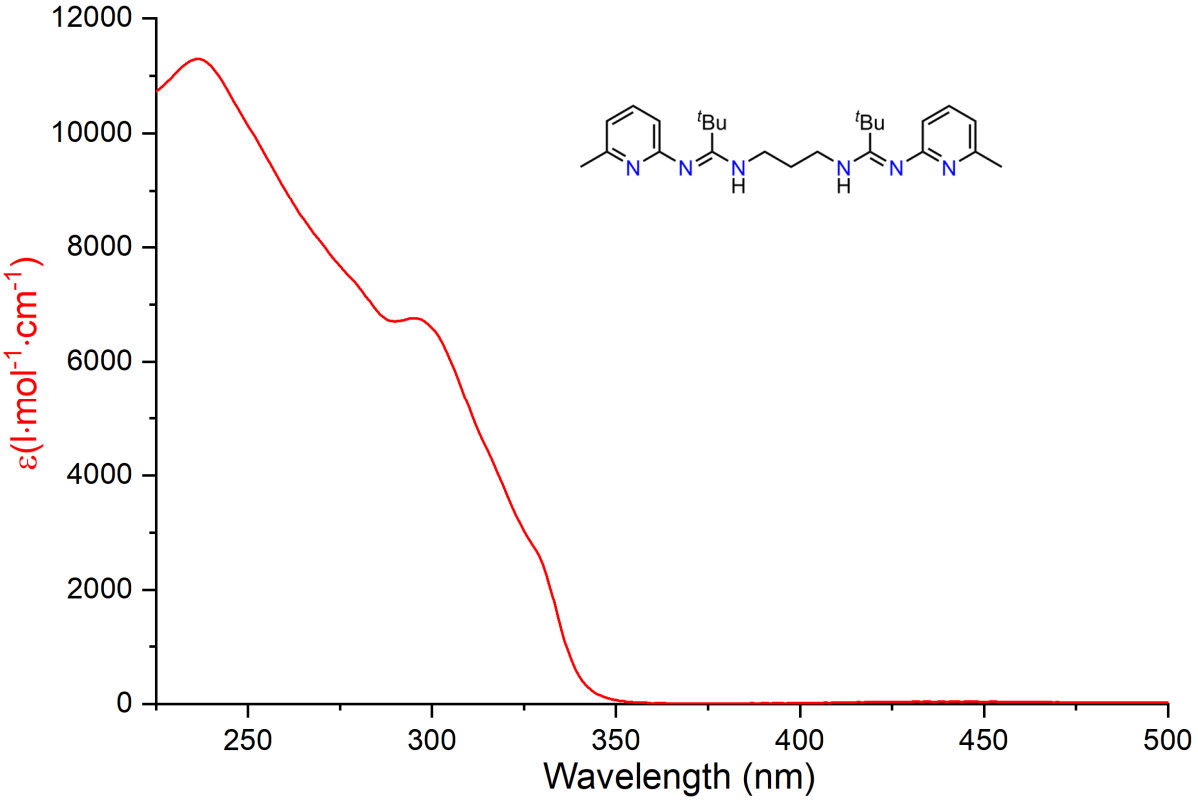

Figure S46: UV–Vis spectrum of $\mathbf{L^2}H_2$ in THF.

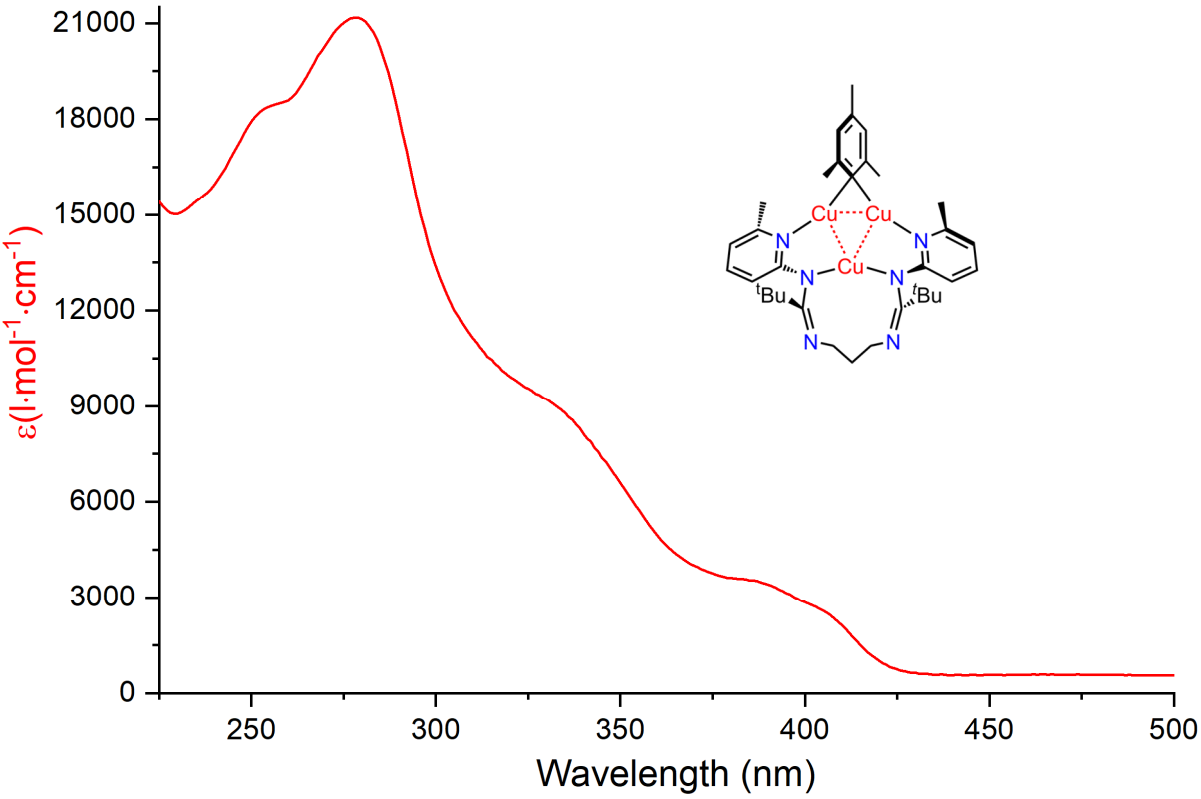

Figure S47: UV–Vis spectrum of **1** in THF.

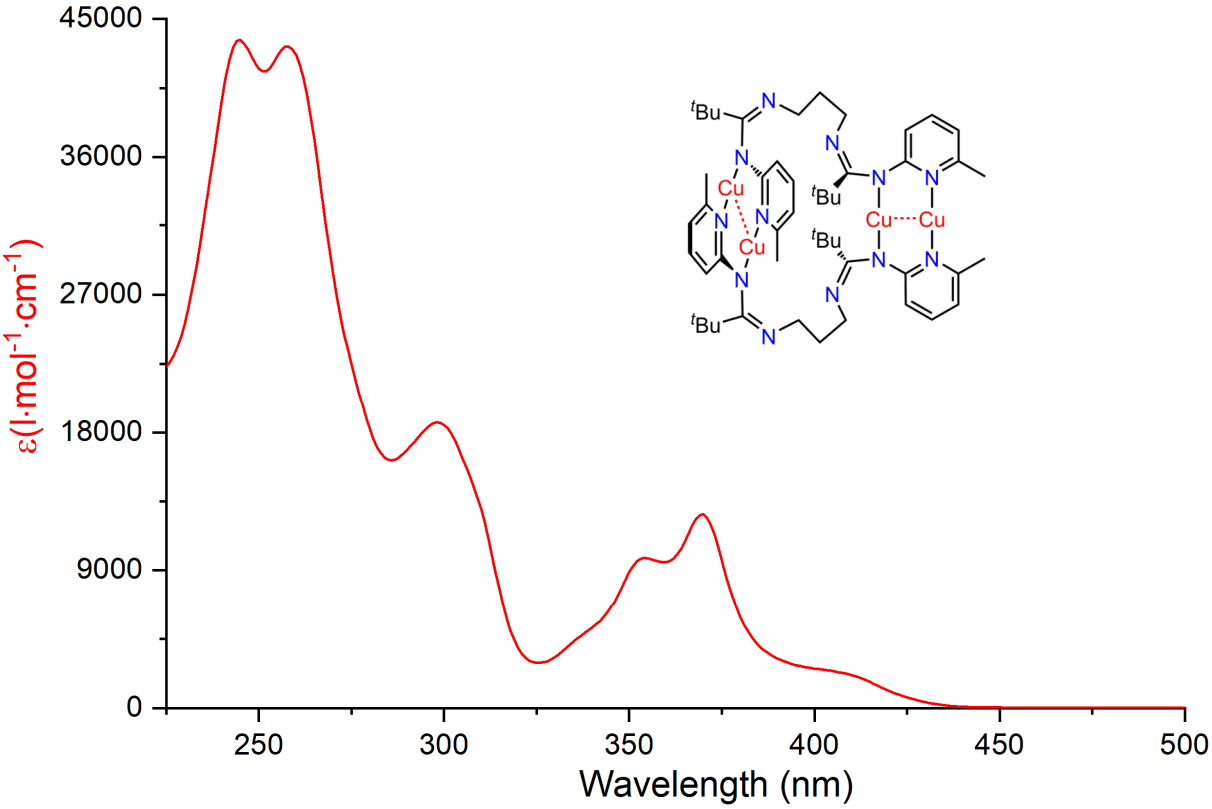

Figure S48: UV–Vis spectrum of **2** in THF.

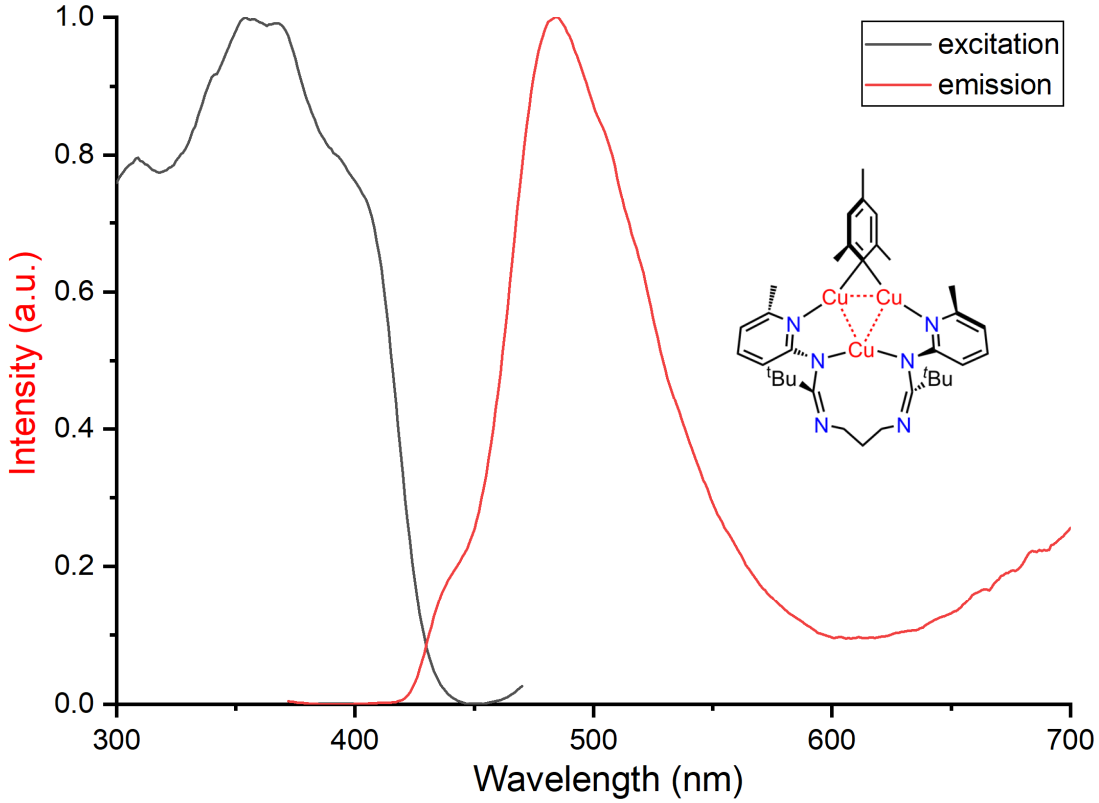

Figure S49: Normalized photoluminescence excitation and emission spectra of **1** in THF at 300 K.

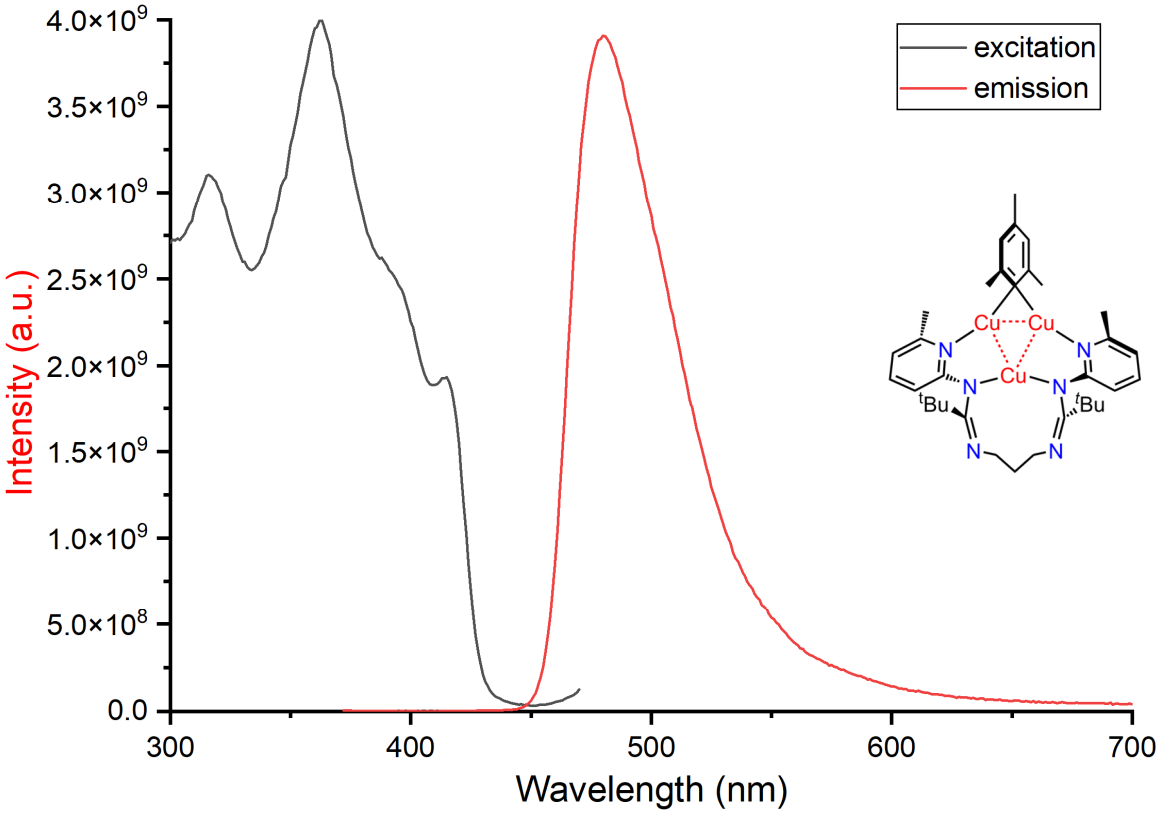

Figure S50: Photoluminescence excitation and emission spectra of **1** in the solid matrix of THF at 77K.

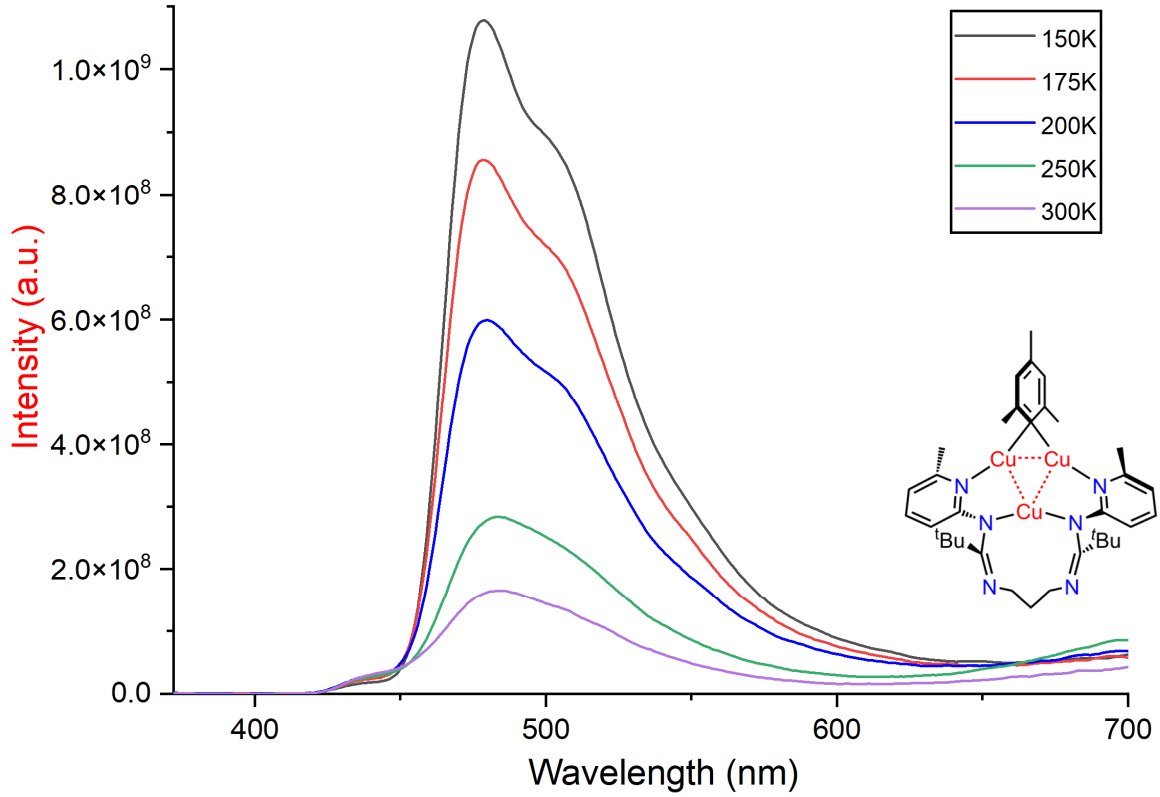

Figure S51: Variable-temperature photoluminescence emission spectra of **1** in solution (THF).

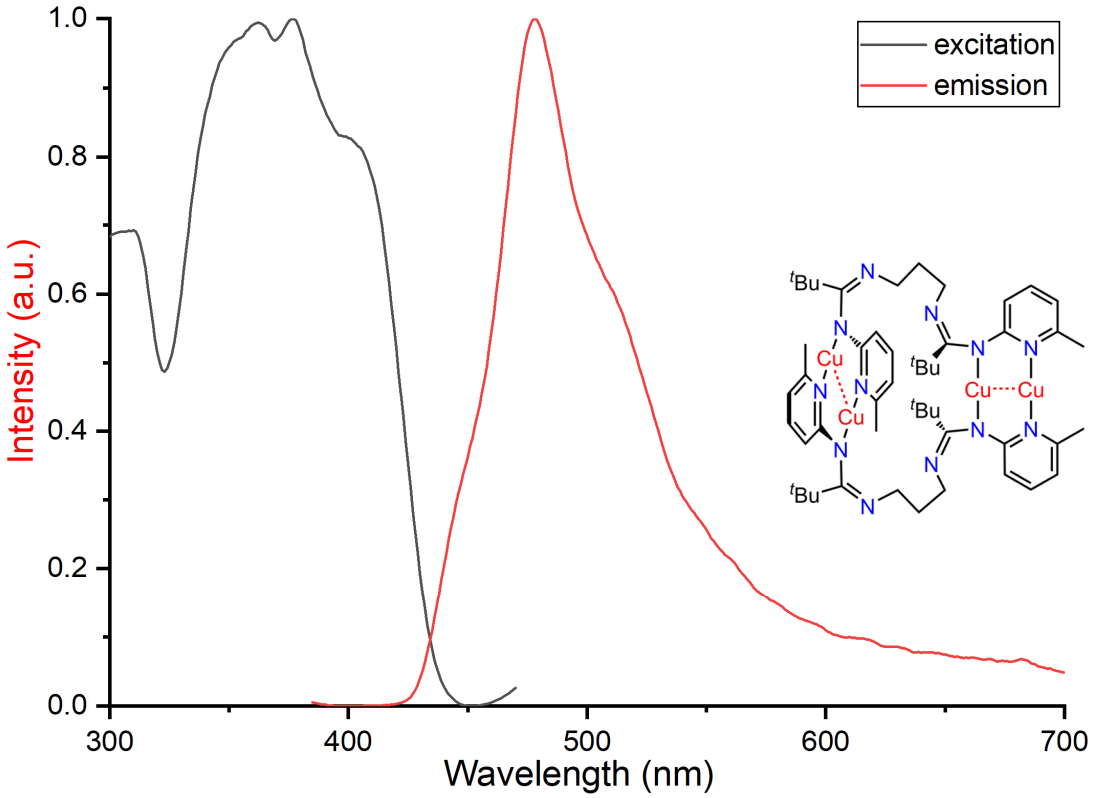

Figure S52: Normalized photoluminescence excitation and emission spectra of **2** in THF at 300 K.

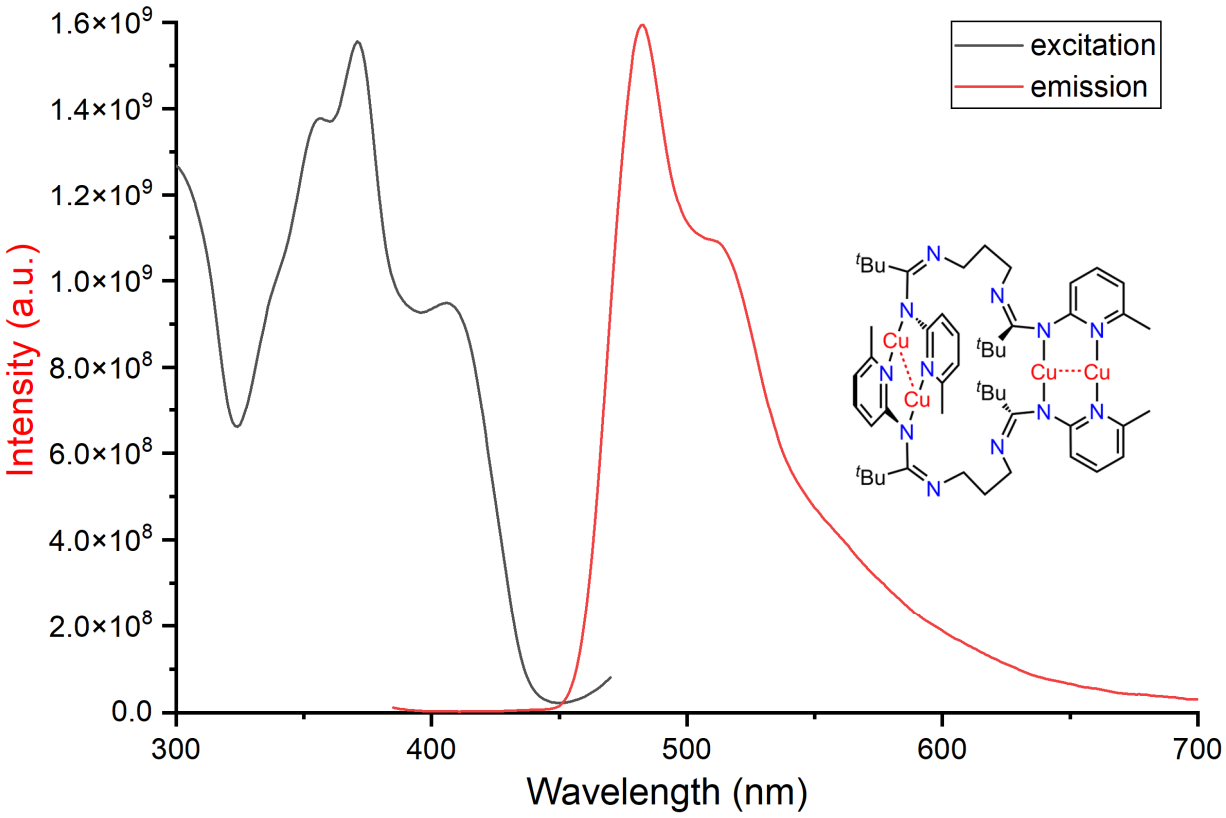

Figure S53: Photoluminescence excitation and emission spectra of **2** in the solid matrix of THF at 77K.

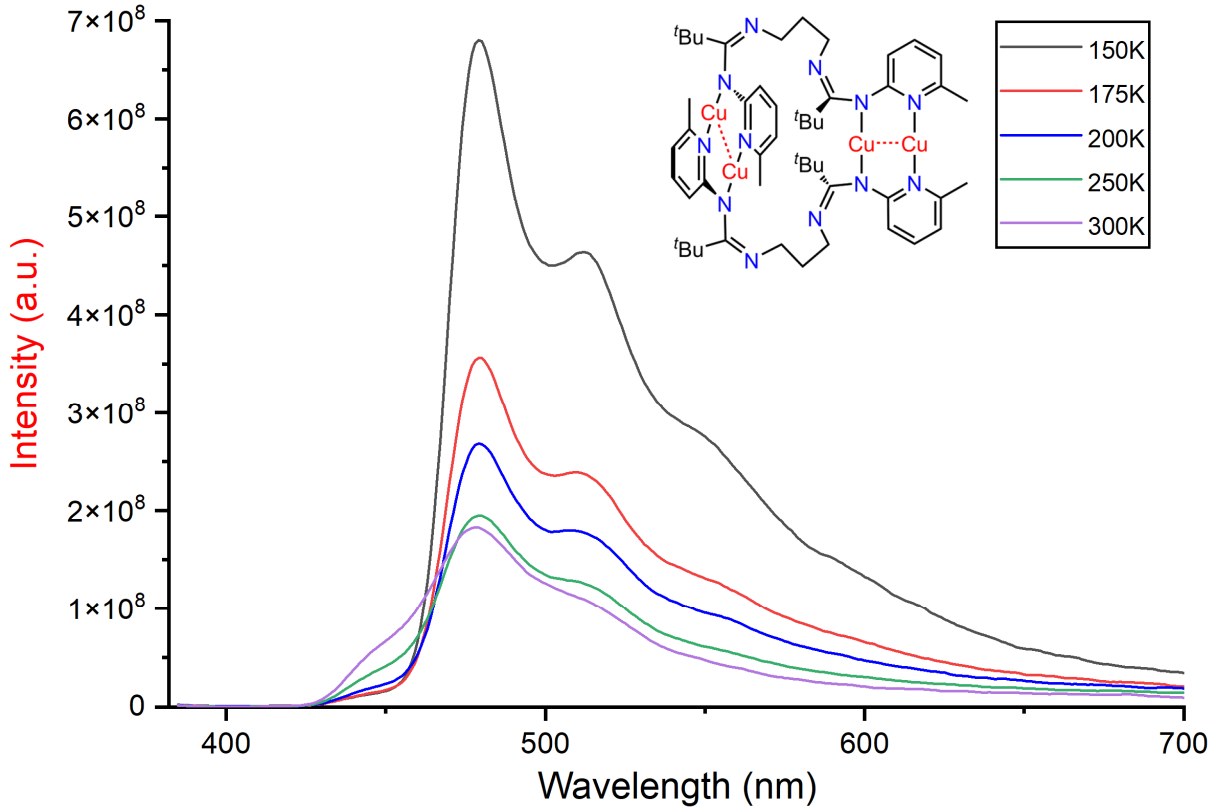

Figure S54: Variable-temperature photoluminescence emission spectra of **2** in solution (THF).

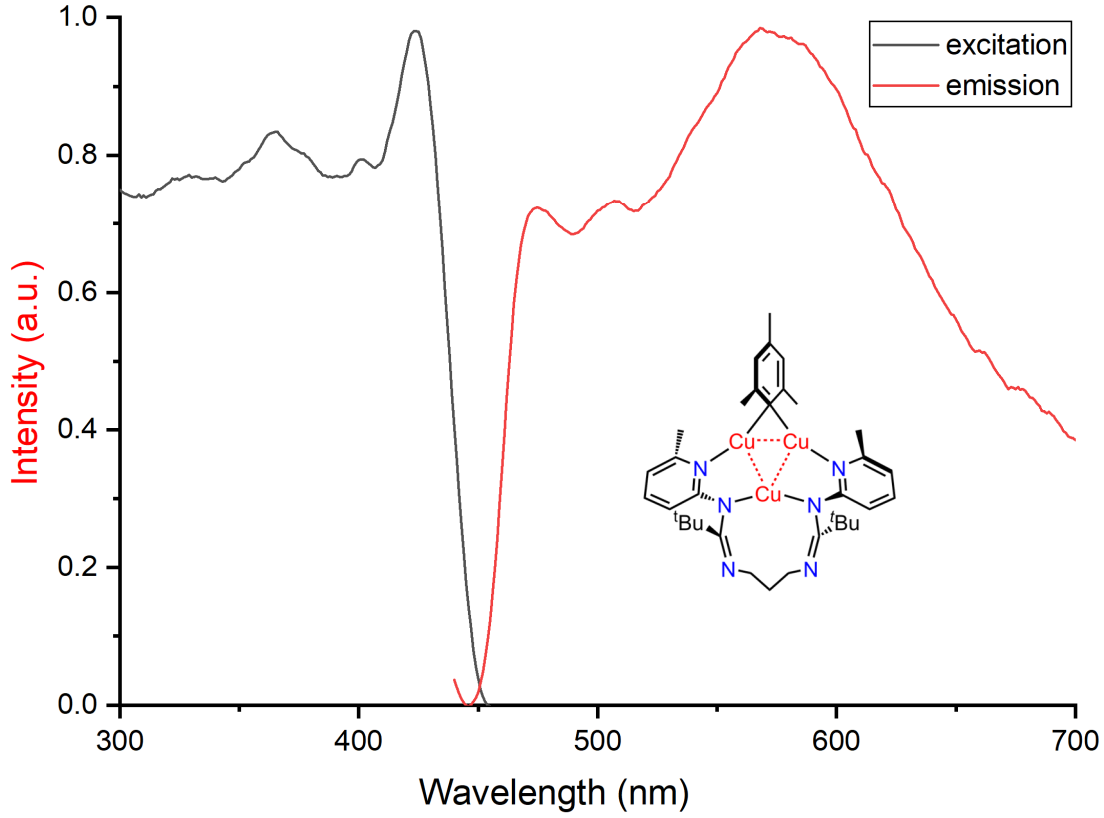

Figure S55: Normalized photoluminescence excitation and emission spectra of **1** in the solid state at 300 K.

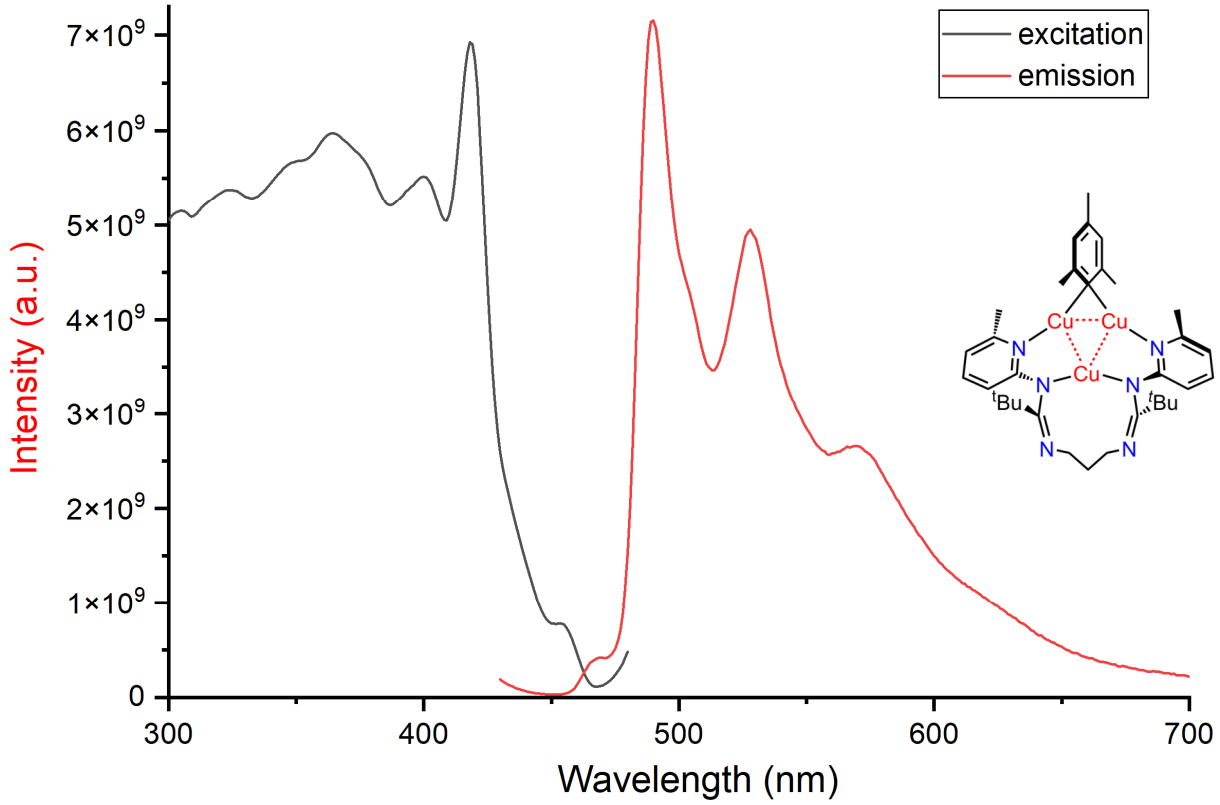

Figure S56: Photoluminescence excitation and emission spectra of **1** in the solid state at 77 K.

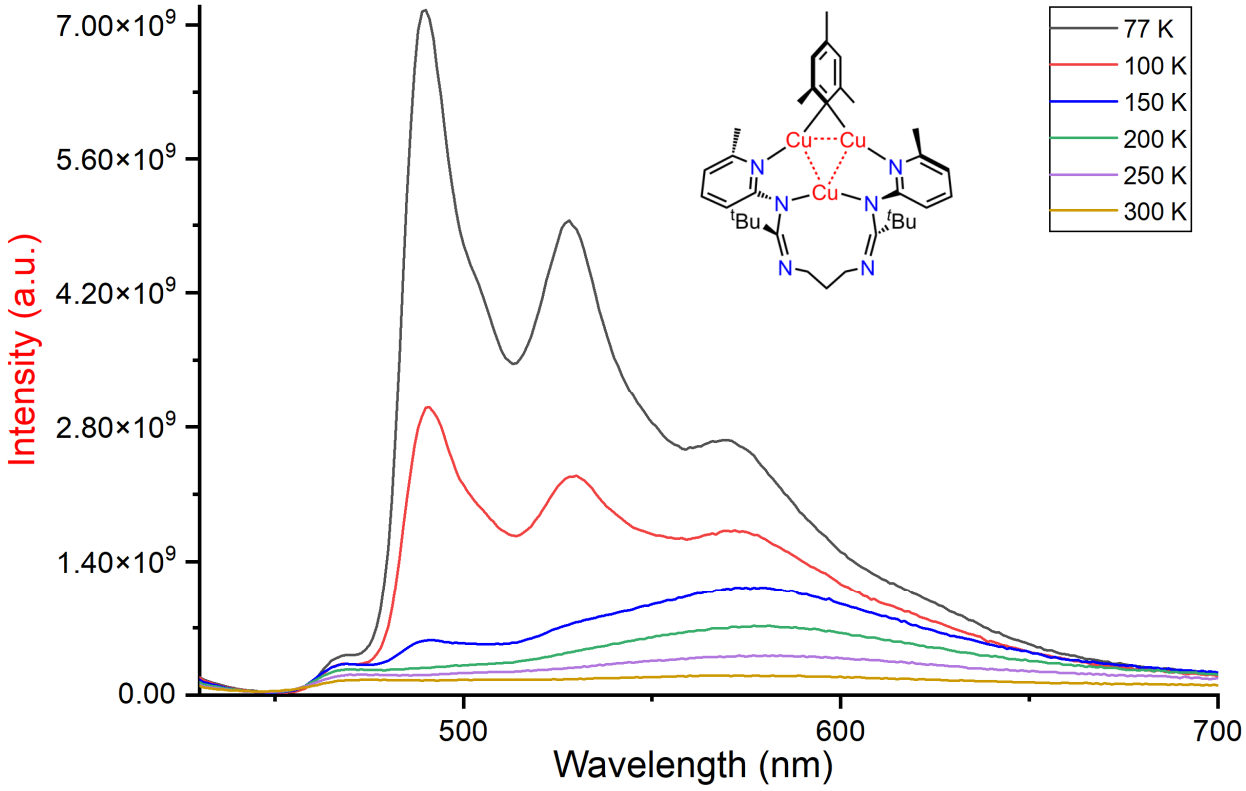

Figure S57: Variable-temperature photoluminescence emission spectra of **1** in the solid state.

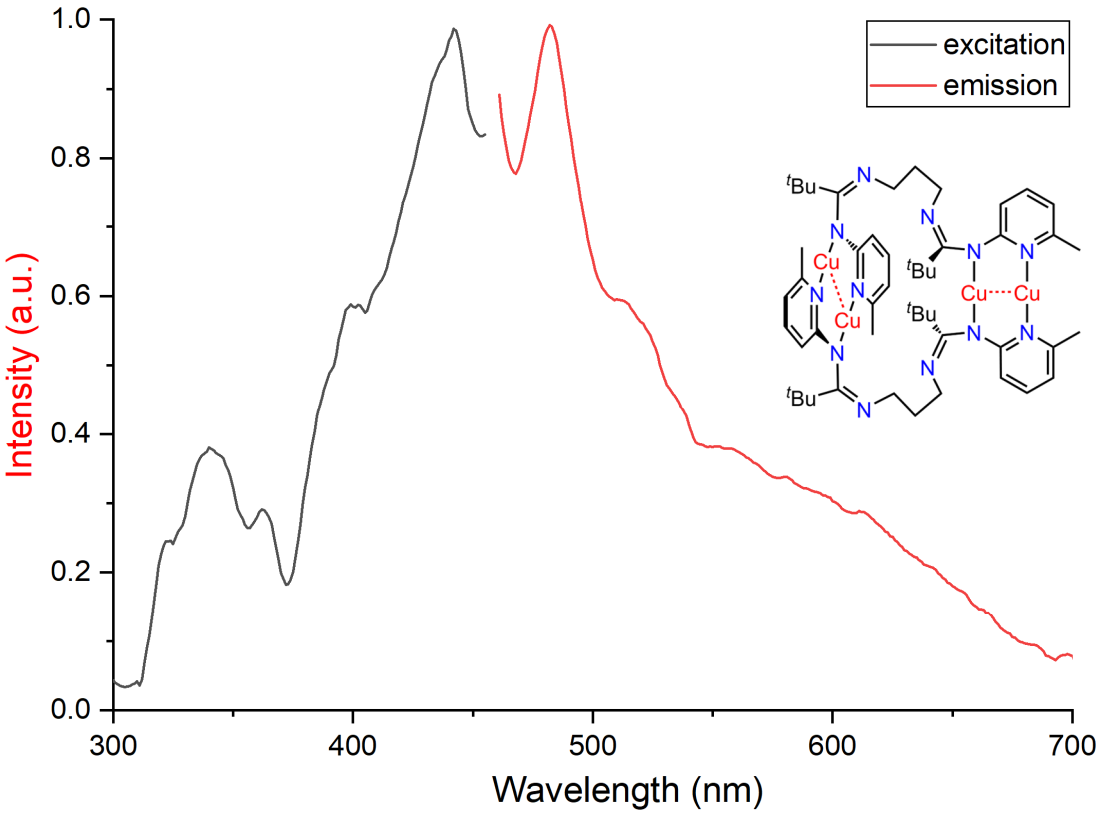

Figure S58: Normalized photoluminescence excitation and emission spectra of **2** in the solid state at 300 K.

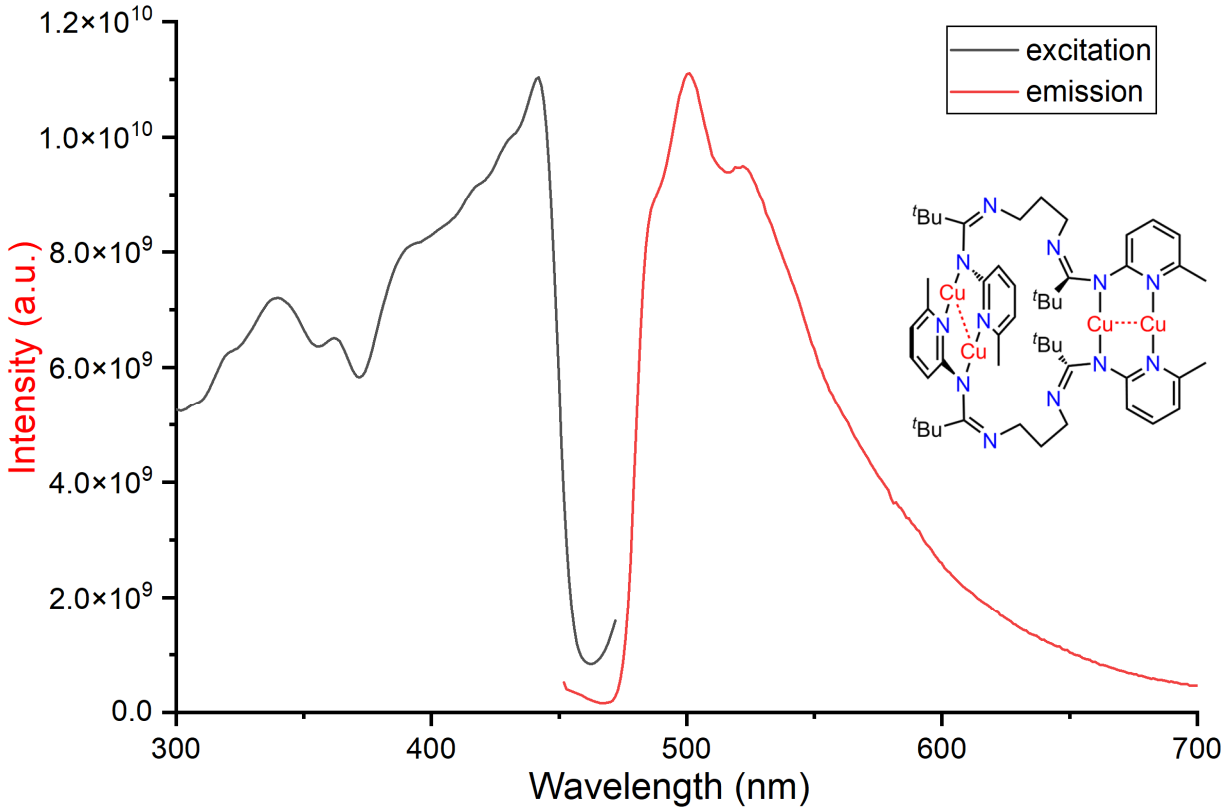

Figure S59: Photoluminescence excitation and emission spectra of **2** in the solid state at 77K.

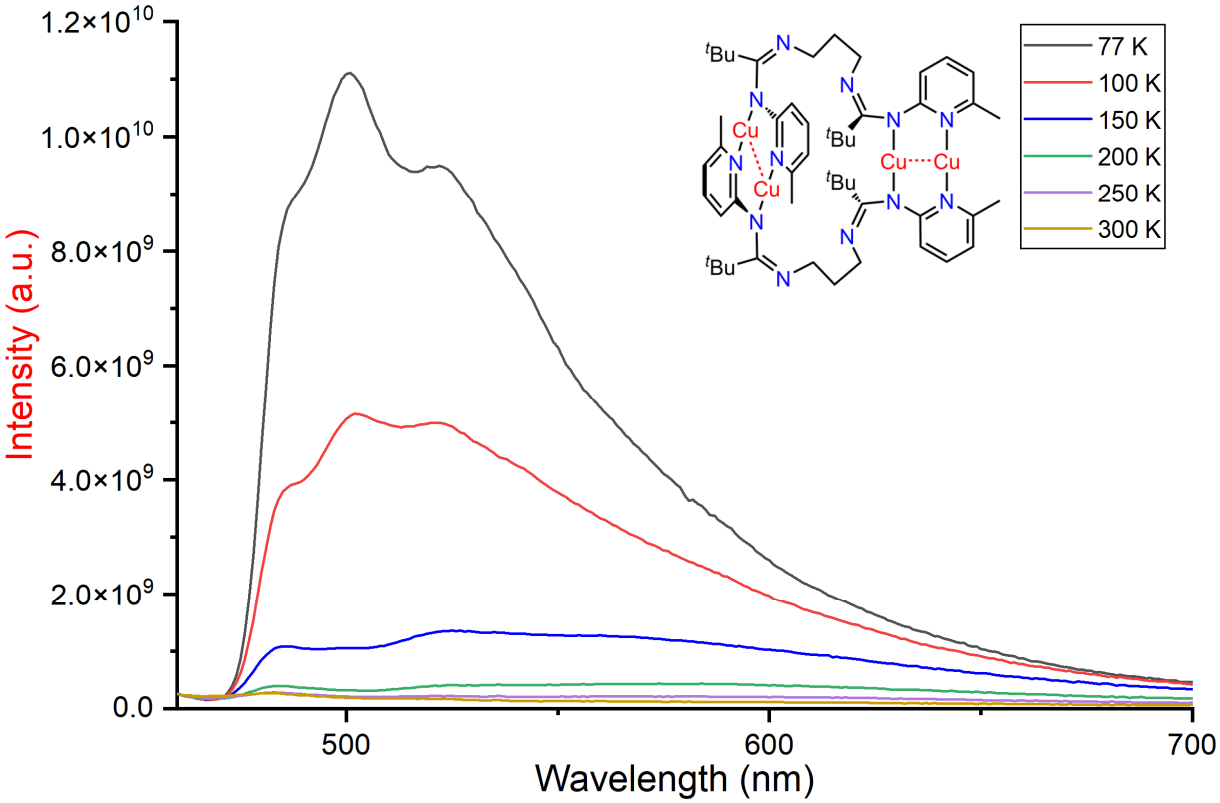

Figure S60: Variable-temperature photoluminescence emission spectra of **2** in the solid state.

Table S7: UV–Vis parameters for $\mathbf{L^2}H_2$, **1**, and **2** in solution (THF).

$\mathbf{L^2}H_2$	**1**	**2**
	λ_{max} [nm] (ε)	
236 (11295)	253 (18285), 279 (21176)	245 (43648), 258 (43216),
295 (6765)	332 (9062)	298 (18662)
	386 (3540)	354 (9809), 370 (12654)

Table S8: Photophysical parameters for **1** and **2*** in solution (THF) and in the solid state.

	1		**2**	
	THF	Solid State	THF	Solid State
Excitation [nm] at 300 K/77 K	367/363	424/419	377/371	442/442
Emission [nm] at 300 K/77 K	484/480	568/490	478/483	482/501
Stokes Shift [eV] at 300 K/77 K	0.82/0.83	0.74/0.43	0.69/0.77	0.23/0.33
Φ_f [%] at 300 K	0.1	6.9	1.0	5.0

*) Samples of **2** were obtained via recrystallization from *n*-hexane solution and dried in oil pump vacuum for 18 h.

References and Footnotes

[S1] Graphics were generated using the following program: DIAMOND—Crystal and Molecular Structure Visualization (version 3.2k), CRYSTAL IMPACT, Dr. H. Putz and Dr. K. Brandenburg GbR, Kreuzherrenstr. 102, 53227 Bonn (Germany).

[S2] (a) Meyer, E. M.; Gambarotta, S.; Floriani, C.; Chiesi-Villa, A.; Guastini, C. *Organometallics* **1989**, *8*, 1067–1079. (b) Eriksson, H.; Håkansson, M. *Organometallics* **1997**, *16*, 4243–4244.

[S3] Fulmer, G. R.; Miller, A. J. M.; Sherden, N. H.; Gottlieb, H. E.; Nudelman, A.; Stoltz, B. M.; Bercaw, J. E.; Goldberg, K. I. *Organometallics* **2010**, *29*, 2176–2179.

[S4] Harris, R. K.; Becker, E. D.; Cabral de Menezes, S. M.; Goodfellow, R.; Granger, P. *Pure Appl. Chem.* **2001**, *73*, 1795–1818.

[S5] Harris, R. K.; Becker, E. D.; Cabral de Menezes, S. M.; Granger, P.; Hoffman, R. E.; Zilm, K. W. *Pure Appl. Chem.* **2008**, *80*, 59–84.

[S6] Burton, A. W. *J. Am. Chem. Soc.* **2007**, *129*, 7627–7637.

[S7] O'Dea, C.; Ugarte Trejo, O.; Arras, J.; Ehnbom, A.; Bhuvanesh, N.; M. *J. Org. Chem.* **2019**, *84*, 14217–14226.

[S8] The ^{15}N chemical shift for the amidine N-atom of $\mathbf{L^2}H_2$ and **2** in 2-py position is expected to be observed through $^3J_{HN}$ coupling from py-H4. It was previously demonstrated in the case of strychnine that a similar tertiary amine did not provide such an observable correlation between N and an *ortho*-positioned aromatic proton. See also (a) Martin, G. E.; Crouch, R. C.; Andrews. C. W. *J. Heterocycl. Chem.* **1995**, *32*, 1759–1766. (b) Koshino, H.; Uzawa, J. *Kagaku to Seibutsu* **1995**, *33*, 252–258.

[S9] Due to its limited solubility, a ^{15}N HMBC NMR spectrum of **1** was not recorded.

[S10] Watkin, D. J. *J. Appl. Cryst.* **1972**, *5*, 250.

[S11] (a) *APEX2: Program for Data Collection on Area Detectors*; BRUKER AXS Inc., 5465 East Cheryl Parkway, Madison, WI 53711–5373 USA. (b) *APEX3: Program for Data Collection on Area Detectors*; BRUKER AXS Inc., 5465 East Cheryl Parkway, Madison, WI 53711–5373 USA. (c) *APEX4: Program for Data Collection on Area Detectors*; BRUKER AXS Inc., 5465 East Cheryl Parkway, Madison, WI 53711–5373 USA.

[S12] Sheldrick, G.M. *SADABS: Program for Absorption Correction of Area Detector Frames*; University of Göttingen, Göttingen, Germany, 2008.

[S13] Sheldrick, G. M. *TWINABS: Program for Performing Absorption Corrections to X-ray Diffraction Patterns Collected from Non-Merohedrally Twinned and Multiple Crystals*; University of Göttingen, Göttingen, Germany, 2013.

[S14] (a) Sheldrick, G.M. *Acta Crystallogr.* **2008**, *A64*, 112–122. (b) Sheldrick, G. M. *Acta Crystallogr.* **2015**, *C71*, 3–8.

[S15] (a) Spek, A. L. *PLATON: A Multipurpose Crystallographic Tool*, Utrecht University, Utrecht, The Netherlands 2008. (b) Spek, A. L. *J. Appl. Cryst.* **2003**, *36*, 7–13.

[S16] (a) Perdew, J. P.; Burke, K.; Ernzerhof, M. *Phys. Rev. Lett.* **1996,** *77*, 3865−3868. (b) Ernzerhof, M.; Scuseria, G. E. *J. Chem. Phys.* **1999**, *110*, 5029−5036. (c) Adamo, C.; Barone, V. *J. Chem. Phys.* **1999**, *110*, 6158−6170.

[S17] Bühl, M.; Reimann, C.; Pantazis, D. A.; Bredow, T.; Neese, F. *J. Chem. Theory Comput.* **2008**, *4*, 1449−1459.

[S18] Grimme, S. *J. Phys. Chem. A* **2005**, *109*, 3067−3077.

[S19] Jesser, A.; Rohrmüller, M.; Schmidt, W. G.; Herres-Pawlis, S. *J. Comput. Chem.* **2014**, *35*, 1−17.

[S20] Hoffmann, A.; Rohrmüller, M.; Jesser, A.; dos Santos Vieira, I.; Schmidt, W. G.; Herres-Pawlis, S. *J. Comput. Chem.* **2014**, *35*, 2146−2161.

[S21] Xu, S.; Gozem, S.; Krylov, A. I.; Christopher, C. R.; Weber, J. M. *Phys. Chem. Chem. Phys.* **2015**, *17*, 31938−31946.

[S22] Dereli, B.; Ortuño, M. A.; Cramer, C. J. *ChemPhysChem* **2018**, *19*, 959−966.

[S23] Frisch, M. J.; Trucks, G. W.; Schlegel, H. B.; Scuseria, G. E.; Robb, M. A.; Cheeseman, J. R.; Scalmani, G.; Barone, V.; Petersson, G. A.; Nakatsuji, H.; Li, X.; Caricato, M.; Marenich, A. V.; Bloino, J.; Janesko, B. G.; Gomperts, R.; Mennucci, B.; Hratchian, H. P.; Ortiz, J. V.; Izmaylov, A. F.; Sonnenberg, J. L.; Williams; Ding, F.; Lipparini, F.; Egidi, F.; Goings, J.; Peng, B.; Petrone, A.; Henderson, T.; Ranasinghe, D.; Zakrzewski, V. G.; Gao, J.; Rega, N.; Zheng, G.; Liang, W.; Hada, M.; Ehara, M.; Toyota, K.; Fukuda, R.; Hasegawa, J.; Ishida, M.; Nakajima, T.; Honda, Y.; Kitao, O.; Nakai, H.; Vreven, T.; Throssell, K.; Montgomery Jr., J. A.; Peralta, J. E.; Ogliaro, F.; Bearpark, M. J.; Heyd, J. J.; Brothers, E. N.; Kudin, K. N.; Staroverov, V. N.; Keith, T. A.; Kobayashi, R.; Normand, J.; Raghavachari, K.; Rendell, A. P.; Burant, J. C.; Iyengar, S. S.; Tomasi, J.; Cossi, M.; Millam, J. M.; Klene, M.; Adamo, C.; Cammi, R.; Ochterski, J. W.; Martin, R. L.; Morokuma, K.; Farkas, O.; Foresman, J. B.; Fox, D. J. *Gaussian 16 Rev. C.01*, Wallingford, CT, 2016.

[S24] These torsion angles were calculated with the program DIAMOND 4.6.8.